Renewable and Sustainable Energy Reviews 217 (2025) 115700

Contents lists available at ScienceDirect

Renewable and Sustainable Energy Reviews

journal homepage: www.elsevier.com/locate/rser

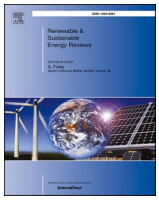

Review on properties, physics, and fabrication of two-dimensional material-based metal-matrix composites (2DMMCs) for heat transfer systems

Hyunjong Lee [a,*], Amir Ardeshiri Lordejani [b], Leonore van Goor [a], Andrea Jurov [d], Apostolos Koutsioukis [c], Siyuan Ruan [c], Neelakandan M. Santhosh [d], Fatemeh Zarei [b], Camila Barreneche [e], Uroš Cvelbar [d], Sergi Dosta [e], Bernard J. Geurts [a], Mario Guagliano [b], Davoud Jafari [a], Valeria Nicolosi [c], Shuo Yin [c], Janez Zavašnik [d], Sara Bagherifard [b], Rocco Lupoi [c], Wessel W. Wits [a,f,**]

[a] *University of Twente, Enschede, the Netherlands*
[b] *Politecnico di Milano, Milano, Italy*
[c] *Trinity College Dublin, The University of Dublin, Dublin, Ireland*
[d] *Jožef Stefan Institute, Ljubljana, Slovenia*
[e] *Universitat de Barcelona, Barcelona, Spain*
[f] *Royal NLR – Netherlands Aerospace Centre, Marknesse, the Netherlands*

A B S T R A C T

In the exploration of new materials development, 2D materials have received much attention due to their outstanding properties in terms of e.g. strength, and electrical and thermal conductivities. Graphene and boron nitride, amongst other 2D materials, are renowned for their exceptional thermal conductivity. In this review, we examine the properties, physics, and fabrication techniques of 2D material-based metal-matrix composites (2DMMCs) with a specific focus on heat transfer systems. The on-going demand for better electronic cooling systems in combination with advancements in mass production techniques of 2D materials facilitates the application of 2DMMCs in heat transfer systems. However, currently, the thermal behaviour of 2DMMCs remains largely uncategorized, strengthening the timely context of this review. Next to recent research progress, material properties, production techniques and strategies for improving thermal conductivity of 2DMMCs are addressed in this work. Methods to reliably assess the thermal conductivity of 2D enhanced materials are discussed alongside the fabrication techniques for 2D-material feedstocks for 2DMMCs production. Also, current limitations in the heat transfer capabilities of 2DMMCs, alongside prospects for enhancing thermal properties through emerging technologies, such as additive manufacturing, are addressed.

Abbreviations

Terms	Abbreviations
2D material-based metal matrix composite	2DMMC
Additive manufacturing	AM
Binder jetting	BJ
Boron nitride nanosheets	BNNS
Ball milling	BM
Black phosphorus	BP
Cold spray	CS
Chemical vapour deposition	CVD
Direct current	DC
Directed energy deposition	DED
Deposition process	DP
Equal channel angular pressing	ECAP
Few layers graphene	FLG
Graphene nanosheets	GNS
Graphene nanoplates	GNP
Graphene oxide	GO
Hexagonal BN	h-BN
Hot extrusion	HE
Hot isostatic pressing	HIP
High pressure torsion	HPT
Integrated circuit	IC
Interfacial thermal conductance	ITC
Liquid base process	LBP
Laser deposition manufacturing	LDM

(*continued on next column*)

(*continued*)

(*continued on next page*)

* Corresponding author.
** Corresponding author. University of Twente, Enschede, the Netherlands.
E-mail addresses: h.lee@utwente.nl (H. Lee), w.w.wits@utwente.nl (W.W. Wits).

https://doi.org/10.1016/j.rser.2025.115700
Received 12 September 2024; Received in revised form 7 February 2025; Accepted 1 April 2025
Available online 23 April 2025

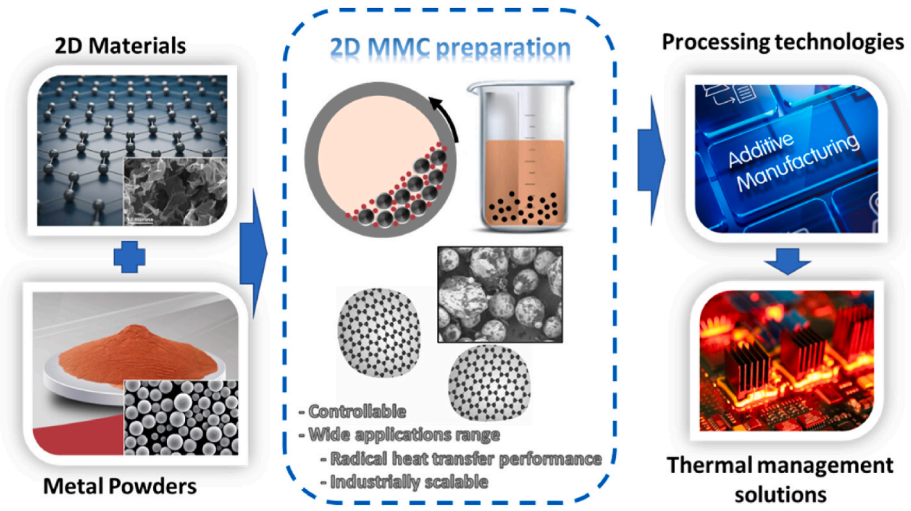

Fig. 1. General synopsis of this review outlining the innovation in 2D-phase materials for heat transfer applications through functional 2DMMCs.

(*continued*)

Laser flash apparatus	LFA
Laser-powder bed fusion	LPBF
Liquid phase exfoliation	LPE
Mechanochemically functionalized graphene	MFG
Metal organic framework	MOF
Powder bed fusion	PBF
Pulsed current	PC
Powder metallurgy	PM
Plasma spray	PS
Reduced graphene film	rGF
Reduced graphene oxide	rGO
Stir casting	SC
Scanning electron microscope	SEM
Single layer graphene	SLG
Severe plastic deformation	SPD
Spark plasma sintering	SPS
Transmission electron microscope	TEM
Transition metal dichalcogenide	TMD
Temperature modulated differential scanning calorimetry	TM-DSC
Transient plane source	TPS
Van Der Waals	vdW
X-ray diffraction	XRD

1. Introduction

The development of 2D (nano)materials has received great attention recently due to their outstanding mechanical properties, electrical and thermal conductivities [1–3]. In particular, the increase in thermal conductivity may lead to innovative applications in thermal management, cooling of electronics and other heat transfer applications. The use of more conventional alternatives, such as diamond, known for its high thermal conductivity, is self-limiting due to processing difficulties and high cost [4]. Implementing 2D materials holds the potential to bring about a significant advancement in this field, reaching performances previously only dreamt of. The thermal conductivity of 2D materials, such as graphene or hexagonal-Boron Nitride (h-BN), has been reported to be ranging between 2 and 5 times higher than synthetic diamond [5,6]. With recent matured 2D materials research, scalable and cost-efficient productions of 2D materials are being developed [7]. Alongside, the rapid progress in metal Additive Manufacturing (AM) allows the use of advanced powder-based processes like Cold Spray (CS), Powder Bed Fusion (PBF), or Binder Jetting (BJ) to fabricate near-net-shape geometries ideal for heat transfer purposes [8–10]. By engineering a metallic-based powder material with embedded 2D phase, it is possible to additively manufacture 3D structures with potentially superior thermal characteristics (see Fig. 1).

2D material-based Metal-Matrix Composites (2DMMCs) have been extensively explored in the literature [11,12]. However, the thermal behaviour of this material class remains largely uncategorized. Metal provides ductility, load-bearing features, printability, and a high melting temperature, while the 2D phase introduces exceptional thermal properties [13–15]. The interaction between these two components in terms of material performances is a critical aspect that has not been thoroughly investigated. It may impact technology and society by generating innovative solutions that can address global challenges, particularly in the realms of energy and manufacturing.

1.1. Materials

The thermal conductivity of graphene ranges from 3080 to 5150 W/mK [16], surpassing that of natural diamond at 2000 W/mK [17]. Also, h-BN and cubic BN exhibit a thermal conductivity of 700 to 2000 W/mK [18,19]. Notably, graphene and h-BN can already be produced in large quantities in laboratory conditions [20], however, an efficient integration into thermal control devices is currently lacking [21]. 2D materials, including graphene and Transition Metal Dichalcogenides (TMDs) like C_3N_4, MoS_2, Bi_2Te_3, and WS_2, offer specific properties crucial for high-end thermal management solutions. Methods for their fabrication include wet exfoliation, Chemical Vapour Deposition (CVD), mechanical cleavage, solvent exfoliation, sonication, and solid-state reaction [7]. On the other hand, processing technologies like PBF and Directed Energy Deposition (DED) are well-established in AM and industrial adoption is upscaling rapidly. These techniques use a high-power energy beam to selectively fuse the feedstock material layer by layer, enabling the rapid production of complex components with fine details [8,22]. In addition, CS, a non beam-based solid-state material deposition process, is considered as the 'next generation' AM technology [23]. While various materials, including metals and ceramics, can be processed via established AM technologies, studies on the direct fabrication of 2DMMCs through AM are still limited. Recent studies, such as Yin et al. [24], demonstrate that CS, assisted by Ball Milling (BM), can produce graphene-reinforced copper MMC materials. More recently, PBF combined with ultrasonic dispersion successfully produced graphene-reinforced aluminium [25] and Inconel 718 MMCs [26]. However, a common challenge in these manufacturing processes is achieving homogeneous dispersion and non-compromised properties of the 2D phase in both the powder feedstock and fabricated products.

Table 1
Data available in the literature on thermal properties test condition and results for the 2D materials.

2D material	Composition	Property	Measured value	Fabrication and measurement condition	Sample Size	Test Temperature	*k* Method applied	REF
Graphene [43] 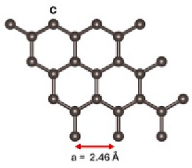	C	k ($Wm^{-1}K^{-1}$)	4840–5300	SLG (suspended) Exfoliation	2–5 μm	RT	–	[21]
			3080–5150	SLG (suspended) Exfoliation	1–5 μm	RT	–	[21]
			2350–3100	SLG (suspended) CVD	2.9–9.7 μm	RT	–	[21]
			579 ± 34	SLG (supported) Exfoliation	2.4 μm	RT	–	[21]
			370	SLG (supported) CVD	1.9 μm	RT	–	[21]
			160	SLG (encased) Exfoliation	–	310 K	–	[21]
			1500–3000	FLG (suspended) Exfoliation	1–5 μm	RT	–	[21]
			170–1250	FLG (supported) Exfoliation	1–5 μm	RT	–	[21]
			30–1000	FLG (encased) Exfoliation	–	310 K	–	[21]
			4800–5300	Optothermal Raman Method	–	–	Raman	[5]
			2400	Np SThM	–	RT	Raman	[5]
			5300 ± 480	SLG	–	–	Laser Flash	[44]
			2300	CVD supported on Cu/Ni	2-3 layer	–	Laser Flash	[44]
			5000	SLG	–	–	–	[45]
			4000–5000	–	–	–	Laser Flash	[46]
			809.5	RGFs (Annealing 1800 °C)	25 μm	300–400 K	–	[21]
			1043.5	RGFs (Annealing 1200 °C)	6 μm	300–400 K	–	[21]
			1102.6	RGFs (Annealing 27 °C)	8.4 μm	300–400 K	–	[21]
			1200	RGFs (Annealing 2000 °C)	13 μm	300–400 K	–	[21]
			1238.3	RGFs (Annealing 2200 °C)	12 μm	–	–	[21]
			1285	RGFs (Annealing 2400 °C)	–	–	–	[21]
			1940	RGFs (Annealing 3000 °C)	10 μm	20 °C	–	[21]
			3214	RGFS (Annealing 2850 °C)	0.8 μm	20 °C	–	[21]
			361–379	SLG (Cu-Graphene)	9 μm	20 °C	Laser Flash	[47]
			346–378	FLG (Cu-Graphene)	9 μm	300–400 K	Laser Flash	[47]
			354–374	SLG (Cu-Graphene)	25 μm		Laser Flash	[47]
			372–377	FLG (Cu-Graphene)	25 μm		Laser Flash	[47]
			1016	GO/poly-naphthylamine	–		–	[21]
			251.23 (in plane)	Cu–rGO	2 mm		Laser Flash	[46]
			28.48 (through plane)	Cu–rGO	2 mm		Laser Flash	[46]
			154	0.1 wt% Al/G composite	5 mm		Laser Flash	[48]
			159	0.2 wt% Al/G composite	5 mm		Laser Flash	[48]
			165	0.3 wt% Al/G composite	5 mm		Laser Flash	[48]
				SLG	9 μm		Laser Flash	[47]
		α ($mm^2\ S^{-1}$)	91–99	FLG	9 μm	300–400 K	Laser Flash	[47]
			95–100	SLG	25 μm	300–400 K	Laser Flash	[47]
			98–99	FLG	25 μm	300–400 K	Laser Flash	[47]
			635	GO/poly-naphthylamine	–	–	–	[21]
			100–104	G/Cu bulk	2.4 nm	–	Laser Flash	[49]
			0.85	SLG	–	RT	Laser Flash	[50]
		C_p ($J\ g^{-1\ -1}$)	0.921	0.1 wt% Al/G composite	5 mm	–	DSC	[48]
			0.928	0.2 wt% Al/G composite	5 mm	–	DSC	[48]
			0.987	0.3 wt% Al/G composite	5 mm	–	DSC	[48]

(*continued on next page*)

Table 1 (*continued*)

2D material	Composition	Property	Measured value	Fabrication and measurement condition	Sample Size	Test Temperature	*k* Method applied	REF
BP [43] 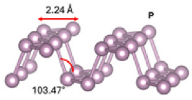	P	k (W m^{-1} K^{-1})	110 (armchair)	–	–	300 K	Raman	[51]
			36 (zigzag)	–	–	300 K	Raman	[51]
			10	–	–	RT	Raman	[51]
h-BN [43] 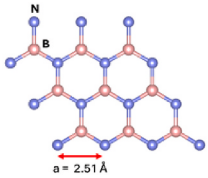	Hexagonal boron nitride	k (W m^{-1} K^{-1})	250	Exfoliated Suspended	5 layers		–	[21]
			360	Exfoliated Suspended	11 layers		–	[21]
			484	Exfoliated Suspended	2 layers		–	[21]
			751	Exfoliated Suspended	1 layer		–	[21]
			646	Exfoliated Suspended	2 layers		–	[21]
			602	Exfoliated Suspended	3 layers		–	[21]
			227	CVD Suspended	9 layers		–	[21]
		C_p (J g^{-1} K^{-1})	0.78	–	–	RT	DSC	[50]
BNNS	Boron nitride nanosheet	k (W m^{-1} K^{-1}) in plane	600	CVD	–	–	Laser Flash	[52]
			20.4	–	–	–	Laser Flash	[53]
			13.2	BNNS/EVA	–	–	Laser Flash	[52]
			31.3	BNNS/ANF@AgNW	8 nm (<20 layers)	30-135 °C	Laser Flash	[53]
			16.3	BNNS/PVDF		–	Laser Flash	[52]
		k (W m^{-1} K^{-1}) through plane	2–30	CVD	8.8 nm	–	Laser Flash	[52]
g-C_3N_4 [43] 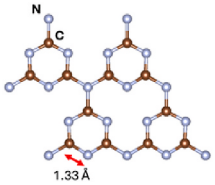		It possesses a condensed and conjugated structure. Properties of low charge recombination, efficient electron conductivity, fast kinetics, high photoabsorbance activity					Laser Flash	[51]
MoS_2 [43] 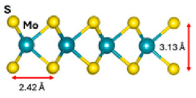	MoS_2	k (W m^{-1} K^{-1})	84	Exfoliated Suspended	1 layer	RT	–	[21]
			77	Exfoliated Suspended	2 layers		–	[21]
			60.3	CVD Suspended	1 layer		–	[21]
			38.4	CVD Suspended	2 layers		–	[21]
			44.8	CVD Suspended	3 layers		–	[21]
			36.9	CVD Suspended	4 layers		–	[21]
			62.2	Exfoliated Supported by SiO_2	1 layer		–	[21]
			60.3	Exfoliated Supported by Glass	4 layers		–	[21]
			52	CVD, transferred, suspended	11 layers		Raman	[51]
Zn-TCPP MOF [54] 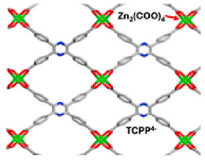		Unique architectures, distinctive features, and desirable structural details.					Raman	[51]
Polymer [55] 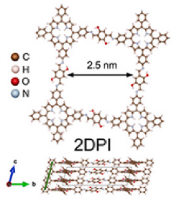	General	k (W m^{-1} K^{-1})	<0.5			–	–	[5]
			0.2			–	Laser Flash	[56]
	EP	k (W m^{-1} K^{-1})	0.22			20-100 °C	Laser Flash	[51]
	(CF)/olefin block copolymer(OBC) composites	k (W m^{-1} K^{-1}) through plane	15.06			–	Laser Flash	[57]
		k (W m^{-1} K^{-1})	1000				Theoretical calculated	[58]
	Graphitized polyimide (PI)	k (W m^{-1} K^{-1})	120			–	Theoretical calculated	[58]
	(FBN)/PVA	k (W m^{-1} K^{-1})	38.27	55 % UHMWPE		25-100 °C	Laser Flash	[57]
						25-100 °C	–	[14]
	UHMWPE	k (W m^{-1} K^{-1})	15.06	30 % loading CF		25-100 °C	Laser Flash	[57]
		through plane	1.17	Random structure		25-100 °C	Laser Flash	[57]
			1.58	Parallel structure		25-100 °C	Laser Flash	[57]
Clays [43]	e.g., Kaolinite $Al_2Si_2O_5(OH)_4$	Low thermal conductivity					TPS	[56]

(*continued on next page*)

Table 1 (*continued*)

2D material	Composition	Property	Measured value	Fabrication and measurement condition	Sample Size	Test Temperature	*k* Method applied	REF
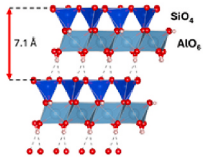								

1.2. Heat transfer applications

Industry demands thermal solutions capable of dissipating high heat fluxes at low thermal resistance. As the integration of "hot" devices advances across various industries, from electric vehicles to aerospace and from defence to consumer products, thermal challenges and cooling issues intensify [27–30]. Heat exchange is increasingly becoming the limiting factor for future innovations, as indicated in recent industry roadmaps [28]. Integrated Circuit (IC) components are adhering to Moore's Law, halving in size and doubling in power roughly every 18 months [31]. While this escalation in power enhances performance, it concurrently elevates heat generation. Moreover, the size reduction imposes detrimental constraints on the available surface area for traditional cooling methods. A review by Nguyen et al. in the early 2000s on cooling methods for laptop CPUs already highlighted the imperative use of heat pipe technology to enhance cooling efficiency [32]. Presently, this scenario continues to persist. With the adoption of miniaturization in electronics, the limitations of standard forced convection cooling methods have been surpassed [33]. Following Moore's Law, heat fluxes exceeding 1000 W/cm^2 are anticipated in the next decade, as well as modern data centres already host servers with power densities reaching 200 W/cm^2 [28,34]. Therefore, the potential revolutionary applications of increased thermal conductivity are of particular interest, along with the need for developing new material systems such as 2DMMCs.

Taking all of this into consideration, the study on the production and application of 2DMMC for single-phase and high-performance cooling systems is essential to keep up with technological advancements. Hence, we review the properties of 2D materials (Section 2), the impact of production technologies on the quality of 2DMMC feedstocks (Section 3), and proper fabrication techniques for 2DMMC parts (Section 4). Furthermore, we propose strategies to improve thermal conductivity in 2DMMCs (Section 5), as well as the current challenges and future potentials in the heat transfer applications of 2DMMCs (Section 6).

2. Properties of 2D materials

The measurement of 2D material properties under characterization requires critical attention. These measurements necessitate special consideration due to the unique nature of 2D materials. For this reason, researchers have developed specific conditions for their measurements to ensure accurate characterization and analyses. In this section, we review the properties of 2D materials, and the corresponding measurement techniques and conditions. In particular, the extraordinary properties of 2D materials that make them stand out compared to commercial bulk materials are highlighted.

2.1. Thermophysical properties of 2D materials

The thermophysical properties of the best 2D materials from a thermal perspective are discussed in this section. In addition, their composition, conditions for the measurements, and sample sizes are also considered.

Graphene is the most extensively studied 2D material in terms of thermophysical properties, as evidenced by the extension of data listed in Table 1. However, the reported thermal conductivity of graphene differs up to one degree of magnitude. This dispersion may also be attributed to the thermal characterization method, as well as the sample size used for the measurements. Therefore, the values obtained from the thermal characterization should be interpreted with consideration of the measurement conditions, such as sample mass, porosity (air), methodology, sample shape, and other aspects. As this concern is evident for graphene, the properties of the other materials listed in Table 1 should also be considered with caution.

Overall, in this subsection, thermophysical properties of 2D materials, including graphene, Black Phosphorus (BP), h-BN, Boron Nitride NanoSheets (BNNS), g-C_3N_4, MoS_2, Zn-TCPP Metal Organic Framework (MOF), polymers, and clay are representatively reviewed, due to their intriguing properties as follows: 1. the exceptional thermal conductivity of graphene [16], h-BN [19], and BNNS [35]; 2. the directional thermal transport along crystal plane in BP [36]; 3. the multifunctionality such as tuneable electrical properties in MoS_2 [37] and photocatalytic activity in g-C_3N_4 [38]; 4. the modifiable thermal conductivity in MOFs based on pore size and shape [39,40]; and 5. the good thermal insulation properties of polymers [41], and clay [42].

2.2. Other properties

In addition to their attractive thermophysical properties, 2D materials can exhibit very interesting physical and mechanical properties. Notably, 2D materials can resist increased mechanical strain due to their single-atomic-layer structures. Their mechanical properties (Young's modulus) are mainly measured by an indentation on circular membranes or on pressurizing membranes and the reported value depends on the processing methods (exfoliation, CVD, SLG, etc) [59]. On the other hand, their electrical properties, mainly characterized by the Eddy Current conductivity meter technique, are less dependent on the fabrication process [60].

The density of 2D materials is mostly measured by Helium Pycnometer or Hg Pycnometer, since these techniques are the most precise for determining true density [61]. Additionally, sample size and test temperature are important variables to consider during characterization, typically requiring single-layer samples and room temperature conditions, respectively. Table 2 summarizes the mechanical, physical, and electrical properties of 2D materials under review.

2.3. Methods for thermal conductivity measurements

There are several methods available to measure thermal conductivity, including steady-state methods such as guarded hot plate [70] and heat flowmeter [71], as well as transient methods such as Transient Plane Source (TPS) [72,73], transient hot wire [74,75], Laser Flash Apparatus (LFA) [76,77], Temperature Modulated Differential Scanning Calorimetry (TM-DSC) [78,79], and 3ω method [80,81]. These techniques, widely used and commercialized for the measurement of thermal conductivity of various materials, will be briefly described.

2.3.1. Steady-state measurements

In steady-state measurements, the measurement of temperature

Table 2
Mechanical, physical and electrical properties of the 2D materials under review.

Material type	Property	Parameter	Value	Fabrication Method	Sample Size	REF
Graphene	Mechanical	Young Modulus (GPa)	1000	Mechanical exfoliated	1 layer	[51,62]
			1000 ± 100	Mechanical exfoliated	1 layer	[51]
			930 ± 48	Mechanical exfoliated	23-43 layer	[51]
			1000 ± 31	Mechanical exfoliated	4 layers	[51]
			2400 ± 400/2000 ± 500	Mechanical exfoliated	1-5 layer	[51]
			800	Mechanical exfoliated	1 layer	[51]
			1550	Mechanical exfoliated	2 layers	[51]
			250 ± 150	Mechanical exfoliated	3-14 layer	[51]
			157	Mechanical exfoliated	1 layer	[51]
			1000	Mechanical exfoliated	1 layer	[51]
			800	Mechanical exfoliated +	1 layer	[51]
				Ar plasma	1 layer	[51]
		Strength (GPa)	130	Gr/Cu composite	1 layer	[63]
			131	Gr/Cu composite	–	[64]
			232	–	5 mm	[48]
			249	–	5 mm	[48]
			260	–	5 mm	[48]
			239	SLG	–	[65]
			663	SLG	5.59 μm	[66]
		Hardness (HV)	49.2 ± 2.5	SLG	5 mm	[48]
			50.7 ± 1.2	Molecular level mixing + SPS	5 mm	[48]
			52.2 ± 1.9	0.1 wt% Al/G composite	5 mm	[48]
			52–67	0.2 wt% Al/G composite	–	[49]
			47–71	0.3 wt% Al/G composite	–	[49]
			226.8 (HV0.1)	–	–	[67]
			145.7 (HV0.1)	–	–	[67]
			188.5 (HV0.1)	–	–	[67]
			74.6 (HV0.1)	–	–	[65]
				–		
				–		
				–		
	Physical	Density (g cm^{-3})	2.2	FLG based composites	1 layer	[63]
			2.27	Cu(111)/Gr heterosystem	1 layer	[21]
	Electrical	Electrical conductivity (S/m)	1400–2100	GO reduced	–	[51]
			2-9 x 10^7	CVD growth	–	[68]
			40000–44000	CVD growth	–	[69]
			35000–40000	CVD growth	–	[69]
MoS_2	Mechanical	Young Modulus (GPa)	280	Mechanical exfoliated	1 layer	[51,62]
			270	Mechanical exfoliated	1 layer	[52]
			270 ± 100	Mechanical exfoliated	2 layer	[51]
			200 ± 60	Mechanical exfoliated	5-25 layer	[51]
			300 ± 10	Mechanical exfoliated	5-25 layer	[51]
			330 ± 70	CVD growth	1 layer	[51]
			260 ± 18	CVD growth	2 layer	[51]
			231 ± 10	CVD growth	–	[51]
			290	$MoS_{2x}Te_{2(1-x)}$	–	[62]
			170 (Pa)	CVD growth	–	[62]
		Strength (GPa)	23	CVD growth	1 layer	[62]
		Stiffness (N m^{-1})	180–183	Circular monolayer	1 layer	[62]
BNNS	Mechanical	Young Modulus (TPa)	0.334	–	–	[62]
			0.6	–	–	[11]
			1.16	CVD	15 nm	[62]
h-BN	Mechanical	Young Modulus (GPa)	711	CVD growth	1 layer	[21]
			865	CVD growth	1 layer	[51,62]
			856	CVD growth	9 layers	[62]
			279 ± 20	CVD growth	2 layers	[51]
			269 ± 13	CVD growth	4 layers	[51]
			252 ± 15	CVD growth	5 layers	[51]
	Physical	Density (g cm^{-3})	2.1	–	1 layer	21]
BP	Mechanical	Young Modulus (GPa)	27 ± 4 (armchair)	Mechanical exfoliated	17-35 layers	[51]
			59 ± 12 (zigzag)	Mechanical exfoliated	17-35 layers	[51]

difference (ΔT) under steady-state heat flow conditions through the sample thickness determines the thermal conductivity and the interfacial thermal conductance [71]. Thermal conductivity can be determined by calculating the slope of the power per thermal gradient between both sample surfaces. The steady-state methods are based on Fourier's law to directly measure the thermal conductivity [82]. These methods are in particular useful for materials that have relatively low thermal conductivity and for composite materials. Furthermore, steady-state methods require relatively large sample sizes, and their testing takes longer compared to transient methods. In addition, these measurements have drawbacks such as systematic heat losses and losses by contact resistance from the usage of temperature sensors, which are difficult to avoid and accurately quantify. However, steady-state measurements can effectively assess anisotropic thermal conductivity and layered composite materials by measuring one-directional heat flow over a large area.

2.3.2. *Transient-state measurements*

In transient-state measurements, thermal conductivity is determined by the temperature change of the specimen over time in response to an

Table 3
Methods to measure the thermal conductivity: scheme, general information, limitations and 2D materials usage.

Method	Scheme of set-up	General information	Limitations	Usage in 2D materials	Reference
Guarded hot plate	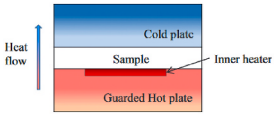	The measurement involves placing a solid sample between two parallel plates at a controlled temperature. The hot plate is heated by a heater that creates the desired temperature gradient. This heat is transferred from the hot surface to the cold plate. To prevent heat losses and to achieve uniaxial heat transfer, the system uses a guarded heater and is thermally insulated.	Once the system reaches a steady-state temperature, Fourier's equation is used to calculate the thermal conductivity. To obtain accurate measurements, it is crucial to determine the contact resistances between the sample and the two plates.	Contact resistance needs to be considered. The sample size should be relatively large (the exact size of sample is adaptable)	[70,72]
Heat flow meter	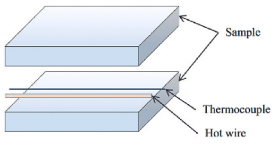	The heat flow meter apparatus is similar to guarded hot plate systems. It differs in the usage of transducers to measure the heat flux density through the sample and follows ASTM E153 for evaluating materials' resistance to thermal transmission.	The temperature range mentioned is quite wide, varying from −20 to 100 °C. However, for 2D materials, the required sample size is relatively large (a diameter between 25.4 mm and 100 mm).	The required sample size is too large to be applied to 2D materials.	[71]
Hot wire	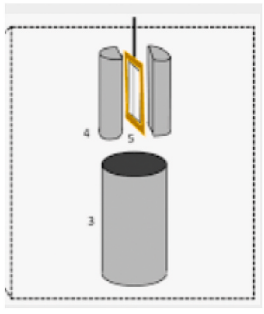	Hot wire is an intrusive technique that can measure the thermal conductivity of non-electrically conductive materials. The wire serves not only as a heater, but also as a temperature sensor. During the process, radial heat flows from the wire to the sample, and the temperature rise slope is proportional to the time elapsed.	The equipment can handle temperatures up to about 150–200 °C, and thermal conductivities ranging from 0.001 W/m K to 20 W/m K. Compared to steady-state methods, the required sample size is much smaller, with a minimum thickness of just 0.3 mm.	Sample size can be adjusted for 2D materials but the materials need to be non-electrically conductive.	[74,75]
Transient Plane Source (TPS)		TPS can be used to measure the thermal conductivity of samples in solid, liquid, and powder forms. It involves using a set of concentric rings, typically made of nickel, as a planar heater, which is then reinforced by insulating gaps. The TPS method can also be modified for bulk thermal conductivity testing to eliminate thermal contact resistance.	This technique allows for a temperature range from −35 °C to about 750–1000 °C and can measure thermal conductivities ranging from 0.001 to 1800 W/m K. The sample must cover the flat sensor and must have a minimum thickness of 0.01 mm (for thin films) to 3 mm (for bulk samples) depending on the actual thermal conductivity.	It is the most versatile technique to measure thermal conductivity and is the best method for 2D material. TPS requires a much smaller sample size compared to the other techniques.	[73]
Laser Flash Apparatus (LFA)	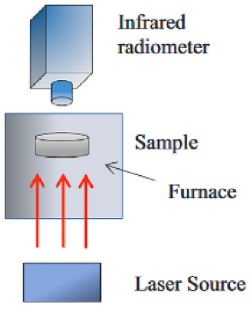	The LFA technique is a highly effective and versatile method used for measuring thermal properties. It is the most accurate technique to determine the thermal diffusivity of conductive solid materials. The LFA method uses non-contact, non-destructive temperature sensing to achieve precise results.	The temperature ranges up to 1200 °C, which is higher than all the other techniques.	The sample size is appropriate to measure 2D materials and it is possible to measure at high temperatures (up to 1200 °C)	[76,77]
Optothermal Raman method	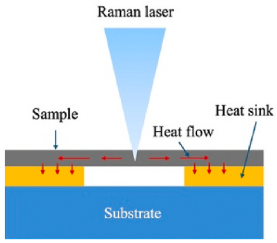	Raman-based method provides non-destructive and direct thermal characterization with high-spatial resolution. Thermal conductivity of nano-sized thin-films or 2D materials can be measured based on the temperature-sensitive Raman peak shifts (e.g., the G or 2D band of graphene).	Accurate calibration between the Raman shift and the temperature rise in a sample is required but challenging due to non-uniform heating at the laser spot and the difficulty in accurate temperature control. Careful consideration of strain, defects, and the effects of heat dissipation in the sample is necessary.	Suitable for the characterization of various 2D materials (e.g., graphene, h-BN, MoS_2, etc.). Generally useful for nano-scale measurements.	[83,84]

(*continued on next page*)

Table 3 (*continued*)

Method	Scheme of set-up	General information	Limitations	Usage in 2D materials	Reference
TM-DSC	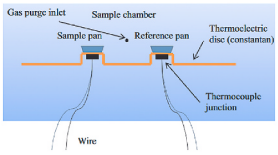	TM-DSC is a variation of the traditional DSC technique. It is used to measure insulating materials like ceramics, glasses, and polymers. The TM-DSC process uses a heating temperature program that combines a linear heating rate with a sinusoidal temperature control. This results in an average constant heating rate.	TM-DSC can be applied in solid bulk samples at temperatures from −125 to 700 °C (depending on the DSC instrument used). However, to have accurate results the sample needs to be in contact with the sensor, which could cause equipment damage or contamination.	The sample size is the same as the DSC crucible dimensions: The typical size of a DSC crucible; is 6 mm in diameter and a height of 4.5 mm. This is a proper size to measure 2D materials.	[78,79]

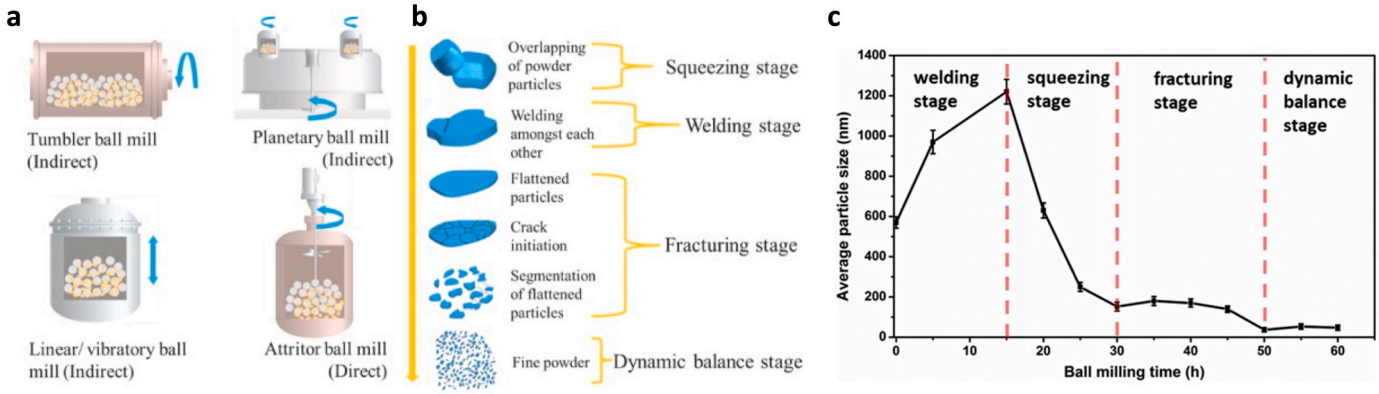

Fig. 2. (a) Schematic diagram illustrating ball milling processes including three indirect and one direct ball milling method, with the key components labelled [86,87], (b) mechanism of powder particle size evolution and reduction in ball milling process, (c) correlation between milling duration and mean diameter of particles during the planetary ball milling process [98,99].

applied heat pulse (e.g., a pulsed laser or an electrical heater). Among them, the TPS method measures the thermal conductivity of materials ranging from 0.001 to 1800 (W/m K), making it widely used [72,73]. Following TPS are the LFA and transient hot wire/hot strip methods. Those methods are able to measure conductivity values between 0.1 and 1000 (W/m K) [76,77], and 0.005 to 500 (W/m K) [74,75], respectively. Regarding the temperature testing range, LFA and TPS range from 120 to 2800 °C and 35 to 1000 °C.

2.3.3. Optothermal Raman method

The Optothermal Raman method is in a category of steady-state measurements, but employs the Raman spectrum as a thermometer to measure the local temperature rise in (nano)materials (e.g., 2D materials or thin films) [83]. The sample is locally heated by the Raman laser, and the temperature rise is extracted from the Raman peak shift, which occurs due to the temperature response of phonons. Thermal conductivity is calculated based on a model incorporating the absorbed laser power (P), temperature rise (ΔT), and the radius of the laser-heated spot. Reported thermal conductivity values range from approximately 1 to 5000 (W/mK) for thin films or 2D materials [83–85]. However, precise calibration between the Raman peak shift and the temperature rise is essential to ensure accurate conductivity measurements (see Table 3).

Table 3 summarizes the most renowned methods to measure thermal conductivity and their limitations when applied to 2D materials.

In the following sections, 2D materials with the greatest potential for practical heat transfer applications will mainly be discussed. The properties reviewed in this section suggest that graphene and h-BN are the most promising candidates to produce 2DMMCs, due to their excellent thermal and mechanical properties. Therefore, the focus will be on graphene and h-BN.

3. Preparation of 2D materials and 2DMMC feedstock powders

3.1. Preparation of 2D materials

3.1.1. Ball milling

As powder preparation and mixing technology has continuously developed over the past half-century, the versatile BM method has received widespread attention due to its simple operation, environmental friendliness, cost-effectiveness, and time-saving features [86–89]. BM offers controlled and decreased particle size, enhanced nanoparticle dispersion, and functionalization for improved product properties [90–93]. Also, BM enables the manufacturing of diverse materials, including polymers, cellulose, catalysts, and 2D (nano)materials [87,94–96].

Previous research classified BM into two principal categories: direct and indirect milling, based on the kinetic energy path—either directly to the grounded powders by mechanical shafts and rollers, or indirectly through the device body [86,88,97]. Typical examples of direct milling involve the attritor mill, pan mill, and roll mill, while indirect milling covers the tumbler mill, vibratory mill, and planetary mill [88], see Fig. 2a. The attritor ball mill is commonly mentioned in direct BM methods due to its reliance on impact and shearing forces for material processing [88]. On the other hand, in the indirect BM method, a vessel is partially filled with the powders and the jars are vibrating or rotating axially or radially [88,97]. During milling, high strain rate loads produced by collisions between particles, milling mediums, and the container walls are indirectly transferred to the powder particles [86].

Fig. 2b illustrates four typical stages in the particle refinement process during BM [86,98,99]. First, two independent approaching particles are gradually overlapped due to particle collisions generated by the localized compressive stresses (squeezing stage) [90,99]. Then, they merge under the effects of impact force (welding stage), and the merged particle undergoes flattening and breaks apart (fracturing stage) by

Table 4
Process parameters of Ball Milling (BM) techniques for 2D material production.

Key Parameters	Common Examples	Supporting References
Ball mill design	Direct milling (attritor mill, pan mill, roll mill) and Indirect milling (tumbler ball mill, vibratory (or shaker) mill, planetary ball mill)	[90,97,102]
Mechanisms	Mechanical forces, including primary shear and secondary impact, that can overcome Van der Waals (vdW) interactions between interlayers	[97,103,104]
Type of the jars/balls	Stainless steels, zirconia, agate, tungsten, alumina and silicon nitride	[89,97,100, 102]
Size of precursor	Depending on the starting material	[87,105,106]
Grinding atmosphere	N_2, CO_2, Ar	[93,97,101, 107]
Liquid process control agents (for wet ball milling)	Water, ethanol, toluene, 1-butanol, hexanoyl chloride	[88,93,94,97]
Milling speed	Customized parameters (determine high or low energy ball milling based on actual energy inputs)	[89,93,97,101, 108,109]
Milling time		[93,97,110, 112]
Milling temperature		[90]
Charge ratio (Ratio of the mass of balls to powder)		[93,97,102, 108,110,112]
Size of balls		[97,109]

further impact and shear forces until it reaches the dynamic balance stage (see Fig. 2b–c) [99]. Fig. 2c complements the BM processes by showing the size variation in each stage [98,99].

Table 4 lists the major variables influencing the BM process including mechanisms of BM [87,88,97]. Numerous parameters tend to interact synergistically with each other, affecting the quality of the final powders, such as crystallinity, particle size, surface activity, and the density of defects [87–89,97,100,101]. Therefore, optimizing suitable BM parameters on the product quality is indispensable. Furthermore, Table 5 provides common strategies that are employed for the optimization of the BM process. Although BM serves as a promising technique for 2D material production, it has both advantages and limitations. Therefore, many efforts have been made to improve BM techniques (see Table 6).

3.1.2. Preparation of 2D materials by ball milling

3.1.2.1. Graphene. Prior research has delineated various methods for synthesizing graphene and other carbon-based materials [124–126], and these approaches are categorized into either top-down or bottom-up strategies in Fig. 3 [94,127]. Prominent techniques for the synthesis or exfoliation of graphene include CVD [128,129], mechanical exfoliation of graphite [130,131], electrochemical liquid-phase exfoliation [94,132, 133], conversion of nanodiamond [134], methods of aqueous exfoliation [130], thermal decomposition of silicon carbide [135], and the reduction of graphitic oxide [136].

Among them, high-energy BM serves as a flexible mechanical exfoliation technique for producing various 2D materials. Especially for costly, but high thermally and electrically conductive graphene, BM offers comparatively less expensive production. BM possesses the potential to peel off the planar carbon nanolayers from the bulk graphite by shearing and collision forces [94,99,130]. During the exfoliation, the kinetic energy applied from the impact and shear forces causes the C-C bonds to cleave and strip away to overcome the weak Van Der Waals (vdW) interactions between layers (Fig. 4) [93,94,103,114,122,131]. Tweaking the parameters in Tables 4 and 5 allows to control the quality and yield of produced graphene. In particular, the use of specific solvents in wet BM or gas atmosphere in dry milling can either modify the surface properties by improving functional groups, or aid in preventing

Table 5
Strategies for the ball milling (BM) process optimization.

Optimization Strategy	Descriptions	Optimization goals	Supporting References
Milling Type Selection & Process Scaling	Select the appropriate milling techniques, either planetary milling or the rotatory milling to increase milling efficiency and reduce processing time	• Planetary BM applies higher shear and impact forces, but relatively smaller flake sizes are obtained. Also, the overall process time is shorter • Rotatory BM is suitable for large-scale productions such as kg-scale BM, but slower processing times and difficulty in particle size control are its main drawbacks	[88,89,101, 105,110, 120]
Starting materials selection & pre-treatment	Apply appropriate pre-treatment methods, such as chemical surface modification or mechanical activation to improve material compatibility or enhance interfacial bonding	• Chemical treatments will assist surface functionalization with improved bonding strength, while mechanical activation improves dispersion and reduces aggregation during milling	[87,88,93, 96,108,111]
Milling gas environment	Modify the milling atmosphere, such as inert gases (e.g., Ar, N_2) to prevent oxidation or reactive gases for functionalization	• Inert gases help maintain the purity of the starting material and prevent oxidation-related degradation, while reactive gases can promote functionalization to enhance particle dispersion and interfacial bonding	[97,107, 108,121]
Milling agents	Select wet or dry milling, introducing process control agents (PCAs) like ethanol, toluene, or polymer surfactants to minimize agglomeration	• Wet milling with PCAs improves material flowability and reduces particle agglomeration. It improves the dispersion and prevents particle welding of 2D materials in the metal matrices. It is known as a milder milling condition compared with dry milling without PCAs	[88,94,97, 105,108, 122]
Parameter control	Milling time: this is a critical factor that decides the exfoliation and fragmentation of 2D materials	• Short milling time results in incomplete exfoliation and larger particle sizes (e.g., less than 2h) • Optimal milling time produces efficient exfoliation and well-dispersed few-layer sheets • Excessive milling time causes unwanted oxidation and structural defects in 2D layers	[97,105, 109,123]
	Milling speed: this is another critical factor that	• Low milling speed results in incomplete and weak exfoliation	

(continued on next page)

Table 5 (*continued*)

Optimization Strategy	Descriptions	Optimization goals	Supporting References
	determines the impact energy and shear force exerted on the materials	with poor milling efficiency • Optimal milling speed leads to balanced exfoliation with proper size control • Excessive milling time causes large defect densities, oxidation, and amorphization, and smaller lateral sizes	
	Ball-to-powder ratio: Adjusting the mass ratio of the grinding ball to the material is crucial for optimizing 2D material dispersion and minimizing agglomeration	• A low ball-to-powder ratio leads to poor yield and weak exfoliation efficiency • Optimal ball-to-powder ratio results in a high yield of 2D layers with better size control and uniformity • A high ball-to-powder ratio causes more fragmentation, resulting in smaller 2D layers, excessive defects, and, low yields	

Table 6
Advantages, limitations, and potential improvements of BM in 2D material production.

Advantages	1. Large-scale synthesis of 2D materials with high yields 2. Functionalization of 2D materials via the addition of solvents, gas, and doping agents	[103, 113–115]
Limitations	1. High defect densities in 2D layers, accompanied by fragmentation 2. Difficult in controlling the flake sizes due to the wide particle size distribution	[103,116, 117]
Potential improvements	1. Careful optimization of each BM parameter assisted by machine learning-based simulations 2. Selection of appropriate liquid milling agents that can improve the quality of 2D materials 3. Post-processing steps such as sonication, centrifugation, and filtration can improve purity and size distribution	[117–119]

the reaggregation of exfoliated graphene sheets [94,106,107,127]. For example, extending the milling time and elevating CO_2 pressure significantly reduces the carbon content by increasing the degree of C-functionalization [94]. Fig. 5 shows that the trend in particle size variation mirrors that observed in Fig. 2b [94]. Interestingly, carboxylation of graphene under high CO_2 pressure improves the exfoliation efficiency, as the complete saturation of dangling bonds helps enhance the mechanochemistry of BM. However, under identical milling conditions of 12 h and 250 rpm, particles that were produced in an Ar atmosphere presented a large cluster of carbon nanoparticles compared to those synthesized in a CO_2 atmosphere, due to the vigorously reactive carbon nanoparticles [94]. Accordingly, reactive carbon nanoparticles form oxides or hydroxides when exposed to air, leading to severe particle agglomeration. Del Rio-Castillo et al. successfully produced high-quality single layer graphene by adding an exfoliating agent (melamine) and proved the feasibility of utilizing Hansen solubility parameters for the selective suspension of exfoliated graphene from the carbon fibres (Fig. 6) [106].

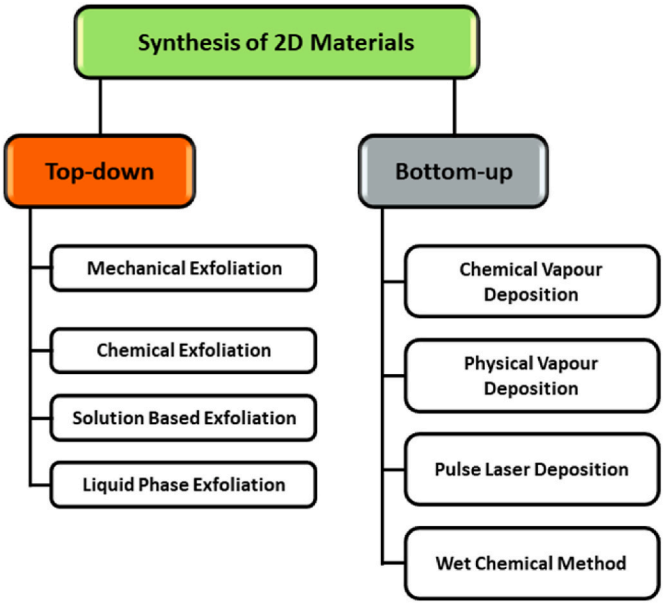

Fig. 3. Flowchart outlining the synthesis techniques for 2D materials, including the top-down and bottom-up routes [137].

3.1.2.2. Hexagonal boron nitride (h-BN). In addition to graphene, BM can also produce other 2D materials, such as h-BN. Similar to graphite, bulk h-BN also exhibits a layered structure stacked by vdW forces. h-BN exhibits higher mechanical strength and chemical stability between the basal planes due to the large difference in electronegativity between boron (2.04) and nitrogen (3.04) atoms [138]. The exfoliation efficiency of h-BN during BM is significantly influenced by its lattice structure and interlayer bonding [120,121]. For instance, h-BN requires exfoliation of 0.068 eV/atom, while graphene requires that of 0.067 eV/atom, suggesting a similar exfoliation efficiency [139]. In other words, when adjusting the BM parameters of h-BN, it is necessary to consider the minimum kinetic energy required for an efficient cleavage (see Fig. 7). Furthermore, high-energy BM with extended milling duration can introduce further crystal defects and non-equilibrium phases [114,140, 141].

As a result, wet BM comes into sight as a milder method compared to dry BM. After introducing NaOH, Lee et al. verified the production scalability for hydroxyl-functionalized BN nanoplatelets (OH-BNNPs) by combining mechanical exfoliation with chemical peeling [145]. Huang et al. explored the exfoliation of h-BN into BNNS with a wet BM method in hydroxyethyl cellulose solution as shown in Fig. 8 [95]. The viscous solution acts as an intercalator and a protective agent during the milling process, which effectively prevents reaggregation and enhances dispersion [95]. After the observed optimal milling time of around 10 h, Deepika et al. concluded smaller balls (0.1–0.2 mm in diameter) and higher speeds (800 rpm) in wet BM provide more effective exfoliation while maintaining uniformity. They further demonstrated an efficient reduction in sizes due to the enhanced interactions between smaller balls and materials, driven by sufficient impact energy and shear forces at higher speed (see Fig. 9) [146]. In other words, the optimization of milling time, rpm, and ball sizes are critical parameters influencing the overall BM efficiency and quality both in dry and wet BM.

3.1.3. Liquid phase exfoliation

Since the successful LPE of graphite, LPE has become a cornerstone method for the scalable and versatile preparation of 2D materials [20, 147], expanding their application range from materials science to

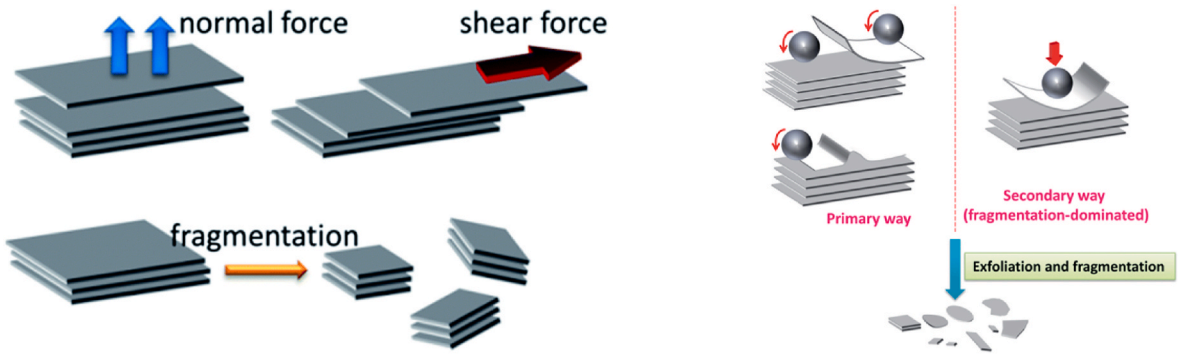

Fig. 4. Two kinds of mechanical routes for exfoliating graphite into graphene flakes and comparison alongside an auxiliary fragmentation process [103].

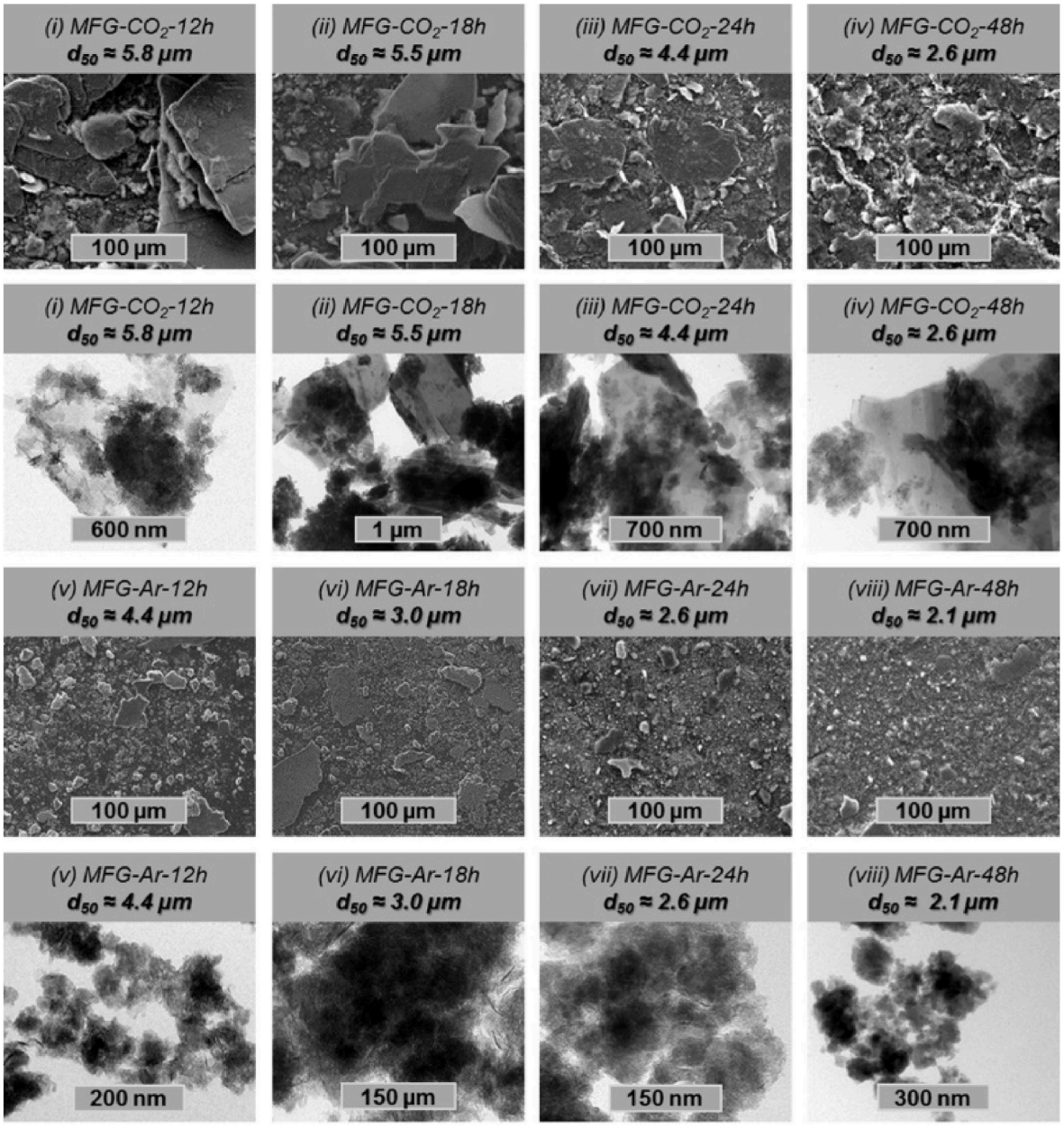

Fig. 5. The Impact of ball-milling time on the morphological characteristics of Mechanochemically Functionalized Graphene (MFG)-CO_2 (first and second row) and MFG-Ar (third and fourth row), as observed through Scanning Electron Microscopy (SEM) (first and third row) and Transmission Electron Microscopy (TEM) (second and fourth row) analysis [94].

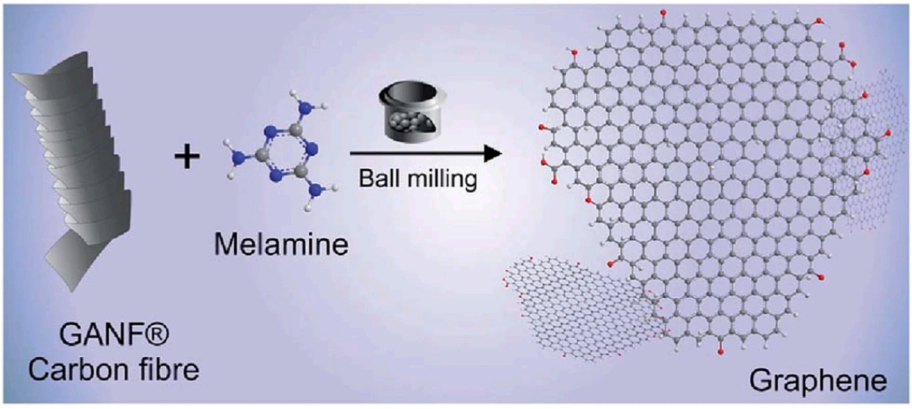

Fig. 6. Schematic of the wet ball milling process implemented for graphene monolayer exfoliation applying melamine as an intercalating agent to separate graphite layers [106].

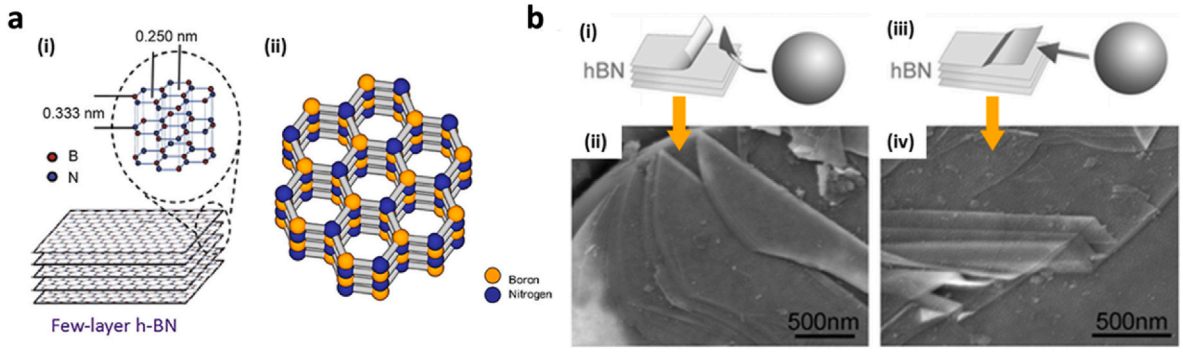

Fig. 7. (a) Characterization of few-layer h-BN nanosheets: (i) depicts the structural composition of the few-layer h-BN nanosheets exhibiting their ultra-thin morphology; (ii) presents the lattice structure of the few-layer h-BN, featuring AAA stacking configuration in which boron and nitrogen atoms are alternately positioned in successive layers, highlighting the precise atomic arrangement within these nanosheets [142,143]. (b) Illustrates the two intermediate stages of cleavage during wet BM: (i and ii) Sketch and SEM image represent the nanosheets peeling off from the edge of an h-BN particle, (iii and iv) The sketch and SEM image represent the nanosheets peeling off from the top surface of an h-BN particle [140,144].

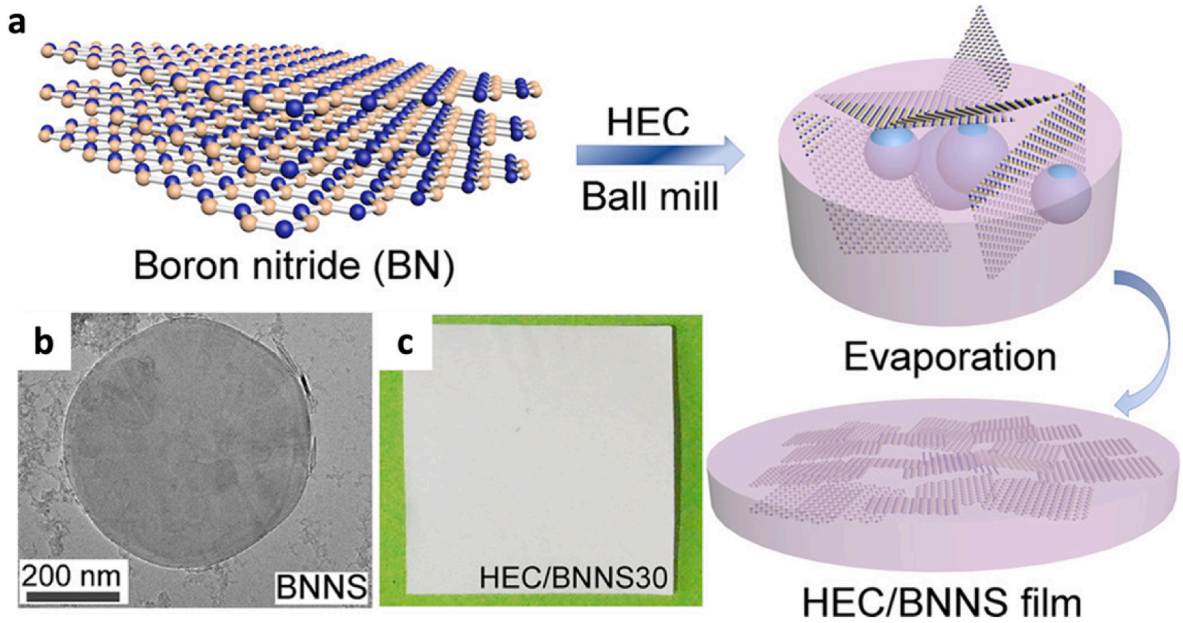

Fig. 8. (a) Schematic demonstration for the fabrication of Boron Nitride NanoSheets (BNNS) and hydroxyethyl cellulose/BNNS composites with ball milling process. (b) TEM of the boron BNNS. (c) Optical images of the hydroxyethyl cellulose/BNNS30 film (30 wt% BNNS+5 wt% hydroxyethyl cellulose) [95].

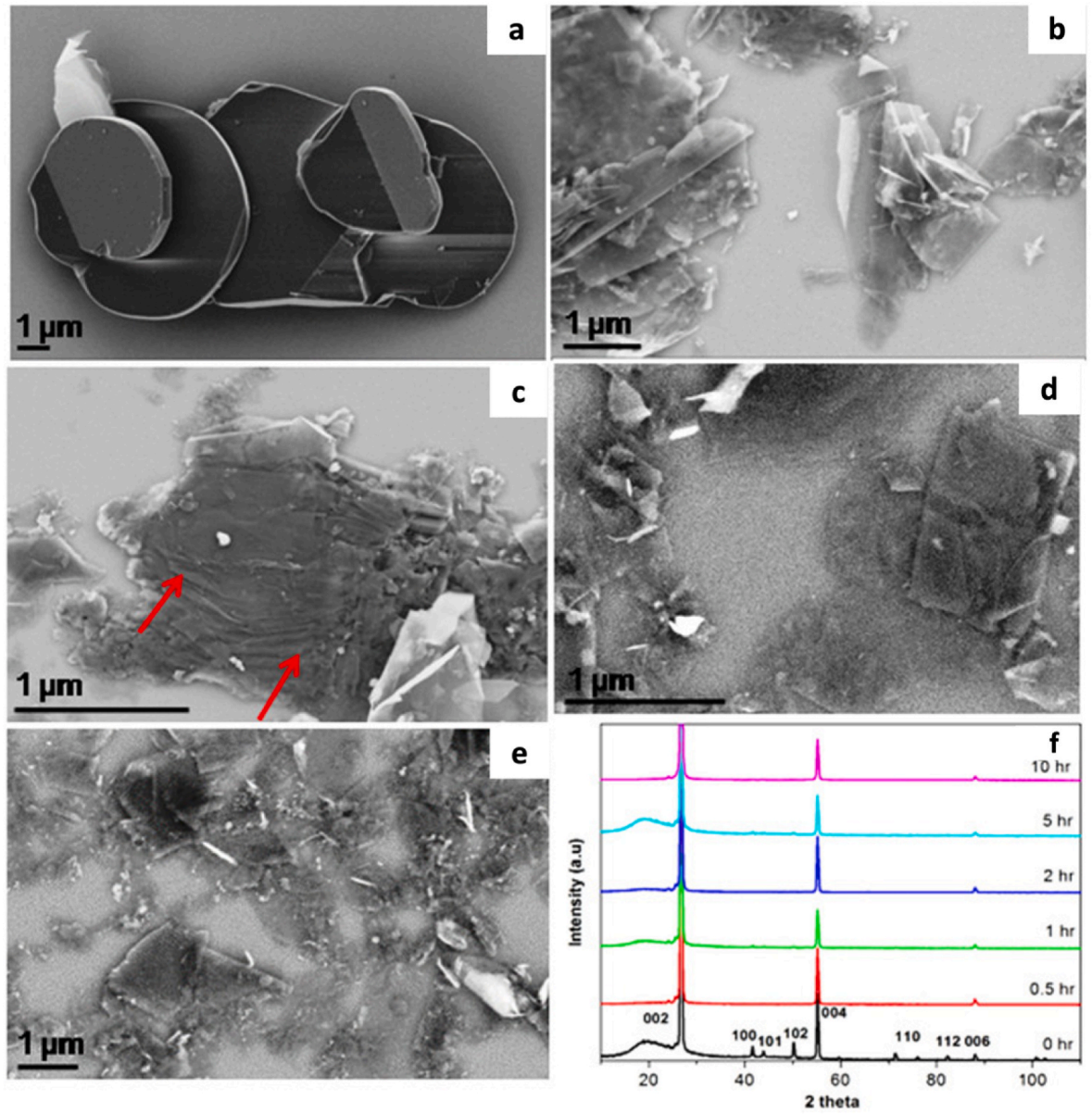

Fig. 9. SEM images of the (a) starting h-BN particles (PT110, Momentive), (b, c) partially exfoliated h-BN particles after 2 h milling, (d) more exfoliated particles after 5 h milling, (e) completely exfoliated particles after 10 h milling, and (f) normalized XRD spectra throughout various stages of ball milling; the initial h-BN particles and the sheets were ball milled for different duration without centrifugation [146].

biomedical and energy field. This technique can be applied to a wide variety of layered materials, primarily for vdW crystals, such as graphite, h-BN, and TMDs (Fig. 10). LPE technique offers the strong possibility that can harness the properties of 2D materials providing the controllability over the thickness and size of exfoliated layers with high quality. These characteristics of LPE can enable the realization of the exceptional thermal conductivity of e.g., graphene up to 5000 W/mK exceeding the conductivity of its bulk counterpart. In addition, LPE enhances the processability of 2D materials with the dispersion in a solvent (2D ink), making the production of solution-processed 2D materials possible [148–150].

In general, LPE techniques for the exfoliation of layered materials to 2D nanosheets involve i) ion intercalation, ii) ion exchange and iii) sonication/shearing assisted exfoliation, peeling thin layers from the bulk crystals (Fig. 11) [152]. Intercalation is the insertion of ions, typically lithium ions, into graphite crystals to facilitate the removal of graphene layers. However, ion intercalation can significantly affect the performance of 2D materials. Extensive research has explored the use of various ions, including alkali metals, magnesium, zinc, and ammonium ions for intercalation. Among these, lithium-ion intercalation appears to be the most effective, despite notable challenges such as the flammability associated with lithium-ion sources, posing safety hazards [124].

The sonication assisted exfoliation process involves three critical steps: a) dispersing the crystals in a solvent (such as organic solvents like N-Methyl-2-pyrrolidone; NMP or Dimethylformamide; DMF, solvent blends like water/ethanol, or hydrophilic polymers with preferred solvents), b) applying ultrasound or shearing with precise control, and c) separating the final product through centrifugation to remove residuals. During sonication assisted LPE, factors such as the type and number of dispersants or surfactants, as well as the centrifugation speed and duration, play pivotal roles in determining the quality of final products. Among three LPE methods, we further discuss the iii) ultrasonication process for 2D material productions due to its scalability and effective exfoliation.

The ultrasonication process is based on the preparation of cavitation bubbles from the ultrasonic waves. Here, cavitation indicates the rapid

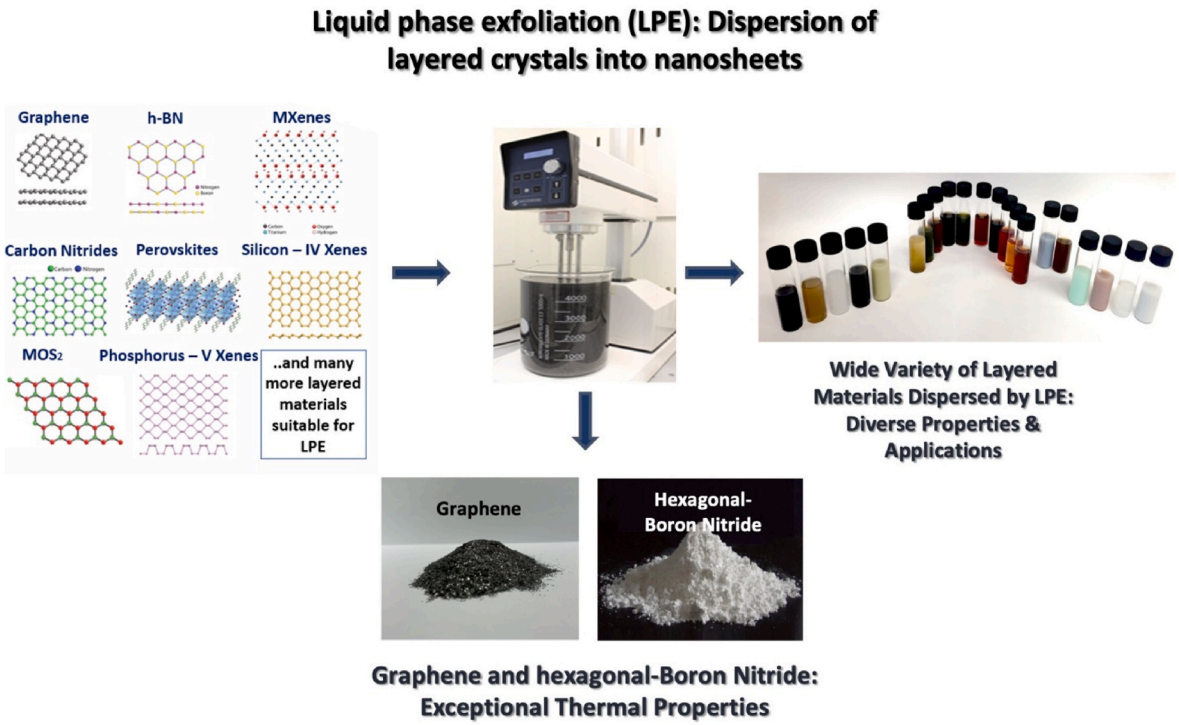

Fig. 10. A wide variety of 2D materials that can be prepared by liquid phase exfoliation. Layered materials bonded by van der Waals (vdW) interactions can be exfoliated using this method, including graphene and h-BN powders [151].

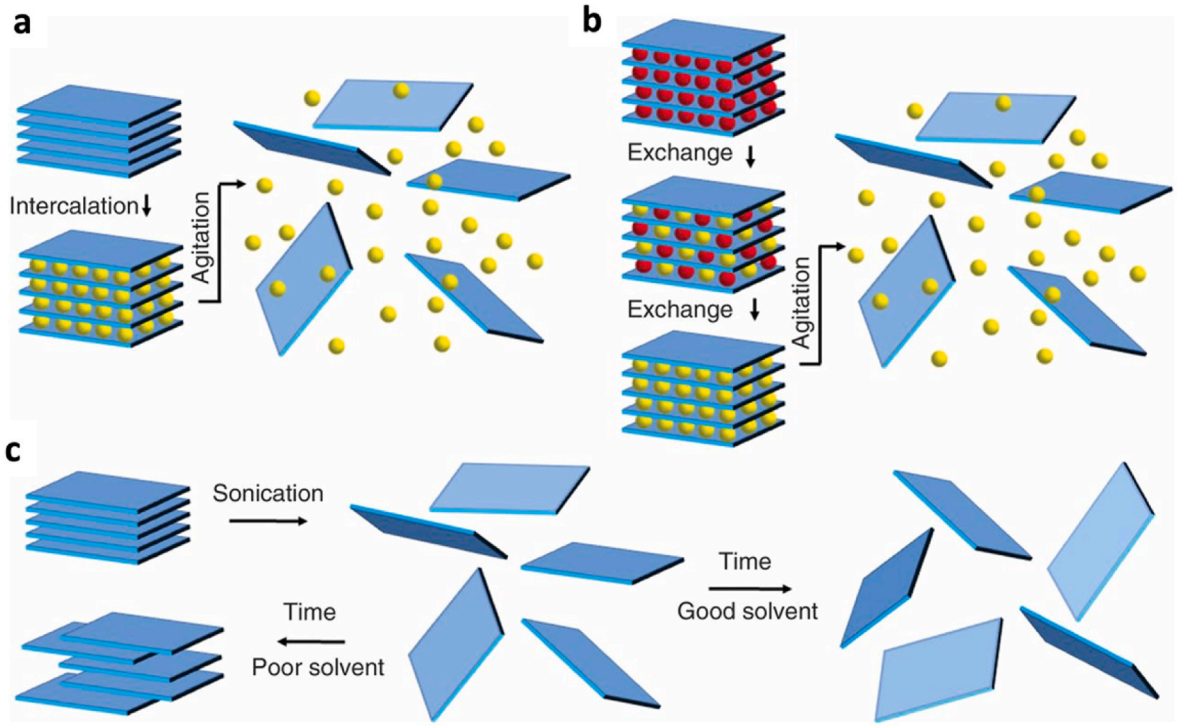

Fig. 11. The main liquid exfoliation mechanisms. a) ion intercalation, where ions inserted between layers swell the crystal and, agitation (shear, ultrasonication, thermal etc) separates the them into an exfoliated dispersion; b) ion exchange, where compounds change the surface charge and these ions are exchanged by larger ones, leading to exfoliation through agitation; c) sonication assisted exfoliation, where sonication in a solvent results in an exfoliation and nanosheet formation – the good solvents with appropriate surface energy provide efficient exfoliations, while the bad solvents cause reaggregation and sedimentation [124].

expansion and collision of micro-sized bubbles or voids due to pressure fluctuations, which will exfoliate the bulk crystals [153,154]. Ultrasonication can take place either using ultrasonic probe or ultrasonic bath, or a combination. These techniques use ultrasonic waves, but significant differences exist in their structure, operational mechanism, and efficiency as illustrated in Fig. 12.

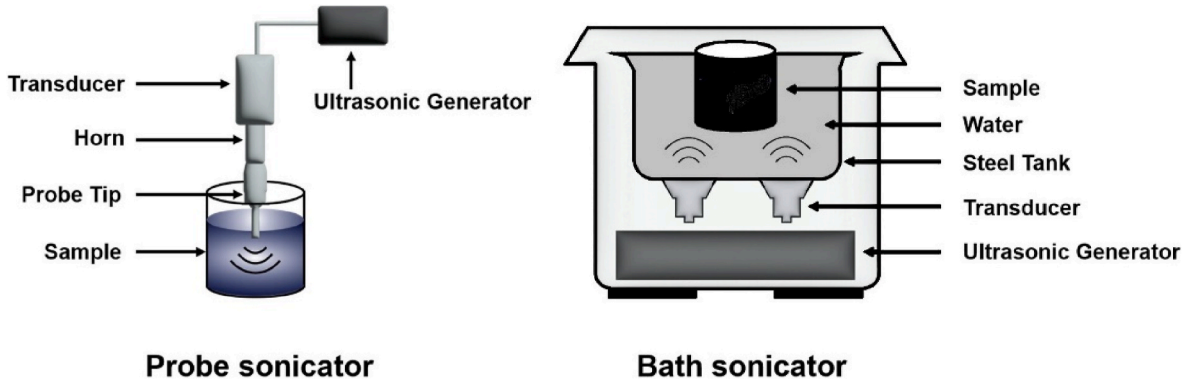

Fig. 12. Probe and bath sonicator as the two main tools for the sonication/shearing liquid exfoliation [155].

Table 7
Sonication/shearing-assisted LPE: Mechanisms, advantages, disadvantages, and parameter optimizations [20,103,155–160].

Mechanisms	Advantages	Disadvantages	Parameter optimizations	Potential improvements
• Sonication-induced cavitation and shearing are the dominant mechanisms • Careful selection of liquid is required to match the intermolecular interactions between 2D materials and solvents by adjusting the surface energy	• Low-cost production of high-quality 2D materials (e.g., a high fraction of monolayer up to 28 %) • Solution-based processing offers advantages for specific applications (e.g., 2D inks for electronics or energy storage systems) • Better controllability over the size and thickness of 2D materials compared to BM	• The low scalability of 2D materials is the main drawback (e.g., Graphene concentration of 0.1–1 mg/mL) •Complex processes require centrifugation and surfactant removal as post-processing • Reaggregation and low reproducibility due to a limited number of controllable parameters (e.g., power, frequency, and duration) • Potential environmental risks related to the water contamination by using organic solvents, surfactants, and polymer stabilizers	Power: • 60 % of the total power (100–300W) for the probe sonicator • Power-to-tank capacity of 10–20 W/L for bath sonicator Frequency: • High frequency (e.g., >80 kHz) produces smaller cavitation bubbles and results in high quality 2D materials with large lateral sizes • Low frequency (e.g., <20 kHz) generates larger cavitation bubbles, providing higher exfoliation efficiency Duration: • Typically 5–7 h for probe sonication • 10–20 h for bath sonicator • Longer sonication results in higher yield (e.g., graphene concentration of 10 mg/mL by 100 h of sonication) but accompanies structural damages in 2D layers Starting concentration: • High concentration (e.g. 0.4 mg/mL) leads to low yield but larger flake sizes • Low concentration (e.g., 0.08 mg/mL) results in higher yield but smaller lateral sizes of flakes Centrifugal speed: • High speed (e.g. > 6000 rpm) leads to low yield but thinner 2D layers • Low speed (at 0–1500 rpm) results in a high yield but thicker 2D layers	• Careful optimization of process parameters, including the selection of solvent, polymer surfactant, power, frequency, etc. • Application of other liquid-based exfoliation techniques such as electrochemical exfoliation to enhance the yield • Recycling of solvents to improve the yield • Gradual centrifugation for size-selective separation of 2D materials

For example, the time duration for probe sonication takes 5–7 h with power ranging from 100 to 300 W, while bath sonication may last up to 12 h with a power-to-tank capacity of 10–20 W/L. For similar volumes of 50–100 mL, starting with concentrations of 20–50 mg/mL, the probe sonicator yields higher graphene concentrations (2 mg/mL after 6 h) compared to the bath sonicator (0.6 mg/mL after 100 h), although it produces smaller sheets. Extended sonication (up to 500 h) can increase yield but also results in smaller sheets due to the overloaded ultrasonic energy. Conversely, shorter sonication reduces costs but may require additional surfactant removal. Therefore, the proper selection of sonicators and processing are crucial to obtain high-quality 2D layers with desired yield and thickness. Key observations for 2D material productions using sonication/shearing liquid exfoliation are provided in Table 7.

3.2. *Preparation of 2DMMC feedstock powders*

3.2.1. *Via ball milling*

2DMMCs are engineered by integrating 2D reinforcing phases into pure metal or alloy powders. This combination aims to capitalize on the unique advantages of both metals and reinforcements by compensating for the shortcomings of a single component [11,161]. Various 2DMMC

Table 8
Examples of techniques for producing 2DMMC. powders [162–165].

	Working Scheme	Advantages	Disadvantages
Molecular mixing	Fine particles of multiple materials are mixed at a molecular level for uniform distribution throughout the composite matrix and are commonly involved with chemical synthesis.	Uniform dispersion of molecular reinforcement	Scale Limitations
		Enhanced interfaces and improved properties	Technical complexity and specific chemical expertise required
		Better material compatibility	Challenging in maintaining process consistency
		More efficient material usage	Potentially time and cost consuming
Electroless plating	A chemical reduction process is supported by suitable catalysts, which initiate the plating on surfaces and generate deposition without the use of electric current.	Homogeneous coating on complex shapes	Involves hazardous chemicals (eg., sodium hypophosphite, formaldehyde, cyanides, acidic and alkaline solvents)
		Precise process control	Limitation to conductive materials
		Enhanced bonding (thus beneficial for electrical and thermal conductivity)	Thickness limitation of plated layers
		Higher quality coatings (enhanced wear resistance and smoother surface finish)	Proper preprocessing of substrates required
Vacuum infiltration	The molten matrix material is drawn into the pores of the porous preform in a heated vacuum chamber by removing air and applying pressure.	Able to fabricate denser composites	Specific equipment dependency (vacuum chambers)
		Suitable for filling the complex preform molds	Additional attention is required to process parameters (temperature and pressure etc.)
		Possess the potential to expand the production scale	Difficult to achieve uniform distribution of nanoparticle reinforcements
		More flexible control of raw materials and processes	Higher energy consumption affects sustainability and lower cost-effectiveness

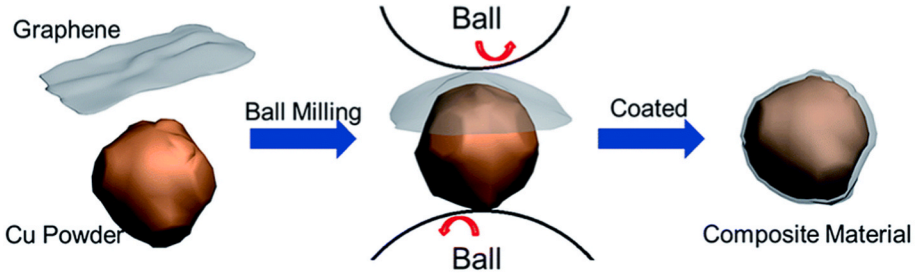

Fig. 13. Schematic diagram of the process for fabricating metal/high-quality graphene composites through high-energy ball milling [168].

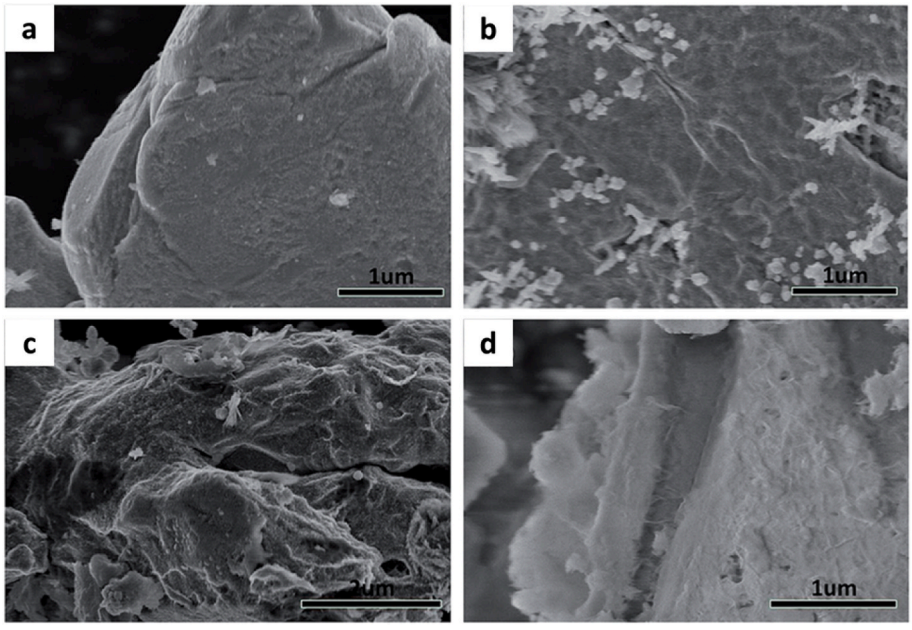

Fig. 14. SEM micrographs showing the morphology of copper powder coated with high-quality graphene throughout the ball milling process. (a) Initial copper powder before milling; (b and c) the surfaces of copper powder after being coated with high quality graphene through milling; (d) the edge of the copper powder coated with high quality graphene after milling [168].

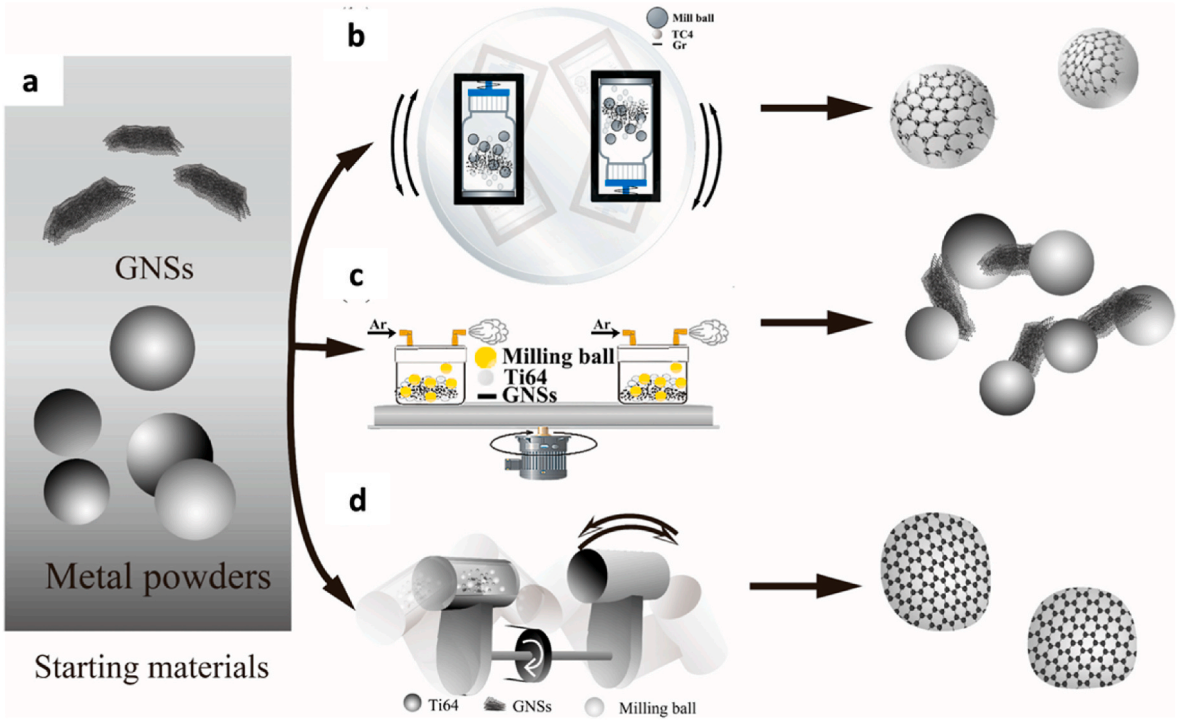

Fig. 15. (a) Schematic of the Ti64-based 2DMMC fabrication process. Ti64 spherical powders (15–300 μm) and aluminum (45 μm) are used alongside graphene nanosheets (3–10 nm thick, 5–10 μm diameter) as starting materials. Where the graphene nanosheets are dispersed into metal matrix powders to form composites, illustrated with three different following milling methods: (b) rocking milling, (c) planetary BM, (d) 3D BM [167].

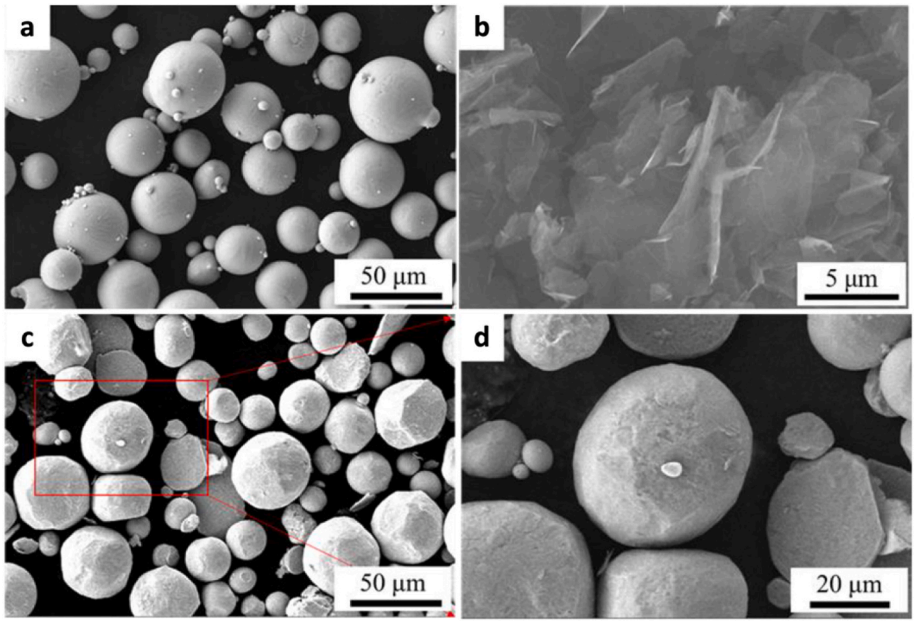

Fig. 16. SEM micrographs of (a) Initial morphology of Ti-6Al-4V powder before milling; (b) graphene morphology; (c and d) morphology of Ti-6Al-4V+0.3 wt% graphene powder after milling [170].

powders have different characteristics, leading to diverse properties depending on the composition and fabrication processes. Molecular mixing, electroless plating, and vacuum infiltration are typical examples of producing 2DMMC feedstock powders, as listed in Table 8.

Compared to the synthesis techniques listed in Table 8, BM emerges as the most effective and environmentally friendly method capable of 2DMMC mass productions [87]. BM can also be used to produce 2DMMC powders by mixing and grinding processes between 2D materials and metal powders. During BM, mechanical forces promote graphene exfoliation and increase the surface roughness of metal powders. Interfacial bonding between graphene and metal particles is depending on vdW interaction, which can be enhanced by repetitive cold welding [166]. For example, graphene and h-BN can be incorporated with various metal powders to improve the thermal and mechanical properties of feedstock powders as shown in Fig. 13 [11].

Among several metal-matrix candidates, ductile copper and

Fig. 17. Enhancing the copper powder with GNP suspension [49].

aluminum alloys are easier to deform during the forceful impact and squeezing process of the BM [86,140,167]. Hence, as shown in Fig. 14, while graphene is well coated on the copper powder, the metal surface and morphology become more irregular after milling at 1700 rpm for 4 h [168]. Similarly, when graphene is replaced with wet ball-milled BNNSs, most of the dendritic copper powders are flattened after milling for only 30 min at 200 rpm, although the BNNSs are homogeneously distributed on the metal surface [169].

In addition to ductile materials, Ti-6Al-4V alloy is also a common candidate for 2DMMC. Many studies have attempted to pair titanium alloy with graphene to enhance properties, as the thermally induced TiC interlayer improves overall mechanical properties [167,170,171]. For all milling methods illustrated in Fig. 15, the defect density on GNS increases with higher milling energy. Meanwhile, the effect of the metal powder size becomes more notable as the milling energy increases [167]. Compared to the copper/graphene powders of Fig. 14, graphene-reinforced Ti-6Al-4V powders remain spherical after milling for 3 h at 240 rpm, see Fig. 16 [170]. Overall, BM processes need to

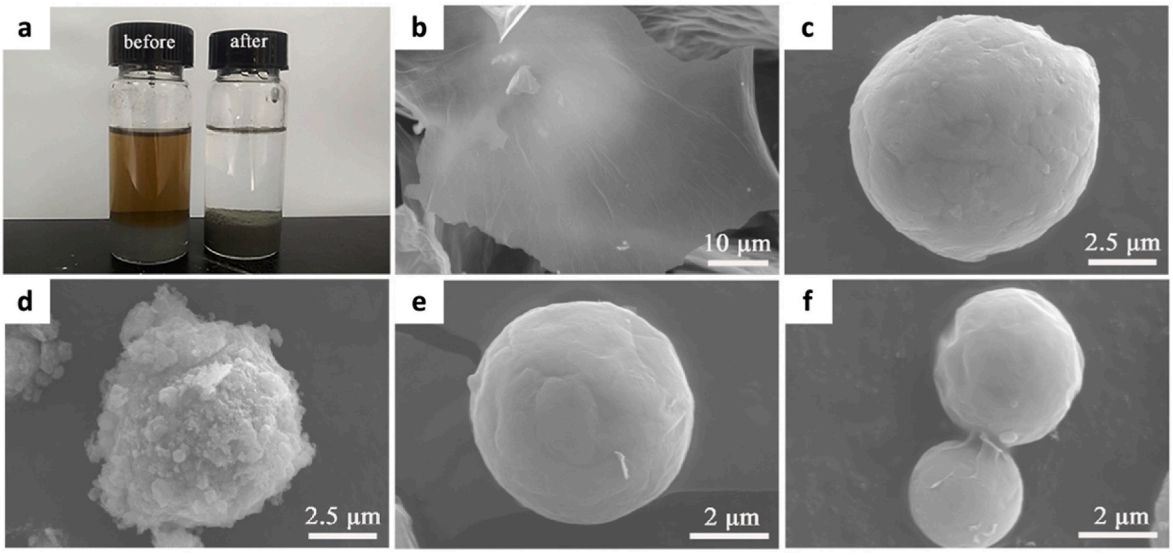

Fig. 18. Enhancing the aluminum powder with graphene oxide dispersion [48].

Table 9
Comparison of Ball Milling (BM) and Liquid Phase Exfoliation (LPE) in terms of process feasibility, scalability, and environmental impact.

	Ball Milling (BM)	Liquid Phase Exfoliation (LPE)	References
Process requirements (Equipment)	Simple equipment (planetary or rotary ball mills): A single motor-driven rotating chamber using jars filled with grinding balls	Complex equipment (combination of ultrasonication and centrifugation process)	[7,89,97, 101,109, 173,174]
2D materials yield per batch	Feasibly achieves high yield per milling cycle, especially with an optimized ball-to-material ratio (e.g., 65–85 % of yields and 20–40 mg/h productions)	Moderate to low yield, requiring multiple steps (e.g., 2–37 % of yields and 0.02–2 mg/h productions)	[7,131,146, 173–175]
Process Scalability	Suitable for large-scale, industrial production with easy parameter control	Moderate scalability, requiring large solvents and high costs	[7,88,89, 101,110, 176]
Control over the final product	Good tuneability with proper parameter control, but may introduce defects	High-quality sheet production, but requires difficult solvent recycling and special handling.	[7,88,89,97, 101,110, 176]
Material recyclability	Low waste production if dry milling is used	Difficult solvent recycling, requiring special handling	[86,97,100, 148, 176–181]
Energy consumption	Moderate to high depends on milling parameters (e.g., 20–50 J/g)	High due to prolonged ultrasonication or solvent recycling (e.g., 50–100 J/g)	[88,97,110, 148, 175–181]
Environmental impact	Moderate, depends on the use of process control agents (PCA) and waste generation	High due to significant solvent consumption	[88,97,105, 108,110, 148, 176–181]

consider the specific properties of metal matrices and their associated costs [11,172]. From a comprehensive assessment, BM unequivocally represents the premier technology for the scalable production of 2DMMC feedstock powders. However, comprehensive studies on how individual BM parameters affect the uniform dispersion of 2D layers in the metal matrix are needed for optimal processing.

3.2.2. *Liquid phase exfoliation principles*

The processability of LPE that offers the preparation of 2D materials makes it also a viable option for the actual preparation of 2DMMCs using sonication/shear methods. For instance, Nazeer et al. demonstrated GNPs are first exfoliated using LPE to create a suspension. This suspension is then mixed with copper powder through vortex mixing and vacuum infiltration to form GNP/Cu paper, resulting in notable improvements in flexural strength. At 0.6 vol% GO, a 22 % increase in flexural strength (127 MPa) was observed compared to pure sintered Cu (Fig. 17) [49].

Similarly, Zhang et al. demonstrated significant enhancements in various mechanical and thermal properties using a procedure akin to LPE with graphene oxide (GO). With the 0.3 wt% graphene addition to pure aluminum, they achieved remarkable improvements: a 15.4 % increase in thermal conductivity, 9.1 % in specific heat capacity, 21.1 % in hardness, and 25.6 % in compressive strength (Fig. 18). These results underscore the versatility and effectiveness of LPE methods in enhancing the properties of 2DMMCs, highlighting their potential for production of 2DMMC powder feedstocks.

In summary, BM and LPE, the two main methods discussed in this section have distinct advantages. BM offers scalability and cost-effectiveness for large-scale production of 2D materials and 2DMMC feedstock powders. However, challenges with size controllability and potential damage during the BM process necessitate a thorough optimization of milling parameters, depending on the selection of 2D material and metal matrices. In comparison, LPE provides better control over size and thickness and can produce higher quality 2D layers than BM. Nevertheless, the complexity of the process, residual solvents, and significantly lower yield compared to BM remain challenges for large-scale production. Therefore, BM and LPE techniques can be applied complementarily for specific 3D consolidation techniques or targeted heat transfer applications. Key characteristics of BM and LPE processes

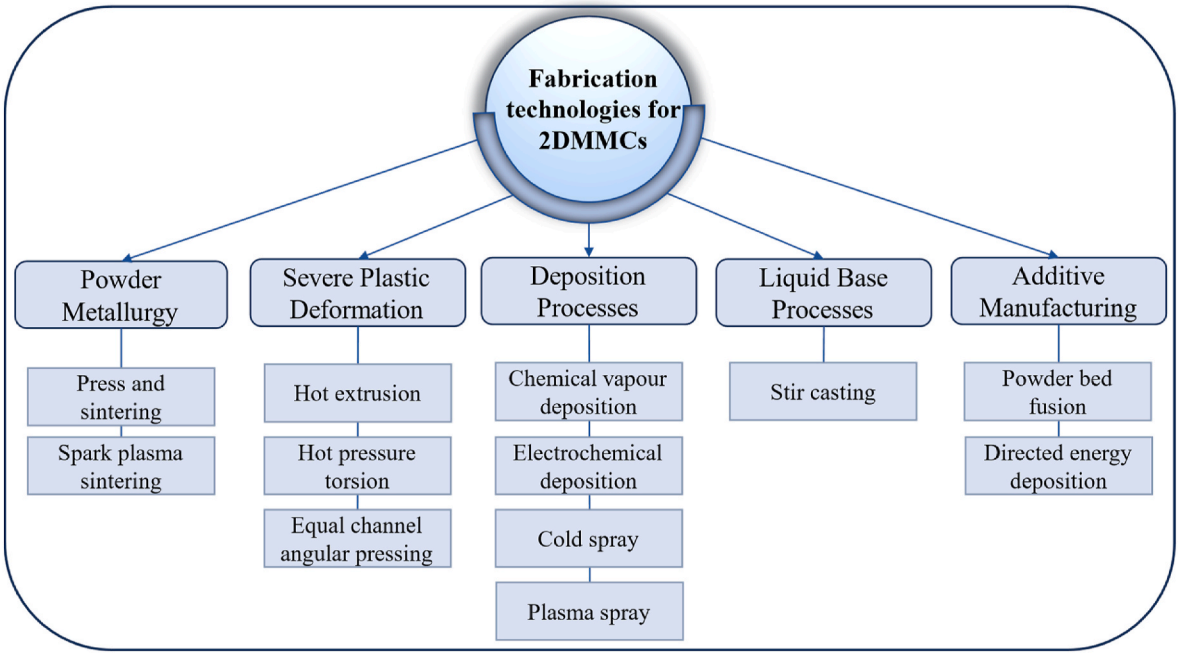

Fig. 19. Summary of fabrication methods for 3D consolidation of 2DMMCs.

are compared and summarized in Table 9.

4. Fabrication methods for consolidation of 3D parts from 2DMMC feedstocks

The properties of 2DMMC parts are significantly influenced by the utilized fabrication process. A key parameter that is affected by the manufacturing route is the distribution of 2D materials within the metal matrix. A uniform dispersion of the reinforcing material ensures effective load-bearing capability, influencing not only the overall strength but also thermal and electrical conductivities. Therefore, an overview of the advantages and shortcomings of the various fabrication techniques is essential in understanding and tailoring the performance of 2DMMC parts.

This section discusses various fabrication methods for the consolidation of 3D parts from 2DMMC feedstocks. The fabrication methods are classified into five main groups: i) Powder Metallurgy (PM), ii) Severe Plastic Deformation (SPD), iii) Deposition Processes (DP), iv) Liquid Base Processes (LBP), and v) Additive Manufacturing (AM), as represented in Fig. 19. The characteristics, advantages and challenges associated with these fabrication methods are summarized.

4.1. Powder metallurgy

PM is a conventional two-step solid-state fabrication method. In the first step metal or metal alloy powder is combined with reinforcing particles (2D materials) to create a uniform powder mixture [182]. The mixing can be implemented through different methods including BM [183], wet mixing [184], vacuum infiltration [49,185], molecular level mixing [162,186] or a combination of them [187]. The second step involves pressing and sintering the mixed feedstock into the final geometry. PM is the most common technique for the development of 2DMMC parts thanks to its exceptional versatility. This section explores the method of press and sintering, and Spark Plasma Sintering (SPS).

4.1.1. Press and sintering

Press and sintering enable powder particles' fusion without melting [182]. Compaction involves pressing metal powders into a desired shape using a die and punch. The goal is to achieve a compact part, which is a pressed, but not fully dense structure. Subsequently, the part undergoes sintering [182] to promote atomic diffusion and particle rearrangement, facilitating the creation of a dense and cohesive structure. Various sintering techniques, such as conventional [188] and microwave [189] methods have been utilized for 2DMMC parts. The incorporation of 2D materials distinctly influences the density variation with sintering time and temperature [120,190]. This arises from the propensity of 2D materials to agglomerate into the matrix [111,190,191]. Microwave sintering induces rapid heating [189] and produces finer, more uniform microstructures than sintering.

Simultaneous application of heating and pressing in hot pressing [111,188,192,193] and Hot Isostatic Pressing (HIP) [194,195] facilitates effective consolidation in 2DMMC part fabrication. However, the slow heating phase of hot pressing may introduce contamination and lead to sub-optimal interfacial bonding [11]. Several factors, including powder size and morphology, 2D phase content, presence of impurities, and sintering parameters (e.g., temperature, time, and gas atmosphere) significantly affect the densification of the final composite [111,192]. Sabouri et al. [196] have recommended incorporating graphene at 0.5 wt% in the aluminium matrix for enhancing thermal conductivity. Surpassing 0.5 wt% was reported to lead to diminished thermal conductivity [196]. Similarly, Ghosh et al. [120] noticed a reduction in mechanical and tribological properties when the h-BN content in aluminium matrix exceeds 3 wt%. This underscores the need for determining the 2D material content to optimize the properties of 2DMMC parts.

4.1.2. Spark plasma sintering

SPS, also known as field assisted sintering, is a rapid technique for consolidating metals, ceramics, and composites powders [197,198]. The process involves passing a low-voltage, pulsed Direct Current (DC) through the material, placed in a graphite-lined die, while applying uniaxial pressure for complex net-shaping of components with minimal grain growth [199–201]. The starting powders are loaded into the graphite-lined die to prevent sticking and interaction with the die walls [202]. The interaction between the die and sample in SPS enhances material purity [203] and affects the microstructure and mechanical properties by using sintering aids like $MoSi_2$ or WC [204,205].

SPS has been successfully used to produce 2DMMC parts [206]. Graphene-aluminium [207] and graphene-copper [208] show enhanced mechanical properties and thermal and electrical conductivities. As demonstrated for graphene reinforced ZrB_2, excessive carbon can adversely affect composite properties, suggesting an optimal concentration range and specific sintering conditions [209–211].

4.2. Severe plastic deformation

SPD techniques encompass processes that subject the metallic materials to substantial plastic strain, thereby significantly altering their microstructural and mechanical properties. Various SPD techniques have been employed for the fabrication of 2DMMC parts, including Equal Channel Angular Pressing (ECAP) [212–215], High Pressure Torsion (HPT) [216–219] and Hot Extrusion (HE) [220–222]. These processes exhibit versatility in terms of implementation across a wide temperature range, encompassing moderate (e.g., ECAP) to high temperatures (e.g., HE). The induced grain refinement enhances the mechanical strength of the matrix material. SPD is employed for both processing and post-processing i.e., i) consolidation of 2DMMC parts [214–218,223,224], and ii) enhancing 2DMMC properties through deformation [219,221]. SPD has been specifically implemented as a post-processing method on 2DMMC parts with magnesium [220], aluminium [212–216,221,222,225] and copper [217,226] matrices. SPD is commonly carried out as post-treatment for 2DMMC parts after PM [212,221] or stir casting [220]. The flow produced by shear deformation inside the matrix can highly promote the dispersion of 2D flakes. Moreover, large plastic deformation can reduce the number of 2D material layers by bending, twisting, and possibly separating them. The combined effect of thinning the layers and reducing flake aggregation enhances overall performance of 2DMMC parts [225,227].

4.2.1. Equal channel angular pressing

In ECAP the metal base composite powder or billet [214] undergoes intense plastic deformation while being pressed through two intersecting channels. ECAP is the most rudimentary and efficient room temperature SPD technique for bulk materials characterized by nanostructured grains [227]. This method avoids agglomeration formation in fine (nano-sized) particles [228]. ECAP can induce exfoliation in graphene layers, as dislocations tend to accumulate behind the carbon reinforcements [229]. The resulting shear stresses can surpass the cohesive vdW forces between graphene nanosheets, and thus may lead to a significant reduction in the number of graphene layers [214]. This effect is particularly pronounced when graphene flakes are aligned parallel to the direction of the shear stress [214].

4.2.2. Hot extrusion

HE is widely employed for shaping metals or alloys through the application of high temperatures. This process provides a unique 3D state of stress on the material, enhancing plasticity and ensuring high formability [225]. During preheating, the material attains a temperature above its recrystallization point while remaining below the melting point. Existing studies predominantly employ HE as a post-treatment for 2DMMC parts, enhancing mechanical properties through grain refinements [221,226]. In contrast, Du et al. [220] opted for combining

stir casting and HE for 2DMMC part fabrication. The results indicated that the distributed GNPs in a magnesium matrix formed beneficial networks that enhanced both strength and thermal conductivity.

4.2.3. High pressure torsion (HPT)

HPT is commonly employed to induce grain refinement in metallic materials through a combination of high pressure and torsional (twisting) deformation. HPT has been investigated for other purposes including consolidation of nanocomposite powders for bulk material production and eliminating the reliance on conventional sintering. The efficient processing of 2DMMC parts through HPT occurs at significantly lower temperatures compared to sintering. Moreover, thanks to being a low temperature process, it mitigates oxidation pick-up and the formation of secondary phases [216,218]. HPT is a potential alternative to liquid casting, although it is constrained by the wettability challenge between 2D materials and metal matrix [218].

4.3. Deposition process (DP)

Deposition of 2DMMC coatings on general parts can be realized in several ways. The most relevant methods are sketched here.

4.3.1. Electrochemical deposition

Electrochemical deposition is a versatile and cost-effective technique for the fabrication of 2DMMC coatings [230–232]. In this process, a conductive substrate serves as an electrode (cathode), immersed in an electrolyte solution containing metal ions and dispersed 2D phases. The application of electric current prompts the reduction of metal ions onto the substrate surface concurrently incorporating the 2D phases. The parameters, including current density [233,234], bath composition [235,236], and deposition temperature [237] are finely tuned to achieve optimal control over the composite properties [231,234,235]. Both DC and Pulsed Current (PC) methods are employed for electrodeposition of 2DMMC coatings. PC may achieve a very uniform surface, effectively controlling the microstructure and chemical composition of the deposits [232–234]. Continuous mechanical stirring during electrochemical deposition [230,238–240] is conducted to ensure uniform dispersion of the 2D material [230,238–240]. Furthermore, for MMCs reinforced with graphene, cluster formation due to hydrophobicity can be addressed by using hydrophilic GO as source material in the electrolyte solution [231]. Sreekumar et al. [232] reviewed the electrodeposition process of 2DMMC coatings onto a nickel matrix yielding nickel nano composite coatings. This method has numerous benefits, such as the uniformity of coatings, easy adaptation to complex geometries, and customization of the composite.

4.3.2. Chemical vapour deposition

CVD is used for depositing monolayers of 2D materials onto metal surfaces using vapour species. A solid layer of coating is achieved through a chemical reaction on the metal substrate. In CVD, the substrate is heated to a specific temperature to reduce surface oxidation and increase the continuity and quality of the grown 2D material [241]. The CVD reactor enables precise adjustment of deposit thickness, and uniformity [242]. An overview of CVD processes including hot wall, cold wall and plasma-enhanced CVD can be found in Ref. [243] for one or more layers of graphene. It explores the issue of precursor selection and discusses the growth mechanisms and applications of graphene [243]. Similarly, Sun et al. [244] present a comprehensive summary of recent advancements in customized CVD production of 2D h-BN on various substrates, including copper, platinum, and nickel.

4.3.3. Cold spray

CS is a solid-state deposition technique for various materials, including 2DMMCs, at temperatures considerably lower than the melting temperature of the metal matrix. CS involves the deposition of powder particles accelerated to supersonic velocities onto a metallic substrate, creating thick coatings as well as additively manufactured parts [245–247]. Low operating temperatures of CS can enable the effective deposition of 2D materials that are sensitive to temperature and oxidation [248]. Powder preparation significantly affects the overall deposition efficiency and the characteristics of the CS 2DMMC deposits. Common methods for preparing 2DMMC feedstock for CS deposition include BM [24,249–252] and *in-situ* reduction techniques [253–259], such as those applied to self-lubricating h-BN encapsulated in nickel [260–263]. CS has been used to deposit copper [253,259], aluminium [254], nickel [264], and zinc [265] reinforced by h-BN or graphene.

Prasad et al. [248] delved into the CS deposition of graphene reinforced MMC parts. Limited studies have investigated the variation of process parameters for the optimization of CS for 2DMMC parts. In terms of deposit quality indexes, literature data discusses enhancing wear and corrosion resistance. Mechanical and thermal characterization is largely missing. The distinctive features of CS, i.e., its notably high deposition rate, low processing temperature, material versatility, and the ability to utilize multiple feeders to tailor material composition, suggest its considerable promise. The main potential of CS is in depositing layers of unrestricted thickness for AM of 2DMMCs [266].

4.3.4. Plasma deposition and spray

Plasma deposition allows for the direct deposition of nanostructures onto substrates from the gas phase [267,268]. Recent developments in plasma deposition techniques have showcased the production of carbon-based structures with freestanding architecture [269] on metallic surfaces [269,270], or intercalated with metallic particles [271]. Plasma deposition offers flexibility in growth rate, surface morphology, orientation, and crystal structure on various substrates by adjusting plasma discharge parameters at low temperatures.

Plasma spray (PS) involves injecting powders into a DC plasma jet, where the particles melt and accelerate toward the substrate, forming thin film coatings. Various types of PS processes have been discussed in Refs. [272,273], highlighting diagnostics of thermal plasma jets, properties of sprayed material, and applications in electronic materials [274]. Plasma computer tomography, laser-based particle shape imaging and control [275], particle motion and air entrainment [276], and their use as thermal barrier coatings [277] are topics of current research. Cold plasma systems, mainly operating at atmospheric pressure in the form of jets, produce reactive species, eliminating the need for higher temperatures. Nanomaterial synthesis, such as gold nanostructures [278,279] is effective with a DC plasma.

Recent advancements include the deposition of graphene-based coatings of metallic particulates, showcasing atmospheric pressure plasma spraying and suspension plasma spraying [280,281]. These composites exhibit improved wear resistance, absorption, and self-lubricating properties, and have potential applications in developing enhanced thermal and mechanical properties of graphene-dispersed aluminium composites [282] or by impregnating cobalt nanoparticles onto graphene using the liquid phase plasma method [283].

4.4. Liquid base process (LBP)

4.4.1. Stir casting

Stir Casting (SC), as a manufacturing technique for 2DMMC parts, includes the dispersion of 2D materials into a molten metal matrix by continuous stirring, followed by casting of the resulting mixture into the desired shape [266]. To achieve a uniform distribution of 2D materials within the metal matrix, wettability and chemical interactions between the reinforcing material and the matrix alloy [284] are crucial factors that can be influenced by the temperature and speed of stirring [285]. Preheating of the 2D materials and their progressive insertion into the molten matrix is reported to improve their dispersion [285,286].

The incorporation of 2D materials through SC can reduce the grain

Table 10
Summary of the fabrication methods used for producing 2DMMC parts, highlighting their advantages and challenges based on the properties of the 2D and matrix materials.

Fabrication method		Post processing	Matrix	Advantages	Challenges
PM	Press and sintering	Hot rolling Hot isostatic pressing Annealing Hot extrusion T6 heat treatment	Cu, Al, Ti stainless steel, Mg Ag, Ni, Fe	Used to prepare complex parts at a low cost [312] Homogeneous dispersion for low content of 2D materials [45]	Formation of void and oxidation [313] Interface bonding of 2D materials and the metal matrix needs to be further improved [312] Prone to damage graphene's intrinsic structure [45]
	SPS	Rapid heating by pulsed or direct current with simultaneously applied uniaxial force	Cu, Al, Stainless steels, refractories	Extensive selection of matrix material powders [314], rapid sintering times mitigating grain growth [315], the ability to pre-forming using dies of complex shapes [316]	Homogeneous dispersion of 2D materials in powder feedstock [314], diffusion zone in contact with the die [317], challenges associated with the stoichiometry [318]
SPD	ECAP	–	Cu, Al	Uniform dispersion of graphene particles, grain refinement [215]	Difficult to prepare large and complex geometries [312]
	HE	–	Cu, Al, Mg	Uniform distribution of 2D materials and the potential alignment of 2D materials within the matrix [319]	High energy consumption. High temperatures can form carbides at the metal-2D material interface [11]
	HPT	–	Al, Cu	Avoids sintering and high temperature deformation [217]	Relatively large agglomerates [312]
DP	Electrochemical deposition	Hot rolling, T6 heat treatment	Cu, Ni, Mg	Low energy and low cost [320]	Controlling the morphology of thin film layers is complex, hindering large-scale manufacturing [320] Prone to the formation of microcracks [321]. Needs stirring or surfactants for homogenous dispersion [266]
	PS	–	Stainless steel, Al, Ti, Au	Flexibility in growth rate, surface morphology, orientation and crystal structure. various possible precursors (solid, liquid or gas) [322]	Possible substrate overheating, porosity in coatings, limited deposition thickness in a single pass, need for substrate pre-preparation for better adhesion [323]
	CS	–	Cu, Ni, Al, Mg	Non-agglomeration and uniformly distributed 2D materials without oxidation and phase transformation [45]. No size limitations, no thermal degradation.	High-pressure CS may potentially damage the structure of 2D materials [312], presence of 2D material can reduce the deposition efficiency [259]
	CVD	Hot rolling	Cu, Ni, Ag, Steel	Good dispersion at high content of 2D material [45]	Complicated process and high cost for complex geometries [312], abnormal coarsening of matrix grains [226]
LBP	SC	Hot extrusion	Al, Mg	Large-scale manufacturing, low cost, and high rates of production [319]	Inhomogeneous distribution of reinforcement [319]. High temperature processes can damage 2D structure [266]. Contamination introduction [11]. Weak interfacial bonding between the reinforcement and the metal matrix [319]
AM	LPBF	–	Cu, Al, Ni	Notable geometrical flexibility and high product quality [324]	Occurrence of pores and inclusions due to the effect of 2D materials on laser energy absorptivity of metal powders; (laser) process parameters must be strictly tailored [312]
	DED	–	Ni, Ti, Al	Functionally graded structures [307], high controllability, capability of surface modification [306]	High fabrication temperature can cause intermetallic or carbides [311]

size within 2DMMC parts [284,287]. Lower grain size arises at higher content of 2D flakes [286], provided particles with sizes less than 1 μm are used [288]. Overall, SC stands out as a cost-effective and efficient fabrication method suitable for large-scale production [289], provided the 2D flakes can withstand the high-temperature processing [266].

4.5. Additive manufacturing

There are limited reports on the application of AM techniques for the fabrication of 2DMMC parts. Here, Laser-Powder Bed Fusion (LPBF) and DED techniques are considered and discussed as major techniques.

4.5.1. Laser-powder bed fusion

LPBF, also known as selective laser melting, constitutes most of the literature for the fabrication of 2DMMC parts using AM technologies. Thin layers of powder are evenly spread across a build plate and then selectively fused using energy provided by a laser beam. This process is repeatedly carried out layer by layer [22]. LPBF is challenged by the absorptivity of the laser energy by the powder [290]. The concentration and the distribution of 2D materials within the metal matrix can influence the absorbability of the feedstock [291,292]. Powder flowability is another key factor [293], defined by the size and morphology of the 2DMMCs' feedstock [292]. Both absorptivity and flowability are intricately linked to the composite powders' preparation method. Therefore, many of the previously mentioned methods have been employed for preparing the feedstock for LPBF processes, including mechanical mixing and BM [294–296], molecular level mixing [297], sonication stirring [26,292,298,299] and electroless deposition [300–302], all in search of a good combination of powder characteristics for LPBF.

Despite the challenges, LPBF has been successfully applied to obtain graphene reinforced composites [15,303] as well as silicon carbide reinforced magnesium [304]. The distribution of 2D materials across the molten pool results in a layered configuration along the build direction, yielding a lamellar structure, that may enhance mechanical properties [299].

Abedi et al. [290] provided a review exploring the properties of LPBF 2DMMC parts for $AlSi_{10}Mg$ reinforced with graphene. There is very limited data on the correlation between the influence of LPBF process parameters like laser power and scanning speed, hatching distance, layer thickness, and build direction on the performance of 2DMMC parts.

4.5.2. Directed energy deposition

DED is another AM process in which material, in the form of wire or

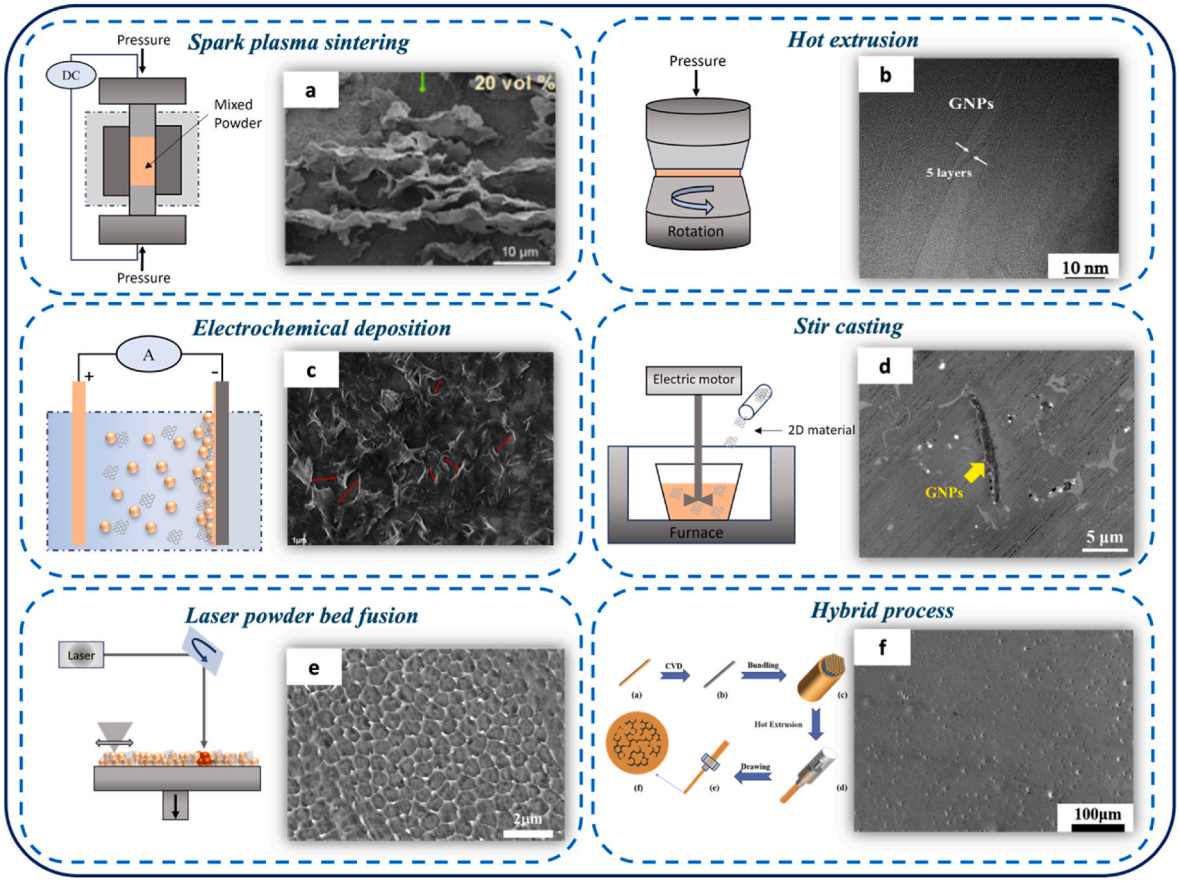

Fig. 20. The most commonly used 2DMMC coating/parts fabrication methods and their corresponding representative 2DMMC structures: (a) spark plasma sintering [49], (b) hot extrusion [325], (c) electrochemical deposition [233], (d) stir casting [326], (e) laser powder bed fusion [299], and (f) the hybrid process of chemical vapour deposition and severe plastic deformation [226].

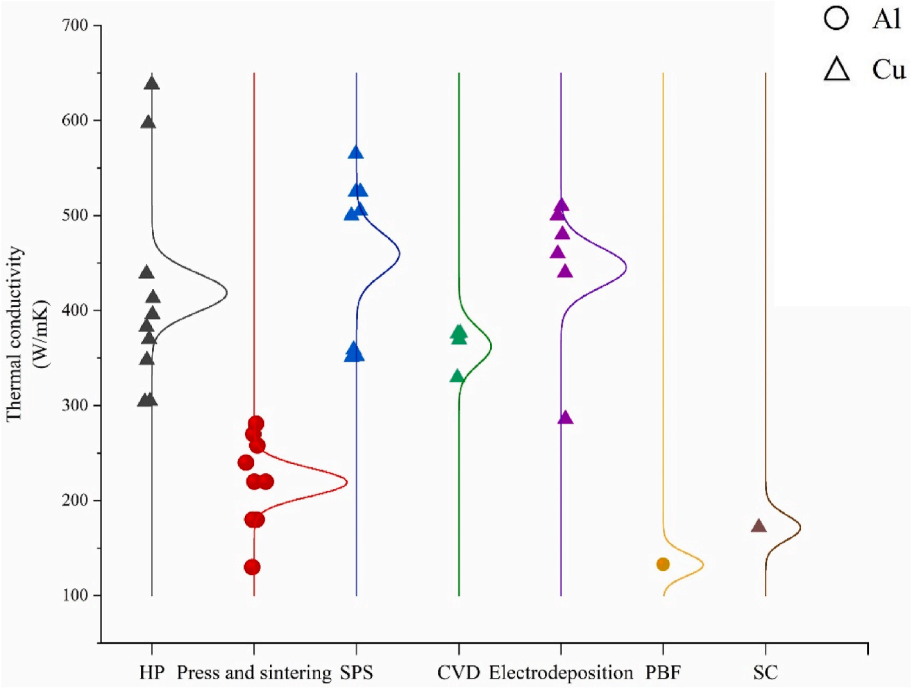

Fig. 21. Diagram of the thermal conductivity of 2DMMCs gathering the data obtained for different fabrication methods and matrixes [45,47–50,64,69,183,187,196,289,327–336], [411].

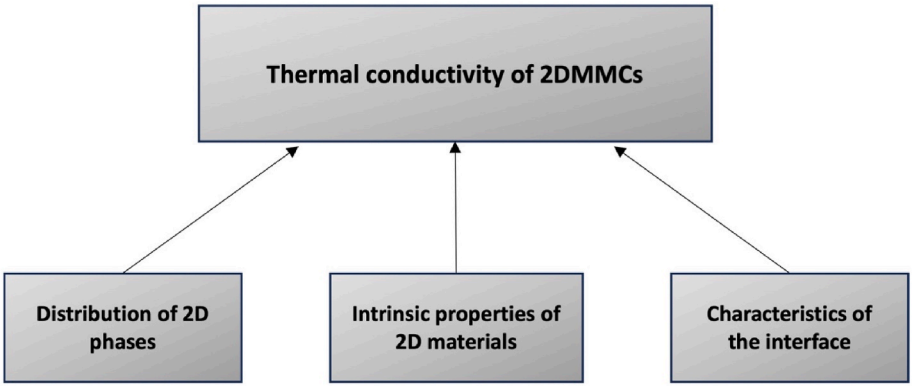

Fig. 22. Dominant factors governing the thermal conductivity of 2DMMC parts.

powder, is deposited layer by layer using a focused energy source, such as a laser or electron beam. The exceptional control offered by DED processes allows for the precise creation of gradient structures with tailored properties [305,306]. This capability is crucial for 2DMMC parts, as the final properties of components depend significantly on the amount and distribution of 2D material [307]. Within DED, laser cladding was used for the fabrication of 2DMMC parts [103]. h-BN was incorporated into various metal matrices using laser cladding for the fabrication of wear resistant coating with thermal stability up to 900 °C [308–310].

Wang et al. [311] investigated the correlation between structure and properties of aluminum alloy reinforced by graphene and demonstrated

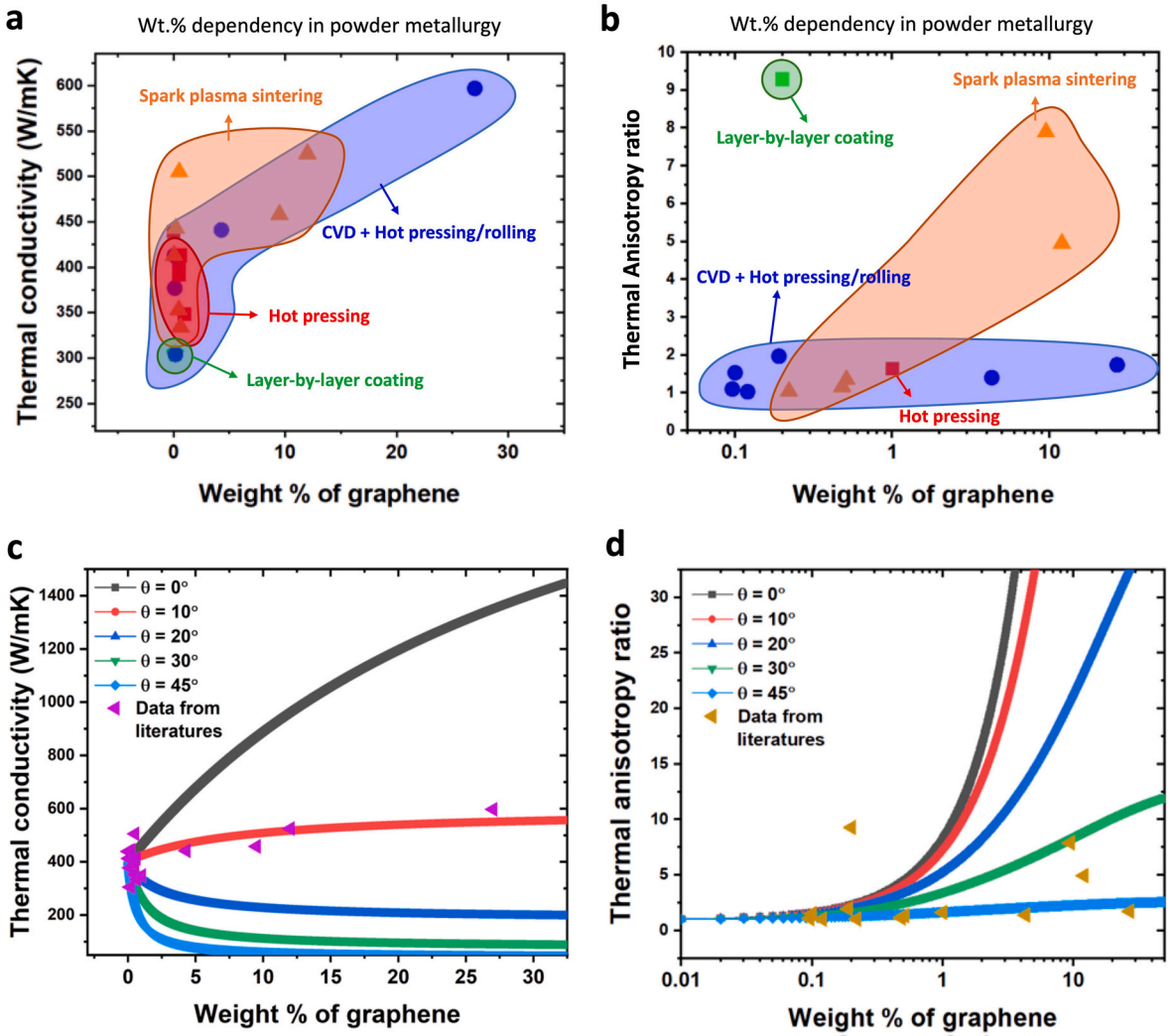

Fig. 23. 2D phase dependency of (a) thermal conductivity and (b) thermal anisotropy ratio for four different copper-graphene production technologies. Comparison of effective medium approximations at different values for the so-called theta parameter θ defined in equations (1) and (2), with literature values of (c) thermal conductivity and (d) thermal anisotropy ratio at different wt.% of graphene in copper-graphene 2DMMC parts [46,49,50,64,69,327,329,330,338–344].

that increasing the graphene nanoplatelet content significantly refines the grain during Laser Deposition Manufacturing (LDM). The high temperature of LDM processes poses a challenge due to the formation of carbides (e.g., Al_4C_3 in aluminium alloys reinforced by graphene). This is mitigated by LDM's rapid heating. Small amounts of Al_4C_3 were found to improve the wettability of the graphene nanoplatelets in the aluminum matrix [311]. Lu et al. [307] reported no carbide formation during LDM used for obtaining Ni_3Al metal-matrix composites. The study demonstrated that the strength enhancement observed in the final composite resulted solely from grain refinement. Further studies into the thermal behavior of DED fabricated 2DMMC parts are much needed.

Table 10 summarizes Chapter 4, outlining the benefits, obstacles, and key characteristics associated with each discussed fabrication method, highlighting aspects such as dispersion, agglomeration, energy consumption, and size limitations.

Current literature advocates hybrid processing strategies, which integrate various techniques to offer customized solutions. Hybrid approaches have been reported to address fabrication hurdles and elevate performance for 2DMMC applications. The research conducted by Li et al. [226] explores a hybrid fabrication method for a copper matrix reinforced by graphene, combining CVD with two SPD methods, i.e., extrusion and cold drawing. In the same vein, Li et al. [411] merged electrophoretic and vacuum hot press techniques to obtain a Cu/rGO film with a thermal conductivity 40.9 % higher than the sole electrophoretic Cu/GO film. These successful examples improve heat dissipation, offering exciting potential for future advancements in thermal management applications.

Fig. 20 represents the predominant manufacturing methodologies within the primary technology categorization, accompanied by schematic representations of the fabrication technique and demonstrative structures obtained for each.

Fig. 21 illustrates the range of thermal conductivity values reported for 2DMMC parts with aluminum and copper matrices achieved through different fabrication methods. Interestingly, the highest reported value, shown in the case of hot pressing, corresponds to a hybrid process of electrophoretic and vacuum hot pressing techniques [411].

The choice of the optimal fabrication method for 2DMMC parts is contingent upon the 2D phase and the metal matrix, and the desired application regarding the required physical, structural, mechanical and thermal attributes. Integrated consideration of these features allows a tailored selection of fabrication methods based on the unique requirements of the target application.

5. Optimizing the thermal conductivity in 2DMMC systems

This section discusses the factors governing the thermal conductivity of 2DMMC parts. The effect of varying parameters governing the production processes on the bulk metal matrix and its interfaces with the 2D material are considered. An overview of the three main factors affecting the thermal conductivity of 2DMMCs is presented in Fig. 22.

5.1. Distribution of 2D phases

The distribution of the 2D phases within the host metal matrix has a significant impact on the thermal conductivity of the 2DMMCs. Next to the wt.%, also the alignment of the 2D phases arising from the material processing and fabrication method is crucial. Fig. 23a depicts the relationship between the thermal conductivity and the wt.% of graphene in a copper matrix, considering four independent production techniques. The results indicate that even low graphene fractions between 0.1 and 1 wt% can induce variations of the thermal conductivity between 300 and 500 W/mK [50,64,66,69,327–330,337]. The thermal conductivity of bulk copper is about 400 W/mK. As the orange area in Fig. 23a indicates, only SPS provides a significant thermal benefit at low graphene wt.%. Chu et al. [338] refer to this as 'aligned graphene', postulating that SPS processing orients the graphene in a favorable position to conduct heat. Fabrication using CVD and hot pressing/rolling, indicated by the blue and red areas in Fig. 23a shows a more modest benefit of enhancing copper with graphene.

The alignment or orientation of the 2D phases can also be observed from the thermal anisotropy ratio, i.e., the ratio between the parallel and normal conductivities (Fig. 23b). Here, SPS stands out with reported anisotropy ratios between 5 and 8. Interestingly, CVD and hot pressing/rolling can combine high conductivity with significant thermal isotropy [336].

Effective medium approximations predict the thermal conductivity of 2DMMC parts [49,345–347]. It provides a prediction for in-plane and through-plane thermal conductivities in terms of interface resistance:

$$K_{//} = K_m \cdot \left\{ \frac{2 + \left(\frac{\alpha}{1+\alpha}\right)\cdot\left[\left(\frac{K_{2D}}{K_m} - 1\right)\cdot(1 + \langle\cos^2\theta\rangle)\right]}{2 - \left(\frac{\alpha}{1+\alpha}\right)\cdot\left[1 - \frac{K_m\cdot\left(\frac{R_k\cdot K_{2D}}{t} + 1\right)}{K_{2D}}\right]\cdot(1 - \langle\cos^2\theta\rangle)} \right\} \quad (1)$$

$$K_{\perp} = K_m \cdot \left\{ \frac{1 + \left(\frac{\alpha}{1+\alpha}\right)\cdot\left[\left(\frac{K_{2D}}{K_m} - 1\right)\cdot(1 - \langle\cos^2\theta\rangle)\right]}{1 - \left(\frac{\alpha}{1+\alpha}\right)\cdot\left[1 - \frac{K_m\cdot\left(\frac{R_k\cdot K_{2D}}{t} + 1\right)}{K_{2D}}\right]\cdot\langle\cos^2\theta\rangle} \right\} \quad (2)$$

where $\alpha = \frac{f_{2D\ phase}}{f_{metal}}\frac{\rho_{metal}}{\rho_{2D\ phase}}$, K_m and K_{2D} are the thermal conductivities of the host metal and 2D phase, respectively, f_{metal} and f_{2D} are the weight fractions of metal and 2D phase, respectively, ρ_{metal} and ρ_{2D} are the mass density of metal and 2D phase, respectively, θ is the angle between the 2D phase and the heat transfer direction, R_k is the interface thermal resistance between the 2D phase and the metal, and t is the thickness of the 2D phase.

In Fig. 23c–d model results are depicted for an assumed thermal conductivity of 400 W/mK and 2000 W/mK for copper and graphene, respectively. Additionally, the interfacial thermal resistance R_k is assumed to be 4×10^{-8} m^2K/W [348] for the copper-graphene interface. The thickness of the graphene layer is taken as $t = 100$ nm. Both the wt. % and 2D phase alignment are varied. Fig. 23c illustrates that with poor alignment ($\theta > 30°$) the thermal conductivity decreases when adding more graphene. Conversely, with perfect alignment ($\theta = 0°$) a large increase is witnessed. The purple diamonds represent the reported values of Fig. 23a. The thermal anisotropy ratio is depicted in Fig. 23d. In this case, the orange triangles represent the values taken from Fig. 23b. There appears to be some general correspondence between the experimental findings and the presented model, but the agreement is insufficient for a quantitative comparison.

5.2. Intrinsic properties of 2D phases

In this subsection, three main properties of 2D phases that are essential in determining the heat transfer characteristics are discussed. Specifically, the thickness of the 2D phase (Subsection 5.2.1), defects contained in the 2D phase (Subsection 5.2.2) and the strain on the 2D phase caused by mechanical deformation or thermal processing (Subsection 5.2.3) are considered.

5.2.1. Thickness

The dependency of the thermal conductivity on the thickness of the 2D material can be expressed using the effective medium approach [49,

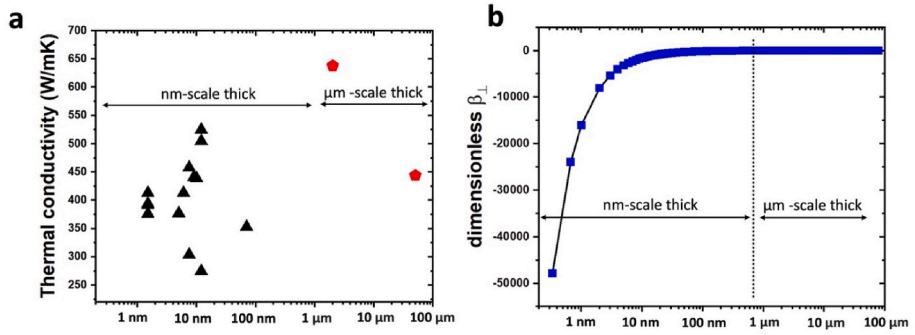

Fig. 24. Dependence of the thermal conductivity on the graphene layer thickness in Cu-graphene 2DMMCs (a) Experimentally determined thermal conductivity versus thickness of graphene derived from Refs. [47,49,50,64,69,329,330,338,339,342,344,349], [411], (b) plot of form-factor $\beta_{\perp}$ as a function of graphene layer thickness.

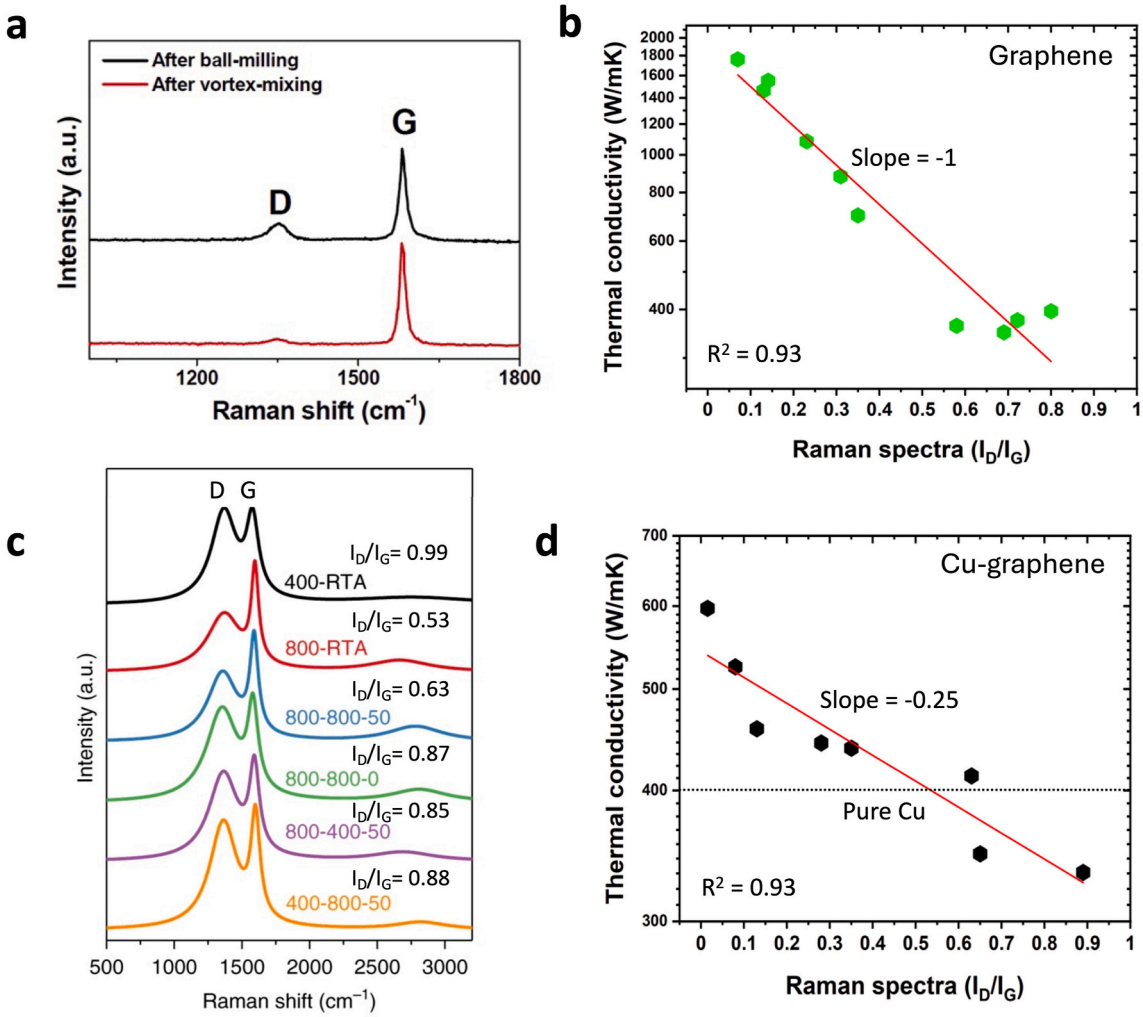

Fig. 25. (a) Raman spectra of graphene after different preparation methods, (b) Thermal conductivity as a function of I_D/I_G taken from the Raman spectrum, (c) Raman spectra of copper-graphene 2DMMC according to their fabrication conditions. The number in the first, second, and third positions presents the experimental condition for thermal annealing temperature, hot-pressing temperature in °C, and hot-pressing pressure in MPa. (d) Thermal conductivity values of copper-graphene as a function of the Raman ratio I_D/I_G taken from the Raman spectrum [49,64,66,327,330,336,338,339,350].

345–347]. The form-factor $\beta_{\perp}$ can be defined, as follows:

$$\beta_{\perp} = 1 - \frac{K_m \cdot \left(\frac{R_k K_{2D}}{t} + 1\right)}{K_{2D}} \tag{3}$$

The symbols are similar to those used in Section 5.1.

In Fig. 24a experimental observations of the thermal conductivity in the in-plane direction are displayed. There is a general trend toward larger values for conductivity as the thickness of the 2D-material layer increases. However, the trend is qualitative and actual measurements are hampered by considerable experimental variations. In Fig. 24b the form-factor $\beta_{\perp}$ as predicted by the effective medium theory is displayed,

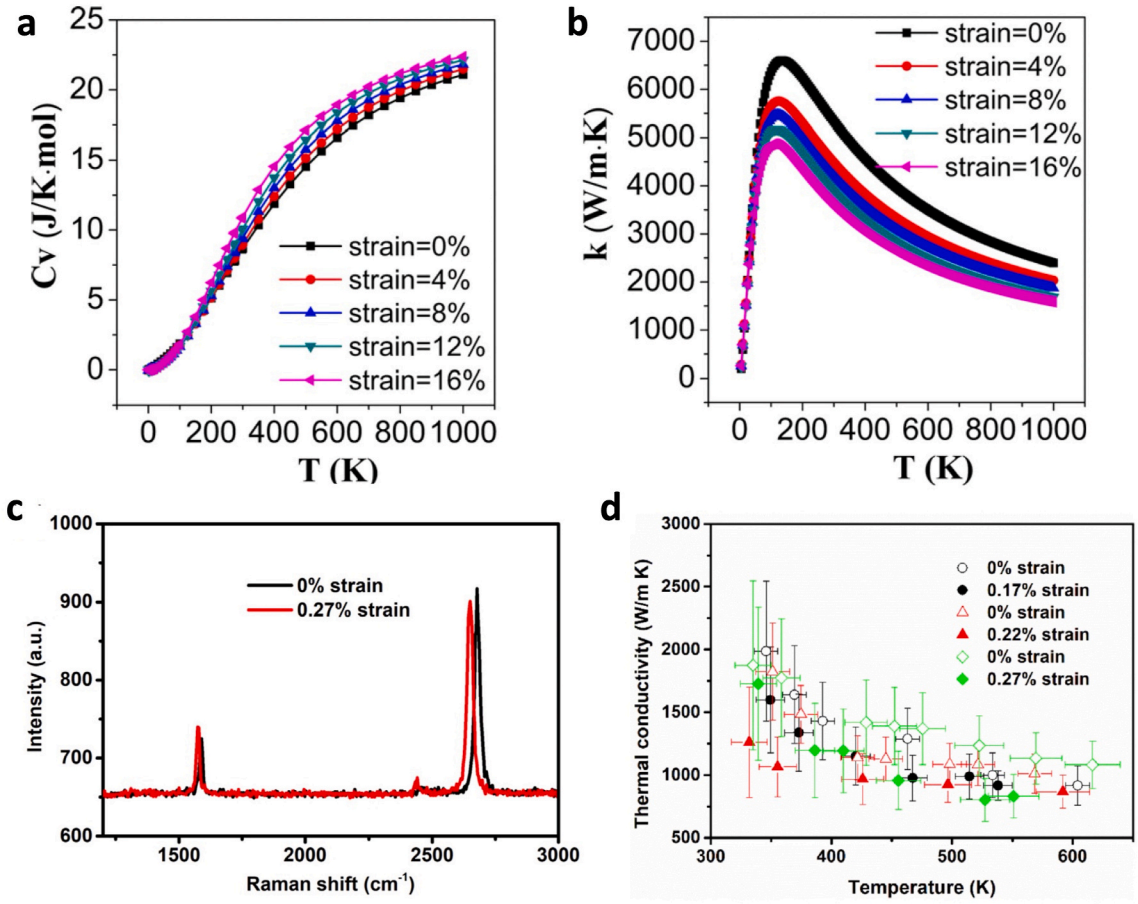

Fig. 26. Effect of strain on (a) heat capacity, (b) thermal conductivity of graphene calculated by density functional theory, and experimentally deduced strain effects on (c) shifted Raman spectra and (d) thermal conductivity data of strained graphene [351,353].

showing saturation with increasing thickness beyond 10 nm. The thermal conductivity changes little by introducing layers thicker than 10 nm. This may help to define the BM times needed to break up graphite into graphene flakes of small enough sizes.

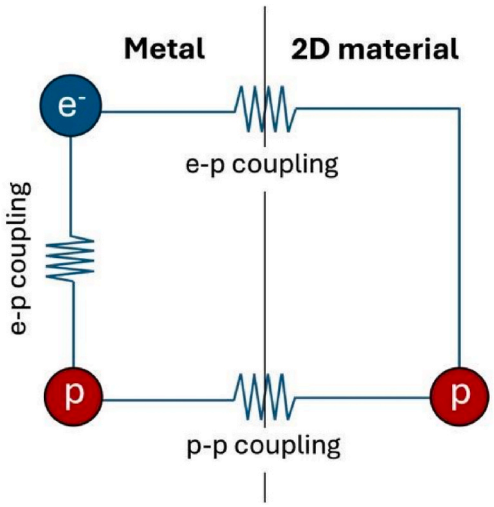

Fig. 27. Heat conduction mechanisms for a metal-2D material interface in 2DMMC systems: electron-phonon (e–p) coupling and phonon-phonon (p–p) coupling, respectively [360].

5.2.2. 2D Layer defects

When premixing metal host particles with a 2D material, the result will have defects in the 2D layer arising from the preparation process used to break up and deposit layers of graphene and graphite. This is quantified in Fig. 25a, in terms of the Raman spectrum of the 2D layer obtained from high-intensity BM, compared to the gentler vortex mixing. The BM procedure appears to introduce a separate Raman shift corresponding to defects, as seen by the secondary peak at the Raman D band. The final quality of the 2D layer influences the resulting thermal conductivity, as, on an atomistic scale, the phonon and electron transport are heavily affected by localized defects. Raman spectra can be used to compare the intensity at the defect scales (I_D) with that at scales of the pristine layer (I_G). The thermal conductivity appears to follow exponential scaling, as depicted in Fig. 25b [207]. Hence, careful preparation of the 2D layer free of defects is an essential approach to increase the thermal conductivity of copper and graphene after 2DMMC fabrication.

The Raman spectrum of actual samples of copper and graphene composites arising from BM and other production methods, at a specific range of parameters, such as temperature and pressure, is displayed in Fig. 25c. In this case, the separation of the *D* and *G* peaks is less outspoken, but the ratio I_D/I_G can be precisely determined. This simple parameter provides a direct index of the resulting thermal conductivity. In fact, a relatively low Raman spectrum ratio I_D/I_G, implying small contributions of defects, is seen to directly relate to a high thermal conductivity. The reverse is also true with low thermal conductivity in case of strong defects in the 2D layer. Quantitatively, there appears to be an exponential relationship between the Raman ratio I_D/I_G and the thermal conductivity for copper-graphene as seen on the semi log-scale presented in Fig. 25d.

Table 11
Interfacial characteristics for 2DMMCs with several metal-2D material combinations.

Materials	Interface bonding	Interatomic distance (Å)	Adhesion strength (J/m^2)	Interfacial thermal conductance (MW/m^2K)	Possible interface reaction	References
Cu-graphene	Physisorbed	3.23–3.32	0.394–0.74	23	No	[348, 371–373]
Al-graphene	Physisorbed	3.41–3.63	0.2	20–31	Yes (Al_4C_3)	[366,374, 375]
Al_4C_3-graphene	Chemisorbed (Covalent/Ionic)	3.48–3.49 (C-termination) 2.02–2.05 (Al-termination)	0.26–0.79 (C-termination) 5.98–6.28 (Al-termination)	–	–	[369]
Fe-graphene	Chemisorbed	2.20–3.00	0.73–1.00	–	Yes (Fe_3C/Fe_7C_3)	[368]
Fe_3C/Fe_7C_3-graphene	Chemisorbed (Covalent)	1.80–2.50	4.32–5.63	–	–	[368]
Ni-graphene	Chemisorbed	2.11–2.17	3.0–3.5	200	No	[367,376, 377]
Ti-graphene	Chemisorbed	2.08–2.15	2.12	31–39	Yes (TiC)	[348,378, 379]
TiC-Ti	Chemisorbed (Covalent/Ionic)	2.08–3.097	0.784–3.102	–	–	[370]
Cu-hBN	Physisorbed	2.91–3.38	0.53	16–29	No	[360,372, 380]

5.2.3. *Strain*

A small block of a metal matrix combined with a layer of 2D material can be strained in several directions, thereby affecting the dispersion of acoustic and optical phonon modes. This alters the thermal transport at a fundamental level [351–354]. Fig. 26a–b depict the calculated heat capacity and thermal conductivity of strained monolayer graphene, respectively, clearly showing modifications under uniaxial tensile strain and deformed crystal symmetry [351]. The altered crystallographic symmetry and resulting frequency shifts of optical phonon modes (Fig. 26c), appear to involve more phonons and increase the heat conductivity. In general, the thermal conductivity of the strained state decreases considerably with increasing temperature [352], as confirmed in Fig. 26d [353].

5.3. *Characteristics of the interface*

In heterogeneous material systems like 2DMMCs, interfaces play a key role in heat transfer, particularly when the mean free path of phonons exceeds the characteristic length of the interface and ballistic transport occurs [355,356]. The interface acts as a barrier for heat conduction, as illustrated in Fig. 27 [357–360]. It has been established that phonon-phonon coupling at the interface forms the main heat

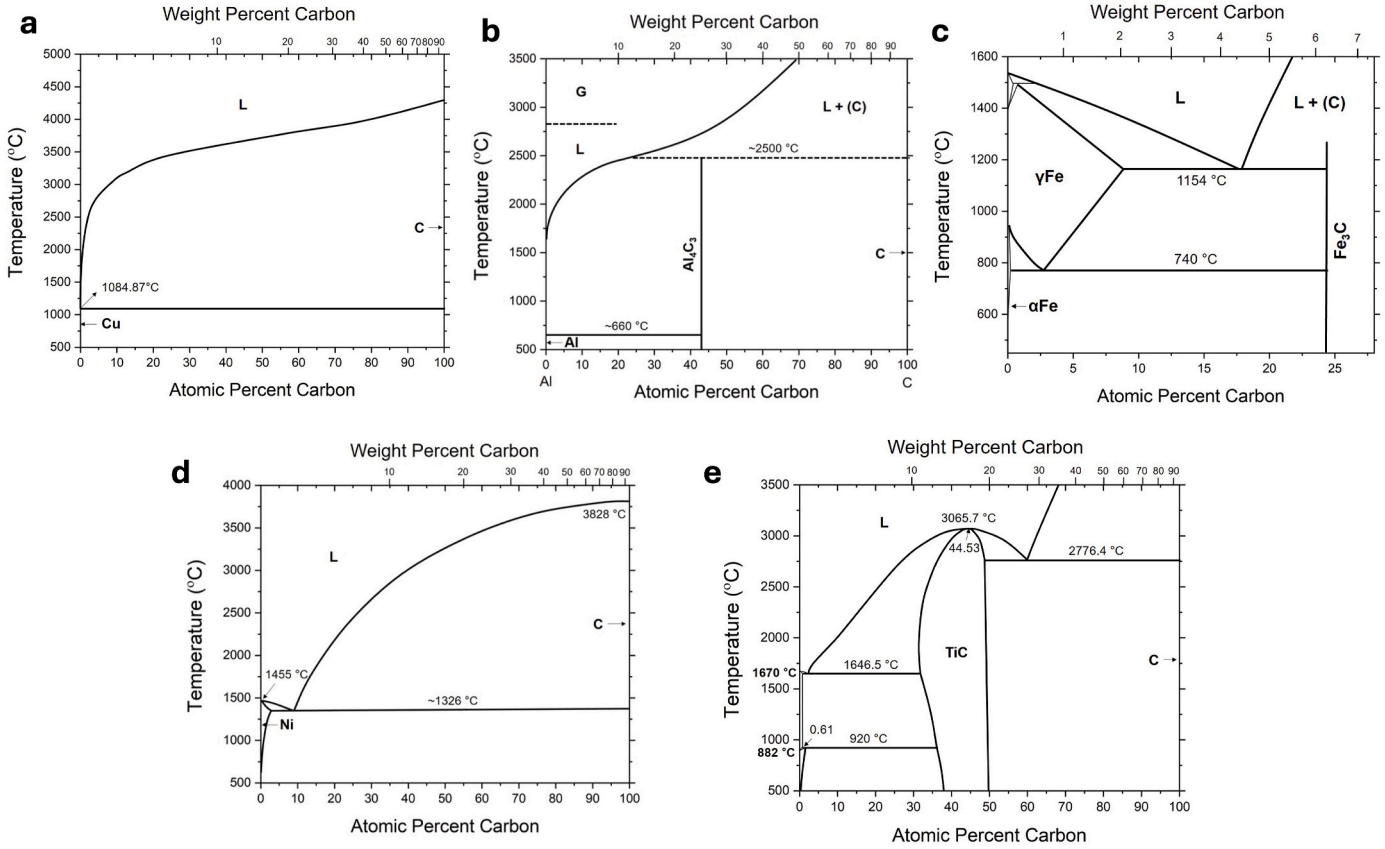

Fig. 28. Phase diagrams of metal-graphene for five representative metal matrices: a-e for Cu, Al. Fe, Ni, and Ti, respectively [381–384].

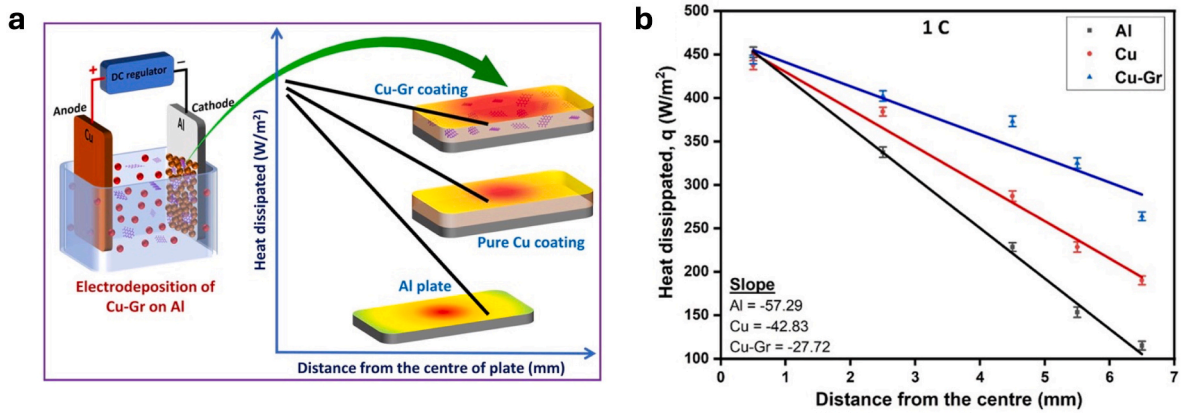

Materials	Filler fraction	Processing technique	Flim thickness	In-plane thermal conductivity	Through-plane thermal conductivity
Cu-graphene	5 vol %	Electrodeposition	45 μm	443.18 W/mK	290.5 W/mK

Fig. 29. Heat spreader applications of copper-graphene composite, processed by electrodeposition. (a) Schematic illustrations of the experimental setup for copper-graphene processing, (b) Heat transfer properties of copper-graphene coatings. Copper-graphene presents the highest heat dissipation rate overall coated areas, (c) Thermal properties of copper-graphene heat spreader coating [392].

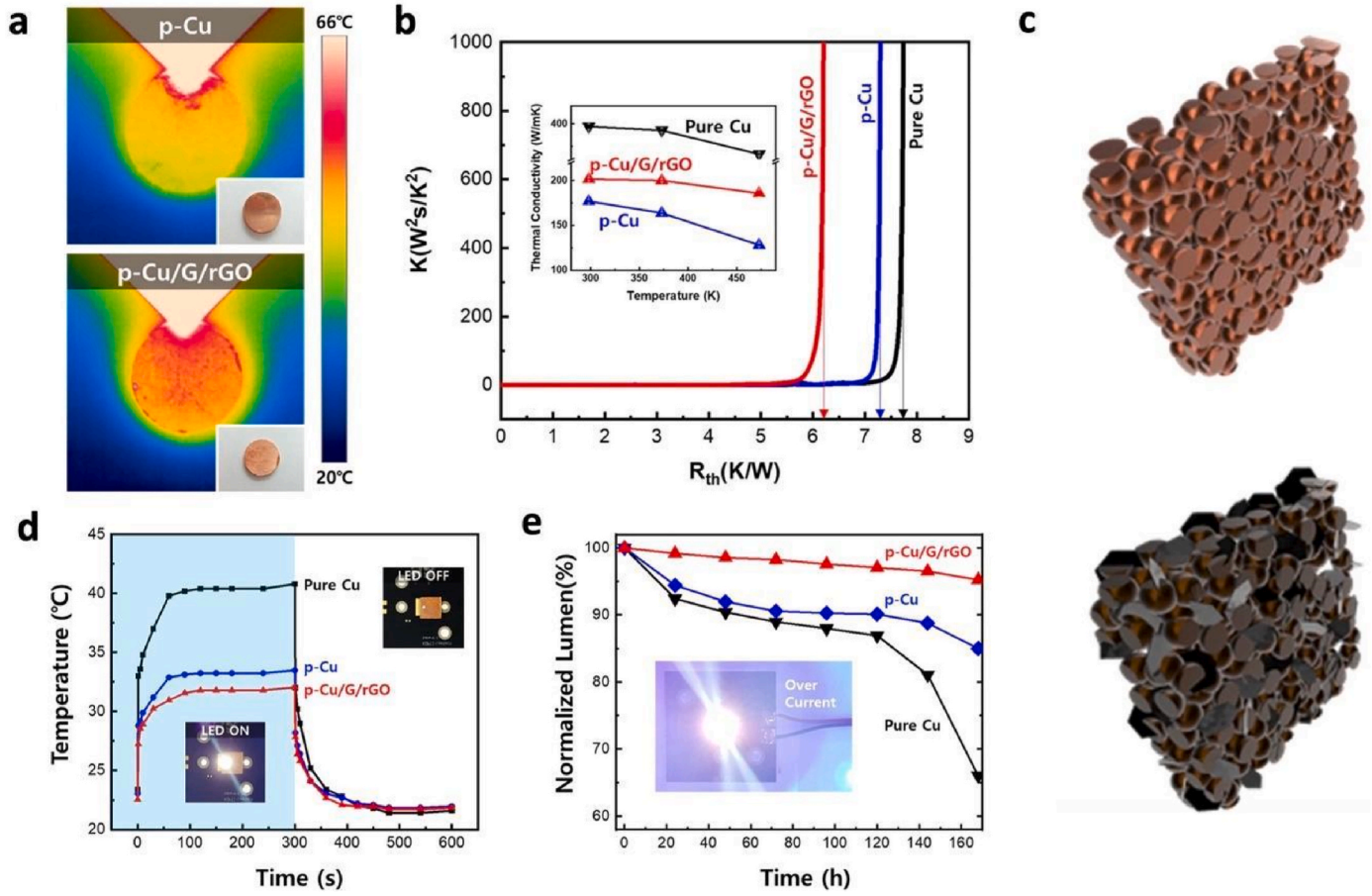

Fig. 30. Heat sink applications of copper-graphene porous structure for microelectronics cooling, processed by chemical vapour deposition and sintering: (a) Thermal infrared images of porous copper and porous copper-graphene, (b) Thermal resistance of LED device with porous heat sink, (c) Schematic images of porous copper (top) and porous copper-graphene (bottom), (d) Temperature distribution of LED devices with heat sinks under on- and off-state LED, (e) LED stability tests with heat sink based on light intensity measurements over time [393].

Table 12
Potential applications for including 2DMMCs in heat transfer: advantages and limitations.

Heat transfer applications using 2DMMCs	Advantages	Limitations	Effects of 2D materials	References
Heat spreader	Higher thermal conductivity and better control over thermal expansion coefficients, compared to traditional materials.	Currently, only available for mm-scale applications using electrodeposition.	Improvement of thermal conductivity.	[334,392, 396,397]
	E.g., the extreme reduction of thermal conductivity of thin metal films (down to 20 % of intrinsic values) due to the high surface roughness can be mitigated by the addition of graphene.	Few manufacturing techniques available for the targeted application sizes.	Reduction of mismatches in thermal expansion coefficients.	
	Thermal properties of a heat spreader can be modified using 2DMMC coatings.	Nano-agglomeration of graphene during processing may hinder potential improvements.	Phonon scattering across interfaces.	
Heat sink	Higher thermal conductivity and better heat transfer performance compared to traditional materials. This applies to low as well as very high temperatures.	Limitation in shape and size during product design.	Surface area enhancements	[393,398, 399]
		Currently, sintering is the main processing technique.	Oxidative protection	
		Application is restricted to low-power electronics, such as LEDs, due to the limited scalability.	Higher thermal conductivity	
		Anisotropic thermal expansion and conductivity.		
Other applications (e.g., heat exchanger)	Higher thermal conductivity	Anticipated potential is not yet realized using applications with large-scale 2DMMC inclusion, e.g., no industrial-scale copper-graphene heat exchanger)	Higher thermal conductivity	[342, 400–402]
	Higher mechanical strength-to-weight		Improved mechanical strength	
	Improved corrosion resistance		Enhanced corrosion resistance	
	Better long-term durability compared to traditional materials		Retainment of a lightweight implementation	

conduction mechanism [357,358,360]. In fact, enhancing phonon-phonon coupling at the interface by modifying interface bonding [357,359–361] was found to increase the interfacial thermal conductance.

5.3.1. Interface bonding

Interface bonding between metal and the 2D material in 2DMMCs is divided into physisorption and chemisorption. Physisorption originates from vdW interactions, while chemisorption derives from chemical interactions, such as covalent or ionic bonding [362,363]. In 2DMMC parts, interface bonding depends on how much the interatomic distance in the metal matrix differs from that of graphene (3.35 Å) and h-BN (3.33 Å) [348,357,359,364,365]. The bonding is considered physisorption if both interatomic distances are comparable. Conversely, chemisorption arises if the metal matrix has a shorter interatomic distance close to covalent bonding, typically around 2.2 Å. It has been observed that the graphene layer is more prone to be physisorbed on Cu, Al, Au, Ag, and Pt (typical interatomic distances of 3.2–3.4 Å), but chemisorbed on Ti, Co, Ni, Pd, Ni, and Fe (typical interatomic distances of 2.0–2.2 Å). In Table 11 the adhesion strength and related Interfacial Thermal Conductance (ITC) are presented for five representative metal matrices Cu, Al, Fe, Ni, Ti, and graphene.

Chemisorbed metal-graphene exhibits stronger adhesion than physisorbed metal-graphene, leading to enhanced phonon-phonon coupling [348,361,366]. For instance, physisorbed metal-graphene shows ITC values in the range of 20–30 MW/m^{2}K [348,366]. Chemisorbed interfaces show values beyond 40 MW/m^{2}K [366], even reaching 200 MW/m^{2}K for nickel-graphene [367]. Furthermore, the interface reaction between metal and graphene needs to be considered, since entirely different adhesion strengths may occur due to interface carbide phases. According to the phase diagrams shown in Fig. 28 of 5 metal matrixes and graphene, copper, and nickel do not show any carbide formations, while other metals can form carbide phases, depending on the fabrication temperatures and processing route. Once a carbide phase forms, adhesion strength increases, which may lead to an increase in ITC values [368–370].

5.3.2. Addition of active elements

Heat conduction at the interfaces in 2DMMC parts can be increased by engineering the interface reactions [340,385,386]. In fact, interface bonding can be enhanced by the addition of active elements. For example, physisorbed copper-graphene can be modified to chemisorbed copper-graphene through carbide phase formations with the addition of Mo [387], Zr [386], Ti [388], Cr [385], and Ni [389]. As a result, thermal conductivity can be increased up to ~800 W/mK or it can be decreased to ~300 W/mK.

6. Future perspectives on heat transfer applications and processing

The aim to enhance efficiency and mitigate the environmental impact of heat management is a catalyst driving innovations in heat transfer technologies. Heating and cooling account for about half of the global energy consumption [390]. It is the largest source of energy use, ahead of electricity (20 %) and transport (30 %), and is responsible for more than 40 % of global energy-related carbon dioxide emissions. Improving heat management using 2DMMC parts in novel devices, is hence crucial for the energy transition from fossil to renewable sources.

This section focuses on future heat transfer applications derived from 2DMMCs and AM processes to realize complex parts. These two areas not only showcase the versatility and potential of 2DMMCs, but also underscore their capacity to revolutionize heat transfer efficiency using novel manufacturing techniques.

6.1. Potential of 2DMMC parts in heat transfer

2DMMC parts are used in many applications such as heat sinks, thermal interfaces, and heat spreaders, displaying augmented thermal conductivity, reduced thermal expansion, expanded operating temperature ranges, and heightened strength-to-weight ratios, as summarized in Table 12 [391]. Striking examples of the technological potential of 2DMMC parts for heat transfer include.

Table 13
Key challenges for 2DMMC research from the perspective of materials, thermal characterizations, powder production, manufacturing and heat transfer applications.

Challenge area	Current status	Future prospects
Materials perspective	• Copper-graphene is the most studied system, capable of achieving thermal conductivity improvements up to 600 W/mK • Enhancements in thermal conductivity beyond 600W/mK are likely limited due to graphene distribution, intrinsic defects, and low interfacial thermal conductance (ITC) • Limited application of 2DMMCs utilizing other combinations of metal-2D materials, such as copper-hBN, and aluminum-graphene	• Broadening the range of material types in 2DMMCs to expand application areas beyond heat transfer systems • Developing high-quality composites by optimized processing of 2D materials and the fabrication of 2DMMCs • Controlling interface reactions between the metal matrix and 2D materials to enhance thermal conductivity, and potentially other properties
Thermal characterization	• Various thermal characterization techniques, including TPS and laser flash analysis, have been well-developed for 2D materials and 2DMMCs • Characterization is applied to mm-scale and nano-scale features	• Applying atomistic-level thermal and structural characterizations to understand heat transfer phenomena • Developing advanced characterization techniques to enable fast, accurate, and reproducible measurements
2DMMC powder production	• BM and LPE are two representative techniques for large-scale 2DMMC powder production • BM offers better scalability, but can easily cause structural damage to the 2D layers and morphology modifications of the powder particles • LPE can provide high-quality exfoliation of 2D layers, but solvent contamination in the final products and low yield are key challenges	• Hybrid processing techniques combining BM and LPE to improve the quality of 2D layers and enhance control over size and thickness • Careful process optimization using machine learning-assisted simulations • Application of appropriate wet BM to minimize structural damage • Recycling of solvent to enhance the yield of LPE
Manufacturing techniques	• Manufacturing 2DMMCs requires careful consideration of various factors, such as uniform distribution of the 2D phase, and potential structural and oxidative damage • To address these challenges, hybrid fabrication techniques are employed for 2DMMCs, leveraging the advantages of each individual method • However, scalability and manufacturing costs remain significant challenges	• Optimizing fabrication techniques and process parameters for targeted applications with desired material properties • AM can offer better control over the distribution of 2D phase within a metal matrix, improving material properties •AM develops scalability and enables the fabrication of complex geometries
Heat transfer applications	• Heat transfer applications, such as heat spreaders and heat sinks, have been demonstrated using copper-graphene • Large-scale production and limitations in geometrical design are the key challenges that need to be addressed	• Expanding application areas to other heat transfer systems, including heat exchangers • AM can provide a solution for scalability and design issues, unlocking new opportunities for heat transfer applications

1. **Heat spreader enhancement:** Sainudeen et al. [392] studied the convective heat transfer of an aluminium heat spreader coated with a copper-graphene nanocomposite (Fig. 29), focusing on spot heating scenarios for battery packs. Using electrodeposition to apply copper and copper-graphene composite materials onto the surface of the aluminium heat spreader, a significant reduction in temperature differentials was observed, with decreases of 66 %, 55 %, and 41 % measured at discharging rates of 0.5 C, 1 C, and 3 C, respectively.
2. **Heat sink:** Rho et al. [393] engineered a novel composite heat sink for an LED chip, consisting of layers of porous copper/single-layer graphene/graphene oxide (p-Cu/SLG/GO) (Fig. 30). Compared to pure copper, the heat dissipation capabilities were much improved – a decrease in overall thermal resistance in p-Cu/Gr/GrO was observed under typical operating conditions. A high bright level of 95.24 % of the initial value after 160 h exposure to rigorous operating conditions was achieved, compared to 66.04 % for pure copper.

Anisotropic thermal control could enhance the operational efficiency of miniature cooling systems [394,395]. Engineering latent heat transfer involving condensation and evaporation of a coolant fluid may accelerate the transfer rate between heat exchangers and 2DMMC parts by an order of magnitude.

6.2. Additive manufacturing of 2DMMC parts

AM, also referred to as 3D printing, can be used to construct a three-dimensional object, from a powder feedstock, layer by layer [403,404]. The manufacturing of 2DMMC parts using AM techniques presents significant challenges.

1. **Fabrication of components using 2DMMCs**: AM feedstock powders must possess nearly spherical morphology for good flowability and uniform printing quality. However, achieving this morphology for composite powders of metal and 2D materials necessitates the exploration of various optimization strategies.
2. **Manufacturability of the composites**: Disparate melting points of metallic components and 2D materials within a single powder mixture can lead to issues with processability. Alinejadian et al. [405] reported on LPBF of MoS_2-based nanocomposites, arising from the different melting points of MoS_2 (1185 °C) and Mo (2623 °C).
3. **Layer mismatches:** Weak vdW forces between layers affect thermal conductivity and thermal expansion at interfaces. Optimization of process parameters is essential for fabricating 2DMMC components.

Several studies have demonstrated improved mechanical properties of 2DMMC parts by incorporating reinforcement 2D materials using AM. Jiang et al. [406] and Wen et al. [407] examined the microstructure and mechanical performance of aluminum/titanium diboride (Al/TiB_2) composites produced via DED. Similarly, Li et al. [408] evaluated the effect of nano-TiB_2 on the microstructural properties of an aluminum-silicon-magnesium alloy produced via LPBF. Hu et al. [303] conducted research on parts manufactured using LPBF with copper-graphene composites. The composites exhibited an average Young's modulus of 118.9 GPa and a hardness of 3 GPa, representing increases of 17.6 % and 50 %, respectively, compared to pure copper.

Compared to the research focusing on mechanically enhanced performance, there has been much less attention on the application of 2DMMC parts to enhance thermal conductivity. Zhang et al. [409] investigated L-PBF of graphene-aluminum-based 2DMMC parts to enhance strength and ductility. The findings underscored the importance of controlling interface characteristics, such as bonding, to improve thermal conductivity.

Developing AM of 2DMMCs requires interdisciplinary efforts to understand the dependencies between materials, processing parameters, and resulting properties. Current drivers of research include:

- **Novel feedstock materials and fabrication techniques**: Research efforts may identify novel feedstock materials and fabrication techniques to address challenges related to powder morphology and processability. This involves exploring alternative sources of 2D materials, optimizing powder compositions, and innovating fabrication processes.
- **Enhanced thermal conductivity:** Developing innovative approaches for interface tailoring and densification control can help improve thermal conductivity.

- **Developing multiscale models:** Advanced computational tools that address AM on a range of important dynamic time and length scales can provide insights into material behavior, phase transformations, and microstructural evolution during processing.
- **Applications beyond heat transfer materials:** While heat transfer materials represent a significant application area for 2DMMC parts, there is a potential for their utilization in other industries such as electronics, aerospace, defence, and automotive.

By addressing these research areas, AM of 2DMMC parts can unlock new opportunities for unprecedented and customizable mechanical and thermal properties of novel parts.

7. Summary and outlook

Over several decades, extensive research on 2DMMC materials has advanced our understanding of their physical and thermal properties, fabrication from powder feedstocks to parts, and their heat transport. Detailed studies on thermal characterization techniques, scalable production, and process optimization have led to significant advancements in a variety of 2DMMC heat transfer applications.

Among 2DMMCs, copper-graphene stands out for its potential in heat transfer systems owing to graphene's high thermal conductivity and the high ductility, toughness and manufacturability of copper. However, the reported maximum thermal conductivity of approximately 600 W/mK for copper-graphene 2DMMC at room temperature is only marginally better than that of pure copper (~400 W/mK) [336,410]. Further improvements of thermal properties of 2DMMCs are crucial for future heat transfer applications – the following generic developments are anticipated in the near future:

1. Developments of thermal characterization techniques at nanometer- and mm-scale for understanding thermal properties
2. Formulation of mass production recipes for 2D materials with excellent crystallinity and minimized oxidation.
3. New techniques for uniform coating of 2D layers on metal surfaces is a timely pacing item for further studies
4. Development of cost-effective fabrication techniques enabling a controlled distribution of 2D phases in a metal matrix, e.g., maintaining good homogeneity or introducing controlled grading of material properties
5. Control of thermal anisotropy for targeted specific heat transfer applications, e.g., when developing a heat spreader or heat exchanger using directional cooling
6. Expansion of research on other 2DMMCs (Cu-h-BN, Al-graphene, etc.)
7. Enhancement of the interface properties between the 2D material and the host metal matrix using controlled interface reactions

Finally, overall specific conclusions regarding the current state-of-the-art and future prospects discussed in this review are summarized in Table 13. Recent progress in advanced thermal characterization and emerging fabrication techniques, such as AM, opens new possibilities for applications of 2DMMCs with unprecedented thermal performances.

Declaration of competing interest

The authors declare that they have no known competing financial interests or personal relationships that could have appeared to influence the work reported in this paper.

Acknowledgements

This work was supported by ThermoDust, a project funded under grant agreement No. 101046835 from the European Union's Horizon and Europe research programme.

Data availability

No data was used for the research described in the article.

References

[1] Novoselov KS, Mishchenko A, Carvalho A, Castro Neto AH. 2D materials and van der Waals heterostructures. Science 2016;353:aac9439.
[2] Gupta A, Sakthivel T, Seal S. Recent development in 2D materials beyond graphene. Prog Mater Sci 2015;73:44–126.
[3] Glavin NR, Rao R, Varshney V, Bianco E, Apte A, Roy A, et al. Emerging applications of elemental 2D materials. Adv Mater 2020;32:e1904302.
[4] Moore AL, Shi L. Emerging challenges and materials for thermal management of electronics. Mater Today 2014;17:163–74.
[5] Song H, Liu J, Liu B, Wu J, Cheng H-M, Kang F. Two-dimensional materials for thermal management applications. Joule 2018;2:442–63.
[6] Fu Y, Hansson J, Liu Y, Chen S, Zehri A, Samani MK, et al. Graphene related materials for thermal management. 2D Mater 2019;7.
[7] Choi SH, Yun SJ, Won YS, Oh CS, Kim SM, Kim KK, et al. Large-scale synthesis of graphene and other 2D materials towards industrialization. Nat Commun 2022;13:1484.
[8] Gu DD, Meiners W, Wissenbach K, Poprawe R. Laser additive manufacturing of metallic components: materials, processes and mechanisms. Int Mater Rev 2012;57:133–64.
[9] Sames WJ, List F, Pannala S, Dehoff RR, Babu SS. The metallurgy and processing science of metal additive manufacturing. Int Mater Rev 2016;61:315–60.
[10] Jafari D, Wits WW. The utilization of selective laser melting technology on heat transfer devices for thermal energy conversion applications: a review. Renew Sustain Energy Rev 2018;91:420–42.
[11] Wen X, Joshi R. 2D materials-based metal matrix composites. J Phys Appl Phys 2020;53.
[12] Tjong SC. Recent progress in the development and properties of novel metal matrix nanocomposites reinforced with carbon nanotubes and graphene nanosheets. Mater Sci Eng R Rep 2013;74:281–350.
[13] Kumar HGP, Xavior MA. Graphene reinforced metal matrix composite (GRMMC): a review. Procedia Eng 2014;97:1033–40.
[14] Anthony Xavior M, Prashantha Kumar HG. Processing and characterization techniques of graphene reinforced metal matrix composites (GRMMC); A review. Mater Today Proc 2017;4:3334–41.
[15] You X, Zhang Q, Yang J, Dong S. Review on 3D-printed graphene-reinforced composites for structural applications. Compos Appl Sci Manuf 2023;167:107420.
[16] Balandin AA, Ghosh S, Bao W, Calizo I, Teweldebrhan D, Miao F, et al. Superior thermal conductivity of single-layer graphene. Nano Lett 2008;8:902–7.
[17] Slack GA. Thermal conductivity of pure and impure silicon, silicon carbide, and diamond. J Appl Phys 1964;35:3460–6.
[18] Chen K, Song B, Ravichandran NK, Zheng Q, Chen X, Lee H, et al. Ultrahigh thermal conductivity in isotope-enriched cubic boron nitride. Science 2020;367:555–9.
[19] Cai Q, Scullion D, Gan W, Falin A, Zhang S, Watanabe K, et al. High thermal conductivity of high-quality monolayer boron nitride and its thermal expansion. Sci Adv 2019;5:eaav0129.
[20] Hernandez Y, Nicolosi V, Lotya M, Blighe FM, Sun Z, De S, et al. High-yield production of graphene by liquid-phase exfoliation of graphite. Nat Nanotechnol 2008;3:563–8.
[21] Wu F, Tian H, Shen Y, Zhu ZQ, Liu Y, Hirtz T, et al. High thermal conductivity 2D materials: from theory and engineering to applications. Adv Mater Interfac 2022;9.
[22] Yap CY, Chua CK, Dong ZL, Liu ZH, Zhang DQ, Loh LE, et al. Review of selective laser melting: materials and applications. Appl Phys Rev 2015;2:041101.
[23] Champagne V, Helfritch D. The unique abilities of cold spray deposition. Int Mater Rev 2016;61:437–55.
[24] Yin S, Zhang Z, Ekoi EJ, Wang JJ, Dowling DP, Nicolosi V, et al. Novel cold spray for fabricating graphene-reinforced metal matrix composites. Mater Lett 2017;196:172–5.
[25] Hu Z, Chen F, Xu J, Nian Q, Lin D, Chen C, et al. 3D printing graphene-aluminum nanocomposites. J Alloys Compd 2018;746:269–76.
[26] Wang Y, Shi J, Lu S, Wang Y. Selective laser melting of graphene-reinforced inconel 718 superalloy: evaluation of microstructure and tensile performance. J Manuf Sci Eng 2016;139.
[27] Mohammadian SK, Rassoulinejad-Mousavi SM, Zhang Y. Thermal management improvement of an air-cooled high-power lithium-ion battery by embedding metal foam. J Power Sources 2015;296:305–13.
[28] Malik A. inNEMI roadmap identifies trends impacting electronics thermal management. Now You Can Cool Your Electron Device Compon Level. 2016. p. 9–15.
[29] Murshed SS, De Castro CN. A critical review of traditional and emerging techniques and fluids for electronics cooling. Renew Sustain Energy Rev 2017;78:821–33.
[30] Tran T-H, Harmand S, Sahut B. Experimental investigation on heat pipe cooling for hybrid electric vehicle and electric vehicle lithium-ion battery. J Power Sources 2014;265:262–72.
[31] Moore GE. Cramming more components onto integrated circuits, reprinted from electronics, volume 38, number 8, April 19, 1965, pp.114 ff. IEEE Solid State Circ Soc Newsl 2006;11:33–5.

[32] Nguyen T, Mochizuki M, Mashiko K, Saito Y, Sauciuc I. Use of heat pipe/heat sink for thermal management of high performance CPUs. Sixteenth annual IEEE semiconductor thermal measurement and management symposium (Cat No00CH37068). 2000. p. 76–9.
[33] Naphon P, Wiriyasart S. Liquid cooling in the mini-rectangular fin heat sink with and without thermoelectric for CPU. Int Commun Heat Mass Tran 2009;36:166–71.
[34] Ebrahimi K, Jones GF, Fleischer AS. A review of data center cooling technology, operating conditions and the corresponding low-grade waste heat recovery opportunities. Renew Sustain Energy Rev 2014;31:622–38.
[35] An L, Yu Y, Cai Q, Mateti S, Li LH, Chen YI. Hexagonal boron nitride nanosheets: preparation, heat transport property and application as thermally conductive fillers. Prog Mater Sci 2023;138:101154.
[36] Lee S, Yang F, Suh J, Yang S, Lee Y, Li G, et al. Anisotropic in-plane thermal conductivity of black phosphorus nanoribbons at temperatures higher than 100 K. Nat Commun 2015;6:8573.
[37] Kayyalha M, Maassen J, Lundstrom M, Shi L, Chen YP. Gate-tunable and thickness-dependent electronic and thermoelectric transport in few-layer MoS2. J Appl Phys 2016;120.
[38] Li W, Sohail M, Anwar U, Taha TA, Al-Sehemi AG, Muhammad S, et al. Recent progress in g–C3N4–Based materials for remarkable photocatalytic sustainable energy. Int J Hydrogen Energy 2022;47:21067–118.
[39] Babaei H, McGaughey AJ, Wilmer CE. Effect of pore size and shape on the thermal conductivity of metal-organic frameworks. Chem Sci 2017;8:583–9.
[40] Balestra SRG, Bueno-Perez R, Hamad S, Dubbeldam D, Ruiz-Salvador AR, Calero S. Controlling thermal expansion: a metal–organic frameworks route. Chem Mater 2016;28:8296–304.
[41] Zhang L, Deng H, Fu Q. Recent progress on thermal conductive and electrical insulating polymer composites. Compos Commun 2018;8:74–82.
[42] Janica I, Del Buffa S, Mikołajczak A, Eredia M, Pakulski D, Ciesielski A, et al. Thermal insulation with 2D materials: liquid phase exfoliated vermiculite functional nanosheets. Nanoscale 2018;10:23182–90.
[43] Momma K, Izumi F. VESTA 3 for three-dimensional visualization of crystal, volumetric and morphology data. J Appl Crystallogr 2011;44:1272–6.
[44] Ali S, Ahmad F, Yusoff PSMM, Muhamad N, Oñate E, Raza MR, et al. A review of graphene reinforced Cu matrix composites for thermal management of smart electronics. Compos Appl Sci Manuf 2021;144.
[45] Hidalgo-Manrique P, Lei X, Xu R, Zhou M, Kinloch IA, Young RJ. Copper/graphene composites: a review. J Mater Sci 2019;54:12236–89.
[46] Nazeer F, Ma Z, Xie Y, Gao L, Malik A, Khan MA, et al. A novel fabrication method of copper-reduced graphene oxide composites with highly aligned reduced graphene oxide and highly anisotropic thermal conductivity. RSC Adv 2019;9:17967–74.
[47] Goli P, Ning H, Li X, Lu CY, Novoselov KS, Balandin AA. Thermal properties of graphene-copper-graphene heterogeneous films. Nano Lett 2014;14:1497–503.
[48] Zhang L, Hou G, Zhai W, Ai Q, Feng J, Zhang L, et al. Aluminum/graphene composites with enhanced heat-dissipation properties by in-situ reduction of graphene oxide on aluminum particles. J Alloys Compd 2018;748:854–60.
[49] Chu K, Wang X-h, Wang F, Li Y-b, Huang D-j, Liu H, et al. Largely enhanced thermal conductivity of graphene/copper composites with highly aligned graphene network. Carbon 2018;127:102–12.
[50] Kostecki M, Cygan T, Petrus M, Jaroszewicz J. Thermal properties of multilayer graphene and hBN reinforced copper matrix composites. J Therm Anal Calorim 2019;138:3873–83.
[51] Qadir A, Le TK, Malik M, Amedome Min-Dianey KA, Saeed I, Yu Y, et al. Representative 2D-material-based nanocomposites and their emerging applications: a review. RSC Adv 2021;11:23860–80.
[52] Wang Z-G, Liu W, Liu Y-H, Ren Y, Li Y-P, Zhou L, et al. Highly thermal conductive, anisotropically heat-transferred, mechanically flexible composite film by assembly of boron nitride nanosheets for thermal management. Compos B Eng 2020:180.
[53] Wang Z-G, Jin Y-F, Hong R, Du J, Dai K, Zhang G-Q, et al. Dual-functional thermal management materials for highly thermal conduction and effectively heat generation. Compos B Eng 2022:242.
[54] Jiang Y, Sun L, Du J, Liu Y, Shi H, Liang Z, et al. Multifunctional zinc metal–organic framework based on designed H4TCPP ligand with aggregation-induced emission effect: CO2 adsorption, luminescence, and sensing property. Cryst Growth Des 2017;17:2090–6.
[55] Ni F, Wang Z, Feng X. On-Water surface synthesis of two-dimensional polymer membranes for sustainable energy devices. Accounts Chem Res 2024;57:2414–27.
[56] Ligati Schleifer S, Regev O. Additive manufacturing of anisotropic graphene-based composites for thermal management applications. Addit Manuf 2023;70.
[57] Zhang G, Xue S, Chen F, Fu Q. An efficient thermal interface material with anisotropy orientation and high through-plane thermal conductivity. Compos Sci Technol 2023;231.
[58] Feng CP, Chen LB, Tian GL, Wan SS, Bai L, Bao RY, et al. Multifunctional thermal management materials with excellent heat dissipation and generation capability for future electronics. ACS Appl Mater Interfaces 2019;11:18739–45.
[59] Akinwande D, Brennan CJ, Bunch JS, Egberts P, Felts JR, Gao H, et al. A review on mechanics and mechanical properties of 2D materials—Graphene and beyond. Extrem Mech Lett 2017;13:42–77.
[60] Zhang J, Doshi M, Fahrenthold EP. Eddy current measurement of chemiresistive sensing transients in monolayer graphene. Appl Mater Today 2022;26:101291.
[61] Sudeep PM, Narayanan TN, Ganesan A, Shaijumon MM, Yang H, Ozden S, et al. Covalently interconnected three-dimensional graphene oxide solids. ACS Nano 2013;7:7034–40.
[62] Shanmugam V, Mensah RA, Babu K, Gawusu S, Chanda A, Tu Y, et al. A review of the synthesis, properties, and applications of 2D materials. Part Part Syst Char 2022;39.
[63] Corona D, Beatrici M, Sbardella E, Di Domenico G, Lucibello F, Zarcone M, et al. 3D printing copper – graphene oxide nanocomposites. The 1st international conference on innovations for computing, engineering and materials. 2021, 20212021. Icem.
[64] Shu S, Yuan Q, Dai W, Wu M, Dai D, Yang K, et al. In-situ synthesis of graphene-like carbon encapsulated copper particles for reinforcing copper matrix composites. Mater Des 2021:203.
[65] Zhan K, Wang W, Li F, Cao J, Liu J, Yang Z, et al. Microstructure and properties of graphene oxide reinforced copper-matrix composite foils fabricated by ultrasonic assisted electrodeposition. Mater Sci Eng 2023;872.
[66] Yang Z, Wang L, Li J, Shi Z, Wang M, Sheng J, et al. Lateral size effect of reduced graphene oxide on properties of copper matrix composites. Mater Sci Eng 2021;820.
[67] Cao J, Yang Q, Zhou L, Chen H, Zhan K, Liu J, et al. Microstructure, properties and synergetic effect of graphene oxide-functionalized carbon nanotubes hybrid reinforced copper matrix composites prepared by DC electrodeposition. Carbon 2023;212.
[68] Samal A, Kushwaha AK, Das D, Sahoo MR, Lanzillo NA, Nayak SK. Thermal and electrical conductivity of copper-graphene heterosystem: an effect of strain and thickness. Adv Eng Mater 2023;25.
[69] Cao H, Xiong D-B, Tan Z, Fan G, Li Z, Guo Q, et al. Thermal properties of in situ grown graphene reinforced copper matrix laminated composites. J Alloys Compd 2019;771:228–37.
[70] Xamán J, Lira L, Arce J. Analysis of the temperature distribution in a guarded hot plate apparatus for measuring thermal conductivity. Appl Therm Eng 2009;29:617–23.
[71] Zhao D, Qian X, Gu X, Jajja SA, Yang R. Measurement techniques for thermal conductivity and interfacial thermal conductance of bulk and thin film materials. J Electron Packag 2016;138:040802.
[72] Al-Ajlan SA. Measurements of thermal properties of insulation materials by using transient plane source technique. Appl Therm Eng 2006;26:2184–91.
[73] Coquard R, Coment E, Flasquin G, Baillis D. Analysis of the hot-disk technique applied to low-density insulating materials. Int J Therm Sci 2013;65:242–53.
[74] Coquard R, Baillis D, Quenard D. Experimental and theoretical study of the hot-wire method applied to low-density thermal insulators. Int J Heat Mass Tran 2006;49:4511–24.
[75] Merckx B, Dudoignon P, Garnier J, Marchand D. Simplified transient hot-wire method for effective thermal conductivity measurement in geo materials: microstructure and saturation effect. Adv Civ Eng 2012;2012.
[76] Campbell RC, Smith SE, Dietz RL. Measurements of adhesive bondline effective thermal conductivity and thermal resistance using the laser flash method. Fifteenth annual IEEE semiconductor thermal measurement and management symposium (cat no 99CH36306). IEEE; 1999. p. 83–97.
[77] Lian T-W, Kondo A, Akoshima M, Abe H, Ohmura T, Tuan W-H, et al. Rapid thermal conductivity measurement of porous thermal insulation material by laser flash method. Adv Powder Technol 2016;27:882–5.
[78] Marcus SM, Blaine RL. Thermal conductivity of polymers, glasses and ceramics by modulated DSC. Thermochim Acta 1994;243:231–9.
[79] Blaine R, Marcus S. Derivation of temperature-modulated DSC thermal conductivity equations. J Therm Anal Calorim 1998;54:467–76.
[80] Kim JH, Feldman A, Novotny D. Application of the three omega thermal conductivity measurement method to a film on a substrate of finite thickness. J Appl Phys 1999;86:3959–63.
[81] Wang H, Sen M. Analysis of the 3-omega method for thermal conductivity measurement. Int J Heat Mass Tran 2009;52:2102–9.
[82] Presley MA, Christensen PR. Thermal conductivity measurements of particulate materials 1. A review. J Geophys Res: Planets 1997;102:6535–49.
[83] Malekpour H, Balandin AA. Raman-based technique for measuring thermal conductivity of graphene and related materials. J Raman Spectrosc 2018;49:106–20.
[84] Wang Y, Xu N, Li D, Zhu J. Thermal properties of two dimensional layered materials. Adv Funct Mater 2017;27:1604134.
[85] Gertych AP, Łapińska A, Czerniak-Łosiewicz K, Dużyńska A, Zdrojek M, Judek J. Thermal properties of thin films made from MoS2 nanoflakes and probed via statistical optothermal Raman method. Sci Rep 2019;9:13338.
[86] Dhiman S, Joshi RS, Singh S, Gill SS, Singh H, Kumar R, et al. A framework for effective and clean conversion of machining waste into metal powder feedstock for additive manufacturing. Cleaner Eng Technol 2021;4.
[87] Piras CC, Fernandez-Prieto S, De Borggraeve WM. Ball milling: a green technology for the preparation and functionalisation of nanocellulose derivatives. Nanoscale Adv 2019;1:937–47.
[88] Gorrasi G, Sorrentino A. Mechanical milling as a technology to produce structural and functional bio-nanocomposites. Green Chem 2015;17:2610–25.
[89] Zhang DL. Processing of advanced materials using high-energy mechanical milling. Prog Mater Sci 2004;49:537–60.
[90] Chen Z, Han G-F, Mahmood A, Hou J, Wei W, Kyong Shon H, et al. Mechanosynthesized electroactive materials for sustainable energy and environmental applications: a critical review. Prog Mater Sci 2024;145:101299.

[91] Wang Z, Xu S-R, Sui Q-X, Wang J, Liu B, Wen H, et al. High-performance martensitic stainless steel nanocomposite powder for direct energy deposition prepared by ball milling. Rare Met 2023;42:2419–32.
[92] Liu X, Kang W, Li X, Zeng L, Li Y, Wang Q, et al. Solid-state mechanochemistry advancing two dimensional materials for lithium-ion storage applications: a mini review. Nano Mater Sci 2023;5:210–27.
[93] Li H, Ni Z, Kang Z, Sheng H, Wang Y, Chen M, et al. Research progress on synthesis mechanism and performance evaluation of ball milling biochar-iron based materials. Npj Mater Sustain 2024;2:18.
[94] Burk L, Gliem M, Mülhaupt R. Mechanochemical routes to functionalized graphene nanofillers tuned for lightweight carbon/hydrocarbon composites. Macromol Mater Eng 2018;304.
[95] Huang J, E S, Li J, Jia F, Ma Q, Hua L, et al. Ball-Milling exfoliation of hexagonal boron nitride in viscous hydroxyethyl cellulose for producing nanosheet films as thermal interface materials. ACS Appl Nano Mater 2021;4:13167–75.
[96] Delogu F, Gorrasi G, Sorrentino A. Fabrication of polymer nanocomposites via ball milling: present status and future perspectives. Prog Mater Sci 2017;86:75–126.
[97] Suryanarayana C. Mechanical alloying and milling. Prog Mater Sci 2001;46:1–184.
[98] Wu ZM, Liang YX, Fan Y, Wang PP, Du JL, Zhao YB, et al. The ball to powder ratio (BPR) dependent morphology and microstructure of tungsten powder refined by ball milling. Powder Technol 2018;339:256–63.
[99] Liang YX, Wu ZM, Fu EG, Du JL, Wang PP, Zhao YB, et al. Refinement process and mechanisms of tungsten powder by high energy ball milling. Int J Refract Metals Hard Mater 2017;67:1–8.
[100] Wei LK, Abd Rahim SZ, Al Bakri Abdullah MM, Yin ATM, Ghazali MF, Omar MF, et al. Producing metal powder from machining chips using ball milling process: a review. Materials 2023;16.
[101] Wagih A, Fathy A, Kabeel AM. Optimum milling parameters for production of highly uniform metal-matrix nanocomposites with improved mechanical properties. Adv Powder Technol 2018;29:2527–37.
[102] Huot J, Cuevas F, Deledda S, Edalati K, Filinchuk Y, Grosdidier T, et al. Mechanochemistry of metal hydrides: recent advances. Materials 2019;12:2778.
[103] Yi M, Shen Z. A review on mechanical exfoliation for the scalable production of graphene. J Mater Chem A 2015;3:11700–15.
[104] Islam MA, Serles P, Kumral B, Demingos PG, Qureshi T, Meiyazhagan A, et al. Exfoliation mechanisms of 2D materials and their applications. Appl Phys Rev 2022;9.
[105] Blázquez JS, Ipus JJ, Moreno-Ramírez LM, Álvarez-Gómez JM, Sánchez-Jiménez D, Lozano-Pérez S, et al. Ball milling as a way to produce magnetic and magnetocaloric materials: a review. J Mater Sci 2017;52:11834–50.
[106] Del Rio-Castillo AE, Merino C, Díez-Barra E, Vázquez E. Selective suspension of single layer graphene mechanochemically exfoliated from carbon nanofibres. Nano Res 2014;7:963–72.
[107] Ning LJ, Wu YP, Fang SB, Rahm E, Holze R. Materials prepared for lithium ion batteries by mechanochemical methods. J Power Sources 2004;133:229–42.
[108] Kaya Y, Kobya V, Mardani A, Mardani N, Beytekin HE. Effect of grinding conditions on clinker grinding efficiency: ball size, mill rotation speed, and feed rate. Buildings 2024;14:2356.
[109] Amannejad M, Barani K. Effects of ball size distribution and mill speed and their interactions on ball milling using DEM. Miner Process Extr Metall Rev 2020;42:1–6.
[110] Lyu H, Gao B, He F, Zimmerman AR, Ding C, Huang H, et al. Effects of ball milling on the physicochemical and sorptive properties of biochar: experimental observations and governing mechanisms. Environ Pollut 2018;233:54–63.
[111] Yue H, Yao L, Gao X, Zhang S, Guo E, Zhang H, et al. Effect of ball-milling and graphene contents on the mechanical properties and fracture mechanisms of graphene nanosheets reinforced copper matrix composites. J Alloys Compd 2017;691:755–62.
[112] Yue H, Yao L, Gao X, Zhang S, Guo E, Zhang H, et al. Effect of ball-milling and graphene contents on the mechanical properties and fracture mechanisms of graphene nanosheets reinforced copper matrix composites. J Alloys Compd 2016:691.
[113] Yao Y, Lin Z, Li Z, Song X, Moon K-S, Wong C-p. Large-scale production of two-dimensional nanosheets. J Mater Chem 2012;22.
[114] Jeon IY, Choi HJ, Jung SM, Seo JM, Kim MJ, Dai L, et al. Large-scale production of edge-selectively functionalized graphene nanoplatelets via ball milling and their use as metal-free electrocatalysts for oxygen reduction reaction. J Am Chem Soc 2013;135:1386–93.
[115] Jeon IY, Bae SY, Seo JM, Baek JB. Scalable production of edge-functionalized graphene nanoplatelets via mechanochemical ball-milling. Adv Funct Mater 2015;25:6961–75.
[116] Lyu H, Gao B, He F, Ding C, Tang J, Crittenden JC. Ball-milled carbon nanomaterials for energy and environmental applications. ACS Sustainable Chem Eng 2017;5:9568–85.
[117] Agrawal A. Top-down strategies for achieving high-quality graphene: recent advancements. J Ind Eng Chem 2025;142:103–26.
[118] Teng C, Xie D, Wang J, Yang Z, Ren G, Zhu Y. Ultrahigh conductive graphene paper based on ball-milling exfoliated graphene. Adv Funct Mater 2017;27:1700240.
[119] Li Y, Bao J, Chen T, Yu A, Yang R. Prediction of ball milling performance by a convolutional neural network model and transfer learning. Powder Technol 2022;403:117409.
[120] Ghosh A, Shukla U, Sahoo N, Ganguly S, Shrivastava P, Kumar L, et al. Effect of ball milling on hexagonal boron nitride (hBN) and development of Al-hBN nanocomposites by powder metallurgy route. Mater Sci Pol 2023;41:68–93.
[121] E S, Huang K, Liu J, Yang J, Ma J, Wang Y, et al. Salting-out effect protected ball-milling exfoliation of hexagonal boron nitride and the scale laws on the thermal conductivities of the exfoliated nanosheet assembled composite films. Chem Mater 2024;36:7909–20.
[122] Stolle A, Szuppa T, Leonhardt SE, Ondruschka B. Ball milling in organic synthesis: solutions and challenges. Chem Soc Rev 2011;40:2317–29.
[123] Mahmoud AED, Stolle A, Stelter M. Sustainable synthesis of high-surface-area graphite oxide via dry ball milling. ACS Sustainable Chem Eng 2018;6:6358–69.
[124] Zhu Y, Murali S, Cai W, Li X, Suk JW, Potts JR, et al. Graphene and graphene oxide: synthesis, properties, and applications. Adv Mater 2010;22:3906–24.
[125] Kim J, Park DB, Hong Choi J, Jo M, Kim S, Oh P, et al. Synthesis of highly dispersible functionalized carbon nanotubes as conductive material through a facile drying process for high-power lithium-ion batteries. ChemSusChem 2023;16:e202201924.
[126] Kosynkin DV, Higginbotham AL, Sinitskii A, Lomeda JR, Dimiev A, Price BK, et al. Longitudinal unzipping of carbon nanotubes to form graphene nanoribbons. Nature 2009;458:872–6.
[127] Kulyk B, Freitas MA, Santos NF, Mohseni F, Carvalho AF, Yasakau K, et al. A critical review on the production and application of graphene and graphene-based materials in anti-corrosion coatings. Crit Rev Solid State Mater Sci 2021;47:309–55.
[128] Alfonso Reina XJ, Ho John, Nezich Daniel, Son Hyungbin, Bulovic Vladimir, Dresselhaus Mildred S, Kong Jing. Large area, few-layer graphene films on arbitrary substrates by chemical vapor deposition. Nano Lett 2009;9:30–5.
[129] Li X, Magnuson CW, Venugopal A, An J, Suk JW, Han B, et al. Graphene films with large domain size by a two-step chemical vapor deposition process. Nano Lett 2010;10:4328–34.
[130] Aparna R, Sivakumar N, Balakrishnan A, Sreekumar Nair A, Nair SV, Subramanian KRV. An effective route to produce few-layer graphene using combinatorial ball milling and strong aqueous exfoliants. J Renew Sustain Energy 2013;5.
[131] Zhao W, Fang M, Wu F, Wu H, Wang L, Chen G. Preparation of graphene by exfoliation of graphite using wet ball milling. J Mater Chem 2010;20.
[132] Abdelkader AM, Cooper AJ, Dryfe RA, Kinloch IA. How to get between the sheets: a review of recent works on the electrochemical exfoliation of graphene materials from bulk graphite. Nanoscale 2015;7:6944–56.
[133] Liu N, Luo F, Wu H, Liu Y, Zhang C, Chen J. One-step ionic-liquid-assisted electrochemical synthesis of ionic-liquid-functionalized graphene sheets directly from graphite. Adv Funct Mater 2008;18:1518–25.
[134] Andersson Blvp Odd E, Sato Hirohiko, Enoki Toshiaki, Hishiyama Yoshihiro, Kaburagi Yutaka, Yoshikawa Masanori, Bandow Shunji. Structure and electronic properties of graphite nanoparticles. Phys Rev B 1998;58.
[135] Ohta Ab T, Seyller T, Horn K. Controlling the electronic structure of bilayer graphene. Science 2006;313:951–4.
[136] Scott Gilje SH, Wang Minsheng, Wang Kang L, Kaner Richard B. A chemical route to graphene for device applications. Chem Mater 2007;7:3394–8.
[137] Batool S, Zhang S-R, Han S-T, Zhou Y. Novel charm of 2D materials engineering in memristor: when electronics encounter layered morphology. Nanoscale Horizons 2022;7.
[138] Gong Y, Xu Z-Q, Li D, Zhang J, Aharonovich I, Zhang Y. Two-dimensional hexagonal boron nitride for building next-generation energy-efficient devices. ACS Energy Lett 2021;6:985–96.
[139] Zhou J, Shen L, Costa MD, Persson KA, Ong SP, Huck P, et al. 2DMatPedia, an open computational database of two-dimensional materials from top-down and bottom-up approaches. Sci Data 2019;6:86.
[140] Bhimanapati GR, Glavin NR, Robinson JA. 2D Boron nitride: synthesis and applications. 2D Mater 2016;95:101–47.
[141] Ghosh J, Mazumdar S, Das M, Ghatak S, Basu AK. Microstructural characterization of amorphous and nanocrystalline boron nitride prepared by high-energy ball milling. Mater Res Bull 2008;43:1023–31.
[142] Molaei MJ, Younas M, Rezakazemi M. A comprehensive review on recent advances in two-dimensional (2D) hexagonal boron nitride. ACS Appl Electron Mater 2021;3:5165–87.
[143] Alem N, Erni R, Kisielowski C, Rossell MD, Gannett W, Zettl A. Atomically thin hexagonal boron nitride probed by ultrahigh-resolution transmission electron microscopy. Phys Rev B 2009;80.
[144] Li LH, Chen Y, Behan G, Zhang H, Petravic M, Glushenkov AM. Large-scale mechanical peeling of boron nitride nanosheets by low-energy ball milling. J Mater Chem 2011;21.
[145] Lee D, Lee B, Park KH, Ryu HJ, Jeon S, Hong SH. Scalable exfoliation process for highly soluble boron nitride nanoplatelets by hydroxide-assisted ball milling. Nano Lett 2015;15:1238–44.
[146] Deepika Li LH, Glushenkov AM, Hait SK, Hodgson P, Chen Y. High-efficient production of boron nitride nanosheets via an optimized ball milling process for lubrication in oil. Sci Rep 2014;4:7288.
[147] Coleman JN, Lotya M, O'Neill A, Bergin SD, King PJ, Khan U, et al. Two-dimensional nanosheets produced by liquid exfoliation of layered materials. Science 2011;331:568–71.
[148] Liu X, Li Y, Zeng L, Li X, Chen N, Bai S, et al. A review on mechanochemistry: approaching advanced energy materials with greener force. Adv Mater 2022;34:e2108327.
[149] Koutsioukis A, Florakis G, Sakellis E, Georgakilas V. Stable dispersion of graphene in water, promoted by high-yield, scalable exfoliation of graphite in natural

aqueous extracts: the role of hydrophobic organic molecules. ACS Sustainable Chem Eng 2022;10:12552–8.
[150] Koutsioukis A, Belessi V, Georgakilas V. Developments in two-dimensional material-based nanoinks for electronics. Smart multifunctional nano-inks. Elsevier; 2023. p. 277–302.
[151] Pinilla S, Coelho J, Li K, Liu J, Nicolosi V. Two-dimensional material inks. Nat Rev Mater 2022;7:717–35.
[152] Nicolosi V, Chhowalla M, Kanatzidis MG, Strano MS, Coleman JN. Liquid exfoliation of layered materials. Science 2013;340:1226419.
[153] Han JT, Jang JI, Kim H, Hwang JY, Yoo HK, Woo JS, et al. Extremely efficient liquid exfoliation and dispersion of layered materials by unusual acoustic cavitation. Sci Rep 2014;4:5133.
[154] Xu Y, Cao H, Xue Y, Li B, Cai W. Liquid-phase exfoliation of graphene: an overview on exfoliation media, techniques, and challenges. Nanomaterials 2018;8:942.
[155] Chavalekvirat P, Hirunpinyopas W, Deshsorn K, Jitapunkul K, Iamprasertkun P. Liquid phase exfoliation of 2D materials and its electrochemical applications in the data-driven future. Precis Chem 2024;2:300–29.
[156] Ng LWT, Hu G, Howe RCT, Zhu X, Yang Z, Jones CG, et al. 2D material production methods. In: Ng LWT, Hu G, Howe RCT, Zhu X, Yang Z, Jones CG, et al., editors. Printing of graphene and related 2D materials: technology, formulation and applications. Cham: Springer International Publishing; 2019. p. 53–101.
[157] Lotya M, Hernandez Y, King PJ, Smith RJ, Nicolosi V, Karlsson LS, et al. Liquid phase production of graphene by exfoliation of graphite in surfactant/water solutions. J Am Chem Soc 2009;131:3611–20.
[158] Kim J, Kwon S, Cho D-H, Kang B, Kwon H, Kim Y, et al. Direct exfoliation and dispersion of two-dimensional materials in pure water via temperature control. Nat Commun 2015;6:8294.
[159] Zheng W, Lee LYS. Beyond sonication: advanced exfoliation methods for scalable production of 2D materials. Matter 2022;5:515–45.
[160] Telkhozhayeva M, Teblum E, Konar R, Girshevitz O, Perelshtein I, Aviv H, et al. Higher ultrasonic frequency liquid phase exfoliation leads to larger and monolayer to few-layer flakes of 2D layered materials. Langmuir 2021;37:4504–14.
[161] Yoo SC, Lee D, Ryu SW, Kang B, Ryu HJ, Hong SH. Recent progress in low-dimensional nanomaterials filled multifunctional metal matrix nanocomposites. Prog Mater Sci 2023;132.
[162] Hwang J, Yoon T, Jin SH, Lee J, Kim TS, Hong SH, et al. Enhanced mechanical properties of graphene/copper nanocomposites using a molecular-level mixing process. Adv Mater 2013;25:6724–9.
[163] Jang J-H, Park H-K, Lee J-H, Lim J-W, Oh I-H. Effect of volume fraction and unidirectional orientation controlled graphite on thermal properties of graphite/copper composites. Compos B Eng 2020:183.
[164] Muench F. Electroless plating of metal nanomaterials. Chemelectrochem 2021;8:2993–3012.
[165] Cantürk SB, Kováčik J. Review of recent development in copper/carbon composites prepared by infiltration technique. Energies 2022;15.
[166] Bidulsky R, Gobber FS, Bidulska J, Ceroni M, Kvackaj T, Grande MA. Coated metal powders for laser powder bed fusion (L-PBF) processing: a review. Metals 2021;11:1831.
[167] Yan Q, Chen B, Zhou X, Kondoh K, Li J. Effect of metal powder characteristics on structural defects of graphene nanosheets in metal composite powders dispersed by ball milling. Crystals 2021;11.
[168] Li W, Li D, Fu Q, Pan C. Conductive enhancement of copper/graphene composites based on high-quality graphene. RSC Adv 2015;5:80428–33.
[169] Wang Y, Huang C, Li R, Liu H, Xu Z, Yu C, et al. Enhanced mechanical properties of boron nitride nanosheets/copper composites with a bioinspired laminated structure. Compos Interfaces 2021;29:999–1012.
[170] Chang S, Du W, Zhao Z, Bai P. Microstructure and high temperature-mechanical properties of TiC/Graphene/Ti6Al4V composite formed by laser powder bed fusion. Metals 2023;13.
[171] Shi X, Wu M, Lu P, Ye X. Preparation and performance study of titanium-based nanocomposites in selective laser melting: microstructure regulation and optimization of mechanical properties. Adv Eng Mater 2024;26:2301994.
[172] Tabandeh-Khorshid M, Ajay K, Omrani E, Kim C, Rohatgi P. Synthesis, characterization, and properties of graphene reinforced metal-matrix nanocomposites. Compos B Eng 2020:183.
[173] Wang Z, Yan X, Hou Q, Liu Y, Zeng X, Kang Y, et al. Scalable high yield exfoliation for monolayer nanosheets. Nat Commun 2023;14:236.
[174] Chen S, Xu R, Liu J, Zou X, Qiu L, Kang F, et al. Simultaneous production and functionalization of boron nitride nanosheets by sugar-assisted mechanochemical exfoliation. Adv Mater 2019;31:1804810.
[175] Zhang C, Tan J, Pan Y, Cai X, Zou X, Cheng H-M, et al. Mass production of 2D materials by intermediate-assisted grinding exfoliation. Natl Sci Rev 2019;7:324–32.
[176] Baláž M. Environmental mechanochemistry. Springer; 2021.
[177] Arvidsson R, Kushnir D, Sandén BrA, Molander S. Prospective life cycle assessment of graphene production by ultrasonication and chemical reduction. Environ Sci Technol 2014;48:4529–36.
[178] Ampah AD, Pagone E, Salonitis K. Life cycle assessment of graphene as heating element. Sustainable design and manufacturing 2019: proceedings of the 6th international conference on sustainable design and manufacturing (KES-SDM 19). Springer; 2019. p. 283–97.
[179] Munuera J, Britnell L, Santoro C, Cuéllar-Franca R, Casiraghi C. A review on sustainable production of graphene and related life cycle assessment. 2D Mater 2021;9:012002.
[180] Beloin-Saint-Pierre D, Hischier R. Towards a more environmentally sustainable production of graphene-based materials: building on current knowledge to offer recommendations. Int J Life Cycle Assess 2021;26:327–43.
[181] Pizza A, Metz R, Hassanzadeh M, Bantignies J-L. Life cycle assessment of nanocomposites made of thermally conductive graphite nanoplatelets. Int J Life Cycle Assess 2014;19:1226–37.
[182] James WB. Powder metallurgy methods and applications. In: Samal P, Newkirk J, editors. Powder metallurgy. ASM International; 2015. p. 9–19.
[183] AbuShanab WS, Moustafa EB, Ghandourah E, Taha MA. Effect of graphene nanoparticles on the physical and mechanical properties of the Al2024-graphene nanocomposites fabricated by powder metallurgy. Results Phys 2020;19:103343.
[184] Yamaguchi M, Meng F, Firestein K, Tsuchiya K, Golberg D. Powder metallurgy routes toward aluminum boron nitride nanotube composites, their morphologies, structures and mechanical properties. Mater Sci Eng 2014;604:9–17.
[185] Chu K, Wang F, Wang X-h, Huang D-j. Anisotropic mechanical properties of graphene/copper composites with aligned graphene. Mater Sci Eng 2018;713:269–77.
[186] Zhang X, Shi C, Liu E, Zhao N, He C. Effect of interface structure on the mechanical properties of graphene nanosheets reinforced copper matrix composites. ACS Appl Mater Interfaces 2018;10:37586–601.
[187] Zarei F, Sheibani S. Comparative study on carbon nanotube and graphene reinforced Cu matrix nanocomposites for thermal management applications. Diam Relat Mater 2021;113:108273.
[188] Wang X, Li J, Wang Y. Improved high temperature strength of copper-graphene composite material. Mater Lett 2016;181:309–12.
[189] Ayyappadas C, Muthuchamy A, Raja Annamalai A, Agrawal DK. An investigation on the effect of sintering mode on various properties of copper-graphene metal matrix composite. Adv Powder Technol 2017;28:1760–8.
[190] Gürbüz M, Can Şenel M, Koç E. The effect of sintering time, temperature, and graphene addition on the hardness and microstructure of aluminum composites. J Compos Mater 2018;52:553–63.
[191] Nautiyal H, Gautam RKS, Singh S, Goswami R, Gautam G, Raturi A, et al. Influence of sintering temperature on mechanical and tribological characteristics of copper based composite reinforced by 2D hybrid material. Proc IME E J Process Mech Eng 2023:09544089231158501.
[192] Chu K, Jia C. Enhanced strength in bulk graphene–copper composites. Phys Status Solidi 2014;211:184–90.
[193] Li G, Xiong B. Effects of graphene content on microstructures and tensile property of graphene-nanosheets/aluminum composites. J Alloys Compd 2017;697:31–6.
[194] Saboori A, Pavese M, Badini C, Fino P. A novel approach to enhance the mechanical strength and electrical and thermal conductivity of Cu-GNP nanocomposites. Metall Mater Trans A 2018;49:333–45.
[195] Cao Z, Wang X, Li J, Wu Y, Zhang H, Guo J, et al. Reinforcement with graphene nanoflakes in titanium matrix composites. J Alloys Compd 2017;696:498–502.
[196] Saboori A, Novara C, Pavese M, Badini C, Giorgis F, Fino P. An investigation on the sinterability and the compaction behavior of aluminum/graphene nanoplatelets (GNPs) prepared by powder metallurgy. J Mater Eng Perform 2017;26:993–9.
[197] Ragulya AV. Fundamentals of spark plasma sintering. Reference module in materials science and materials engineering. Elsevier; 2016.
[198] Cavaliere P, Sadeghi B, Shabani A. Spark plasma sintering: process fundamentals. In: Cavaliere P, editor. Spark plasma sintering of materials: advances in processing and applications. Cham: Springer International Publishing; 2019. p. 3–20.
[199] Olevsky E, Khaleghi E, Garcia C, Bradbury W. Fundamentals of spark-plasma sintering: applications to net-shaping of high strength temperature resistant components. Mater Sci Forum 2010;654–656:412–5.
[200] Šestan A, Sreekala L, Markelj S, Kelemen M, Zavašnik J, Liebscher CH, et al. Non-uniform he bubble formation in W/W2C composite: experimental and ab-initio study. Acta Mater 2022;226.
[201] Herrmann M, Räthel J, Schulz I. Spark plasma sintering/field assisted sintering of ceramic materials. Interceram: Int Ceram Rev 2009;58:109–14.
[202] Šestan A, Jenuš P, Krmpotič SN, Zavašnik J, Čeh M. The role of tungsten phases formation during tungsten metal powder consolidation by FAST: implications for high-temperature applications. Mater Char 2018;138:308–14.
[203] Chua AS, Brochu M, Bishop DP. Spark plasma sintering of prealloyed aluminium powders. Powder Metall 2015;58:51–60.
[204] Sciti D, Nygren M. Spark plasma sintering of ultra refractory compounds. J Mater Sci 2008;43:6414–21.
[205] Novak S, Kocen M, Šestan Zavašnik A, Galatanu A, Galatanu M, Tarancón S, et al. Beneficial effects of a WC addition in FAST-Densified tungsten. Mater Sci Eng 2020;772.
[206] Mamedov V. Spark plasma sintering as advanced PM sintering method. Powder Metall 2002;24:322–8.
[207] Tian W-m, Li S-m, Wang B, Chen X, Liu J-h, Yu M. Graphene-reinforced aluminum matrix composites prepared by spark plasma sintering. Int J Miner Metall Mater 2016;23:723–9.
[208] Qu D, Li FZ, Zhang HB, Wang Q, Zhou TL, Hu CF, et al. Preparation of graphene nanosheets/copper composite by spark plasma sintering. Adv Mater Res 2014;833:276–9.
[209] Yadhukulakrishnan GB, Karumuri S, Rahman A, Singh RP, Kaan Kalkan A, Harimkar SP. Spark plasma sintering of graphene reinforced zirconium diboride ultra-high temperature ceramic composites. Ceram Int 2013;39:6637–46.
[210] Hussainova I, Ivanov R, Shamshirgar AS. Spark plasma sintering of layered γ-Al_2O_3/graphene reinforced nanocomposites. Proc Est Acad Sci 2019;68.

[211] Klébert S, Balázsi C, Balázsi K, Bódis E, Fazekas P, Keszler AM, et al. Spark plasma sintering of graphene reinforced hydroxyapatite composites. Ceram Int 2015;41:3647–52.
[212] Güler Ö, Bağcı N, Güler SH, Canbay CA, Safa H, Yılmaz TA, et al. The effect of equal-channel angular pressing (ECAP) on the properties of graphene reinforced aluminium matrix composites. J Compos Mater 2021;55:1749–68.
[213] Brodova IG, Petrova AN, Shirinkina IG, Rasposienko DY, Yolshina LA, Muradymov RV, et al. Mechanical properties of submicrocrystalline aluminium matrix composites reinforced by "in situ" graphene through severe plastic deformation processes. J Alloys Compd 2021;859:158387.
[214] Hasanzadeh Azar M, Sadri B, Nemati A, Angizi S, Shaeri MH, Minárik P, et al. Investigating the microstructure and mechanical properties of aluminum-matrix reinforced-graphene nanosheet composites fabricated by mechanical milling and equal-channel angular pressing. Nanomaterials 2019;9:1070.
[215] Ramesh Kumar S, Gudimetla K, Mohanlal S, Ravisankar B. Effect of mechanically alloyed graphene-reinforced aluminium by equal channel angular pressing (ECAP). Trans Indian Inst Met 2019;72:1437–41.
[216] Zhao L, Lu H, Gao Z. Microstructure and mechanical properties of Al/Graphene composite produced by high-pressure torsion. Adv Eng Mater 2015;17:976–81.
[217] Korznikova G, Czeppe T, Khalikova G, Gunderov D, Korznikova E, Litynska-Dobrzynska L, et al. Microstructure and mechanical properties of Cu-graphene composites produced by two high pressure torsion procedures. Mater Char 2020;161:110122.
[218] Huang Y, Bazarnik P, Wan D, Luo D, Pereira PHR, Lewandowska M, et al. The fabrication of graphene-reinforced Al-based nanocomposites using high-pressure torsion. Acta Mater 2019;164:499–511.
[219] Pu B, Zhang X, Zhao D, He C, Shi C, Liu E, et al. Achieving prominent strengthening efficiency of graphene nanosheets in Al matrix composites by hybrid deformation. Carbon 2021;183:530–45.
[220] Du X, Du W, Wang Z, Liu K, Li S. Simultaneously improved mechanical and thermal properties of mg-zn-zr alloy reinforced by ultra-low content of graphene nanoplatelets. Appl Surf Sci 2021;536:147791.
[221] Jiang Y, Xu R, Tan Z, Ji G, Fan G, Li Z, et al. Interface-induced strain hardening of graphene nanosheet/aluminum composites. Carbon 2019;146:17–27.
[222] Li JL, Xiong YC, Wang XD, Yan SJ, Yang C, He WW, et al. Microstructure and tensile properties of bulk nanostructured aluminum/graphene composites prepared via cryomilling. Mater Sci Eng 2015;626:400–5.
[223] Shin SE, Bae DH. Deformation behavior of aluminum alloy matrix composites reinforced with few-layer graphene. Compos Appl Sci Manuf 2015;78:42–7.
[224] El-Ghazaly A, Anis G, Salem HG. Effect of graphene addition on the mechanical and tribological behavior of nanostructured AA2124 self-lubricating metal matrix composite. Compos Appl Sci Manuf 2017;95:325–36.
[225] Mei Y, Shao P-z, Sun M, Chen G-q, Hussain M, Huang F-l, et al. Deformation treatment and microstructure of graphene-reinforced metal matrix nanocomposites: a review of graphene post-dispersion. Int J Miner Metall Mater 2020;27:888–99.
[226] Li T, Wang Y, Yang M, Hou H, Wu S. High strength and conductivity copper matrix composites reinforced by in-situ graphene through severe plastic deformation processes. J Alloys Compd 2021;851:156703.
[227] Fattahi M, Hsu C-Y, Ali AO, Mahmoud ZH, Dang NP, Kianfar E. Severe plastic deformation: nanostructured materials, metal-based and polymer-based nanocomposites: a review. Heliyon 2023;9:e22559.
[228] Šnajdar-Musa M, Schauperl Z. ECAP - new consolidation method for production of aluminium matrix composites with ceramic reinforcement. Process Appl Ceram 2013;7:63–8.
[229] Zare H, Jahedi M, Toroghinejad MR, Meratian M, Knezevic M. Compressive, shear, and fracture behavior of CNT reinforced Al matrix composites manufactured by severe plastic deformation. Mater Des 2016;106:112–9.
[230] Badrayyana S, Bhat DK, Shenoy S, Ullal Y, Hegde AC. Novel Fe–Ni-Graphene composite electrode for hydrogen production. Int J Hydrogen Energy 2015;40:10453–62.
[231] Biswal HJ, Vundavilli PR, Gupta A. Perspective—electrodeposition of graphene reinforced metal matrix composites for enhanced mechanical and physical properties: a review. J Electrochem Soc 2020;167:146501.
[232] Sreekumar R, Nair AS, S.s S. Recent trends and developments in two-dimensional materials based electrodeposited nickel nanocomposite coatings. Flat Chem 2022;36:100434.
[233] Pavithra CLP, Sarada BV, Rajulapati KV, Rao TN, Sundararajan G. A new electrochemical approach for the synthesis of copper-graphene nanocomposite foils with high hardness. Sci Rep 2014;4:4049.
[234] Sangeetha S, Kalaignan GP. Tribological and electrochemical corrosion behavior of Ni–W/BN (hexagonal) nano-composite coatings. Ceram Int 2015;41:10415–24.
[235] Li H, He Y, He T, Qing D, Luo F, Fan Y, et al. Ni-W/BN(h) electrodeposited nanocomposite coating with functionally graded microstructure. J Alloys Compd 2017;704:32–43.
[236] Cui R, Han Y, Zhu Z, Chen B, Ding Y, Zhang Q, et al. Investigation of the structure and properties of electrodeposited Cu/graphene composite coatings for the electrical contact materials of an ultrahigh voltage circuit breaker. J Alloys Compd 2019;777:1159–67.
[237] Jabbar A, Yasin G, Qamar Khan W, Yousaf Anwar M, Mustafa Korai R, Naeem Nizam M, et al. Electrochemical deposition of nickel graphene composite coatings: effect of deposition temperature on its surface morphology and corrosion resistance. RSC Adv 2017;7:31100–9.
[238] Mathew RT, Singam S, Kollu P, Bohm S, Prasad MJNV. Achieving exceptional tensile strength in electrodeposited copper through grain refinement and reinforcement effect by co-deposition of few layered graphene. J Alloys Compd 2020;840:155725.
[239] Ünal E, Karahan İH. Effects of ultrasonic agitation prior to deposition and additives in the bath on electrodeposited Ni-B/hBN composite coatings. J Alloys Compd 2018;763:329–41.
[240] Ünal E, Karahan İH. Production and characterization of electrodeposited Ni-B/hBN composite coatings. Surf Coating Technol 2018;333:125–37.
[241] Kim SM, Hsu A, Lee Y-H, Dresselhaus M, Palacios T, Kim KK, et al. The effect of copper pre-cleaning on graphene synthesis. Nanotechnology 2013;24:365602.
[242] Tang L, Tan J, Nong H, Liu B, Cheng H-M. Chemical vapor deposition growth of two-dimensional compound materials: controllability, material quality, and growth mechanism. Acc Mater Res 2021;2:36–47.
[243] Saeed M, Alshammari Y, Majeed SA, Al-Nasrallah E. Chemical vapour deposition of graphene—synthesis, characterisation, and applications: a review. Molecules 2020;25:3856.
[244] Sun J, Lu C, Song Y, Ji Q, Song X, Li Q, et al. Recent progress in the tailored growth of two-dimensional hexagonal boron nitride via chemical vapour deposition. Chem Soc Rev 2018;47:4242–57.
[245] Bagherifard S, Monti S, Zuccoli MV, Riccio M, Kondás J, Guagliano M. Cold spray deposition for additive manufacturing of freeform structural components compared to selective laser melting. Mater Sci Eng 2018;721:339–50.
[246] Bagherifard S, Kondas J, Monti S, Cizek J, Perego F, Kovarik O, et al. Tailoring cold spray additive manufacturing of steel 316 L for static and cyclic load-bearing applications. Mater Des 2021;203:109575.
[247] Yin S, Cavaliere P, Aldwell B, Jenkins R, Liao H, Li W, et al. Cold spray additive manufacturing and repair: fundamentals and applications. Addit Manuf 2018;21:628–50.
[248] Prasad K, Rahman Rashid RA, Hutasoit N, Palanisamy S, Hameed N. Fabrication of metal/graphene composites via cold spray process: state-of-the-art and the way forward, vol. 8. C; 2022. p. 65.
[249] Kulkarni A, Rice S, Ansell TY. Enhancing mechanical and tribological properties of cold-sprayed aluminum through graphene nanoplatelet and boron carbide reinforcement. J Therm Spray Technol 2023;32:2351–63.
[250] Saha DC, Sripada JVSN, Saha GC, Jahed H. Microstructure and interfacial bonding evolution of cold spray deposited graphene-reinforced composite feedstock on AZ80 magnesium substrate. J Therm Spray Technol 2023;32:984–1001.
[251] Sripada JVSN, Saha DC, Saha GC, Jahed H. Study the effect of milling parameters on HE-MA nanostructured Al6061-graphene cermet feedstock particles. J Alloys Compd 2021;859:157759.
[252] Sun W, Tan AW-Y, Bhowmik A, Xue F, Marinescu I, Liu E. Evaluation of cold sprayed graphene nanoplates–inconel 718 composite coatings. Surf Coating Technol 2019;378:125065.
[253] Dardona S, Hoey J, She Y, Schmidt WR. Direct write of copper-graphene composite using micro-cold spray. AIP Adv 2016;6:085013.
[254] Wang X, Zhang L, Zhou X, Wu W, Jie X. Corrosion behavior of Al2O3-reinforced graphene encapsulated Al composite coating fabricated by low pressure cold spraying. Surf Coating Technol 2020;386:125486.
[255] Wu H, Zhang L, Liu C, Mai Y, Zhang Y, Jie X. Deposition of Zn-G/Al composite coating with excellent cathodic protection on low-carbon steel by low-pressure cold spraying. J Alloys Compd 2020;821:153483.
[256] Zhang L, Wang X, Wu H, Mai Y, Liu C, Jie X. High densification and anti-corrosion of graphene-coated aluminum coating deposited on AZ31B magnesium by low-pressure cold spray. Carbon Lett 2020;30:581–4.
[257] Zhao Z-p, Tang J-r, Du H, Gyansah L, Wang J-q, Xiong T-y. In-situ chemical interaction in cold-sprayed Zn/Cu composite coating. Mater Lett 2018;228:246–9.
[258] Wang Y, Zhu Y, Li R, Wang H, Tian L, Li H. Microstructure and wear behavior of cold-sprayed Cu-BNNSs composite coating. J Therm Spray Technol 2021;30:1482–92.
[259] Choi J, Okimura N, Yamada T, Hirata Y, Ohtake N, Akasaka H. Deposition of graphene–copper composite film by cold spray from particles with graphene grown on copper particles. Diam Relat Mater 2021;116:108384.
[260] Neshastehriz M, Smid I, Segall AE. In-Situ agglomeration and De-agglomeration by milling of nano-engineered lubricant particulate composites for cold spray deposition. J Therm Spray Technol 2014;23:1191–8.
[261] Neshastehriz M, Smid I, Segall AE, Eden TJ. On the bonding mechanism in cold spray of deformable hex-BN-Ni clusters. J Therm Spray Technol 2016;25:982–91.
[262] Neshastehriz M. Influence of PRE-process work hardening of nickel encapsulated hexagonal boron nitride powders on cold spray.
[263] Stark LM, Smid I, Segall AE, Eden TJ, Potter J. Self-lubricating cold-sprayed coatings utilizing microscale nickel-encapsulated hexagonal boron nitride. Tribol Trans 2012;55:624–30.
[264] Smid I, Segall A, Walia P, Aggarwal G, Eden T, Potter J. Cold-sprayed Ni-hBN self-lubricating coatings. Tribol Trans 2012;55:599–605.
[265] Wu H, Shen G, Li R, Zhang L, Jie X, Liu G. Influence of embedded reduced graphene oxide on the corrosion-wear performance of cold sprayed Zn-rGO/Al coating in NaCl solution. Surf Coating Technol 2022;429:127856.
[266] Naseer A, Ahmad F, Aslam M, Guan BH, Harun WSW, Muhamad N, et al. A review of processing techniques for graphene-reinforced metal matrix composites. Mater Manuf Process 2019;34:957–85.
[267] Santhosh NM, Filipič G, Tatarova E, Baranov O, Kondo H, Sekine M, et al. Oriented carbon nanostructures by plasma processing: recent advances and future challenges. Micromachines 2018;9:565.
[268] Zheng J, Yang R, Xie L, Qu J, Liu Y, Li X. Plasma-assisted approaches in inorganic nanostructure fabrication. Adv Mater 2010;22:1451–73.

[269] Tatarova E, Dias A, Dankov P, Kissovski J, Botelho do Rego AM, Bundaleska N, et al. Plasma-driven tuning of dielectric permittivity in graphene. Small 2024;20:2303421.
[270] Kovacevic E, Strunskus T, Santhosh N M, Zavašnik J, Unger WES, Sauvage T, et al. Thermal stability studies of plasma deposited hydrogenated carbon nitride nanostructures. Carbon 2021;184:82–90.
[271] Dias A, Bundaleska N, Felizardo E, Tsyganov D, Almeida A, Ferraria AM, et al. N-Graphene-Metal-Oxide(Sulfide) hybrid nanostructures: single-Step plasma-enabled approach for energy storage applications. Chem Eng J 2022;430:133153.
[272] Fauchais PL, Heberlein JV, Boulos MI. Thermal spray fundamentals: from powder to part. Springer Science & Business Media; 2014.
[273] Brossa F, Lang E. Plasma spraying — a versatile coating technique. In: Gissler W, Jehn HA, editors. Advanced techniques for surface engineering. Dordrecht: Springer Netherlands; 1992. p. 199–234.
[274] Plasma spraying: theory and applications. World scientific; 1993.
[275] Landes K. Diagnostics in plasma spraying techniques. Surf Coating Technol 2006;201:1948–54.
[276] Pfender E. Fundamental studies associated with the plasma spray process. Surf Coating Technol 1988;34:1–14.
[277] Xu JL, Khor KA. 5 - plasma spraying for thermal barrier coatings: processes and applications. In: Xu H, Guo H, editors. Thermal barrier coatings. Woodhead Publishing; 2011. p. 99–114.
[278] Vasudevan A, Shvalya V, Košiček M, Zavašnik J, Jurov A, Santhosh NM, et al. From faceted nanoparticles to nanostructured thin film by plasma-jet redox reaction of ionic gold. J Alloys Compd 2022;928:167155.
[279] Shvalya V, Vasudevan A, Modic M, Abutoama M, Skubic C, Nadižar N, et al. Bacterial DNA recognition by SERS active plasma-coupled nanogold. Nano Lett 2022;22:9757–65.
[280] Li J, Song C, Lu D, Zhao Y, Sun B, Sun Y. Fabrication of graphite/graphene composite coatings by atmospheric pressure plasma spraying. 2023 IEEE 6th international electrical and energy conference (CIEEC). 2023. p. 4104–9.
[281] Ganvir A, Björklund S, Yao Y, V. S. S, Vadali S, Klement U, Joshi S. A facile approach to deposit graphenaceous composite coatings by suspension plasma spraying. Coatings 2019;9:171.
[282] Gao F, Choi Y, Dobashi Y, Matsugi K. Development of graphene reinforced metal matrix composite by spark plasma sintering. Int J Eng Technol 2018;7:76–9.
[283] Kim S, Kim B, Kim S-J, Lee Y-S, Kim H-G, Lee H, et al. Preparation and characterization of cobalt/graphene composites using liquid phase plasma system. J Nanosci Nanotechnol 2015;15.
[284] Xiao H, Ma G, Ye J, He Y. Preparation of graphene reinforced AZ31B magnesium-based composites by stirring casting. Vacuum 2021;191:110281.
[285] Khatavkar MRA, Mandave AK, Baviskar DD. Influence of hexagonal boron nitride on tribological properties of AA2024-hBN metal matrix composite. IRJET 2018;5:3792.
[286] Awate PP, Barve SB. Enhanced microstructure and mechanical properties of Al6061 alloy via graphene nanoplates reinforcement fabricated by stir casting. Funct Compos Struct 2022;4:015005.
[287] Madhukar P, Selvaraj N, Punugupati G, Kumar GBV, Rao CSP, Mishra SK. Microstructure studies of AA7150-hBN nanocomposites fabricated by ultrasonic assisted stir casting. Mater Res Express 2019;6:116545.
[288] Rashad M, Pan F, Liu Y, Chen X, Lin H, Pan R, et al. High temperature formability of graphene nanoplatelets-AZ31 composites fabricated by stir-casting method. J Magnesium Alloys 2016;4:270–7.
[289] Hu Z, Wu Z, Luo S, Wang X, Nian Q, Chen Y, et al. Large scale production of graphene aluminum composites by stir casting: process, microstructure and properties. J Mater Res Technol 2023;27:681–91.
[290] Abedi M, Moskovskikh D, Romanovski V, Ozherelkov D, Gromov A. Unlocking the potential of graphene-reinforced AlSi10Mg nanocomposites in laser powder bed fusion: a comprehensive review. J Alloys Compd 2024;978:173441.
[291] Gu D, Yang Y, Xi L, Yang J, Xia M. Laser absorption behavior of randomly packed powder-bed during selective laser melting of SiC and TiB2 reinforced Al matrix composites. Opt Laser Technol 2019;119:105600.
[292] Dong M, Zhou W, Kamata K, Nomura N. Microstructure and mechanical property of graphene oxide/AlSi10Mg composites fabricated by laser additive manufacturing. Mater Char 2020;170:110678.
[293] Balbaa MA, Ghasemi A, Fereiduni E, Elbestawi MA, Jadhav SD, Kruth JP. Role of powder particle size on laser powder bed fusion processability of AlSi10mg alloy. Addit Manuf 2021;37:101630.
[294] Yan Q, Chen B, Li JS. Super-high-strength graphene/titanium composites fabricated by selective laser melting. Carbon 2021;174:451–62.
[295] Jin Y, Zhao X, Bai P, Du W, Liao H, Li Y, et al. The graphene/AlSi10Mg composites with fine cells and nano-Si precipitates fabricated using selective laser melting. Mater Lett 2022;324:132775.
[296] Mandal A, Tiwari JK, Sathish N, Srivastava AK. Microstructural and mechanical properties evaluation of graphene reinforced stainless steel composite produced via selective laser melting. Mater Sci Eng 2020;774:138936.
[297] Wen S, Chen K, Li W, Zhou Y, Wei Q, Shi Y. Selective laser melting of reduced graphene oxide/S136 metal matrix composites with tailored microstructures and mechanical properties. Mater Des 2019;175:107811.
[298] Zhou W, Dong M, Zhou Z, Sun X, Kikuchi K, Nomura N, et al. In situ formation of uniformly dispersed Al4C3 nanorods during additive manufacturing of graphene oxide/Al mixed powders. Carbon 2019;141:67–75.
[299] Han Y, Zhang Y, Jing H, Lin D, Zhao L, Xu L, et al. Selective laser melting of low-content graphene nanoplatelets reinforced 316L austenitic stainless steel matrix: strength enhancement without affecting ductility. Addit Manuf 2020;34:101381.
[300] Li Y, Feng Z, Huang L, Essa K, Bilotti E, Zhang H, et al. Additive manufacturing high performance graphene-based composites: a review. Compos Appl Sci Manuf 2019;124:105483.
[301] Lin K, Fang Y, Gu D, Ge Q, Zhuang J, Xi L. Selective laser melting of graphene reinforced titanium matrix composites: powder preparation and its formability. Adv Powder Technol 2021;32:1426–37.
[302] Li X, Yi D, Liu B, Zhang J, Yang X, Wang C, et al. Graphene-strengthened inconel 625 alloy fabricated by selective laser melting. Mater Sci Eng 2020;798:140099.
[303] Hu Z, Chen F, Lin D, Nian Q, Parandoush P, Zhu X, et al. Laser additive manufacturing bulk graphene–copper nanocomposites. Nanotechnology 2017;28:445705.
[304] Wits WW, Smit Md, Al-Hamdani K, Clare AT. Laser powder bed fusion of a Magnesium-SiC metal matrix composite. Procedia CIRP 2019;81:506–11.
[305] Hu Y, Wang H, Cong W. Laser deposition-additive manufacturing of graphene oxide reinforced IN718 alloys: effects on surface quality, microstructure, and mechanical properties. International manufacturing science and engineering conference. American Society of Mechanical Engineers; 2019. p. V002T03A50.
[306] Li Y, Zhang D, Ye Z, Ye G, He R, Wang H, et al. The reinforcement mechanisms of graphene oxide in laser-directed energy deposition fabricated metal and ceramic matrix composites: a comparison study. Int J Adv Des Manuf Technol 2021:1–14.
[307] Lu G, Shi X, Liu X, Zhou H, Chen Y, Yang Z, et al. Tribological performance of functionally gradient structure of graphene nanoplatelets reinforced Ni3Al metal matrix composites prepared by laser melting deposition. Wear 2019;428–429:417–29.
[308] Lu X-L, Liu X-B, Yu P-C, Qiao S-J, Zhai Y-J, Wang M-D, et al. Synthesis and characterization of Ni60-hBN high temperature self-lubricating anti-wear composite coatings on Ti6Al4V alloy by laser cladding. Opt Laser Technol 2016;78:87–94.
[309] Heer B, Sahasrabudhe H, Khanra AK, Bandyopadhyay A. Boron nitride-reinforced SS316 composite: influence of laser processing parameters on microstructure and wear resistance. J Mater Sci 2017;52:10829–39.
[310] Yan H, Zhang P, Gao Q, Qin Y, Li R. Laser cladding Ni-based alloy/nano-Ni encapsulated h-BN self-lubricating composite coatings. Surf Coating Technol 2017;332:422–7.
[311] Wang T, Meng Q, Araby S, Yang G, Li P, Cai R, et al. Non-oxidized graphene/metal composites by laser deposition additive manufacturing. J Alloys Compd 2021;882:160724.
[312] Zhao Z, Bai P, Du W, Liu B, Pan D, Das R, et al. An overview of graphene and its derivatives reinforced metal matrix composites: preparation, properties and applications. Carbon 2020;170:302–26.
[313] Chen C, Guo L, Luo J, Hao J, Guo Z, Volinsky AA. Aluminum powder size and microstructure effects on properties of boron nitride reinforced aluminum matrix composites fabricated by semi-solid powder metallurgy. Mater Sci Eng 2015;646:306–14.
[314] Oketola A, Jamiru T, Adegbola AT, Ogunbiyi O, Rominiyi AL, Smith S. Spark plasma sintering of ceramic-reinforced binary/ternary nickel and titanium metal matrix composites: mechanical properties, microstructure, and densification-A review. J Alloy Metall Syst 2023:100031.
[315] Chaim R, Chevallier G, Weibel A, Estournès C. Grain growth during spark plasma and flash sintering of ceramic nanoparticles: a review. J Mater Sci 2018;53:3087–105.
[316] Manière C, Nigito E, Durand L, Weibel A, Beynet Y, Estournes C. Spark plasma sintering and complex shapes: the deformed interfaces approach. Powder Technol 2017;320:340–5.
[317] Tokita M. Progress of spark plasma sintering (SPS) method, systems, ceramics applications and industrialization. Ceramics 2021;4:160–98.
[318] Smetanina K, Andreev P, Nokhrin A, Lantsev E, Chuvildeev V. Carbon contamination during spark plasma sintering of powder materials: a brief overview. J Alloys Compd 2023:172823.
[319] Sadhu KK, Mandal N, Sahoo RR. SiC/graphene reinforced aluminum metal matrix composites prepared by powder metallurgy: a review. J Manuf Process 2023;91:10–43.
[320] Alinejadian N, Kollo L, Odnevall I. Progress in additive manufacturing of MoS2-based structures for energy storage applications – a review. Mater Sci Semicond Process 2022;139:106331.
[321] Sayyar Z, Jamshidi Z. The role of novel composite of 2D materials and their characterization, properties, and potential applications in different fields. Composite materials. IntechOpen; 2020.
[322] Tejero-Martin D, Rezvani Rad M, McDonald A, Hussain T. Beyond traditional coatings: a review on thermal-sprayed functional and smart coatings. J Therm Spray Technol 2019;28:598–644.
[323] Karthikeyan J. The advantages and disadvantages of the cold spray coating process. The cold spray materials deposition process. Elsevier; 2007. p. 62–71.
[324] Chen T, Lin YC. Feasibility evaluation and optimization of a smart manufacturing system based on 3D printing: a review. Int J Intell Syst 2017;32:394–413.
[325] Shao P, Chen G, Ju B, Yang W, Zhang Q, Wang Z, et al. Effect of hot extrusion temperature on graphene nanoplatelets reinforced Al6061 composite fabricated by pressure infiltration method. Carbon 2020;162:455–64.
[326] Li M, Guo Q, Chen L, Li L, Hou H, Zhao Y. Microstructure and properties of graphene nanoplatelets reinforced AZ91D matrix composites prepared by electromagnetic stirring casting. J Mater Res Technol 2022;21:4138–50.
[327] Nazeer F, Ma Z, Gao L, Wang F, Khan MA, Malik A. Thermal and mechanical properties of copper-graphite and copper-reduced graphene oxide composites. Compos B Eng 2019;163:77–85.
[328] Nazeer F, Ma Z, Xie Y, Gao L, Malik A, Khan MA, et al. A novel fabrication method of copper–reduced graphene oxide composites with highly aligned reduced

graphene oxide and highly anisotropic thermal conductivity. RSC Adv 2019;9:17967–74.
[329] Yang KM, Ma YC, Zhang ZY, Zhu J, Sun ZB, Chen JS, et al. Anisotropic thermal conductivity and associated heat transport mechanism in roll-to-roll graphene reinforced copper matrix composites. Acta Mater 2020;197:342–54.
[330] Zhang X, Xu Y, Wang M, Liu E, Zhao N, Shi C, et al. A powder-metallurgy-based strategy toward three-dimensional graphene-like network for reinforcing copper matrix composites. Nat Commun 2020;11:2775.
[331] Tiwari JK, Mandal A, Sathish N, Kumar S, Ashiq M, Nagini M, et al. Effect of graphene addition on thermal behavior of 3D printed graphene/AlSi10Mg composite. J Alloys Compd 2022:890.
[332] Saboori A, Pavese M, Badini C, Fino P. Microstructure and thermal conductivity of Al–Graphene composites fabricated by powder metallurgy and hot rolling techniques. Acta Metall Sin 2017;30:675–87.
[333] Harichandran R, Kumar RV, Venkateswaran M. Experimental and numerical evaluation of thermal conductivity of graphene nanoplatelets reinforced aluminium composites produced by powder metallurgy and hot extrusion technique. J Alloys Compd 2022;900:163401.
[334] Wang X, Wang X, Liu M, Crimp MA, Wang Y, Qu Z. Anisotropic thermal expansion coefficient of multilayer graphene reinforced copper matrix composites. J Alloys Compd 2018;755:114–22.
[335] Firkowska I, Boden A, Boerner B, Reich S. The origin of high thermal conductivity and ultralow thermal expansion in copper–graphite composites. Nano Lett 2015;15:4745–51.
[336] Cao H, Tan Z, Fan G, Guo Q, Su Y, Li Z, et al. Wide and fine alignment control and interface modification for high-performance thermally conductive graphite/copper composite. Compos B Eng 2020:191.
[337] Nazeer F, Ma Z, Gao L, Abrar S, Malik A, Khan MA, et al. Higher mechanical and thermal properties of Cu-rGO composites. Vacuum 2020;180:109584.
[338] Chu K, Wang X-h, Li Y-b, Huang D-j, Geng Z-r, Zhao X-l, et al. Thermal properties of graphene/metal composites with aligned graphene. Mater Des 2018;140:85–94.
[339] Guo S, Zhang X, Shi C, Liu E, He C, He F, et al. In situ synthesis of high content graphene nanoplatelets reinforced Cu matrix composites with enhanced thermal conductivity and tensile strength. Powder Technol 2020;362:126–34.
[340] Zhang X, Wan D, Peng K, Zhang W. Enhancement of thermal conductivity and mechanical properties of Cu-Reduced graphene oxide composites by interface modification. J Mater Eng Perform 2019;28:5165–71.
[341] Pu F, Zhou C, Liang P, Bai Y, Wang G, Yang Z, et al. In-situ synthesized graphene reinforced copper matrix composites with enhanced thermal properties and corrosion resistance. Diam Relat Mater 2023;138.
[342] Wang J, Guo L-n, Lin W-m, Chen J, Zhang S, Chen S-d, et al. The effects of graphene content on the corrosion resistance, and electrical, thermal and mechanical properties of graphene/copper composites. N Carbon Mater 2019;34:161–9.
[343] Ryu H, Rho H, Lee SW, Lee S-K, Lee H, Bae S, et al. Swift isotropic heat transport of 3D graphene platform-based metal-graphene composites. Carbon 2021;183:93–9.
[344] Wu M, Chen Z, Huang C, Huang K, Jiang K, Liu J. Graphene platelet reinforced copper composites for improved tribological and thermal properties. RSC Adv 2019;9:39883–92.
[345] Nan C-W, Birringer R, Clarke DR, Gleiter H. Effective thermal conductivity of particulate composites with interfacial thermal resistance. J Appl Phys 1997;81:6692–9.
[346] Simoncini A, Tagliaferri V, Ucciardello N. High thermal conductivity of copper matrix composite coatings with highly-aligned graphite nanoplatelets. Materials 2017;10.
[347] Jagannadham K. Thermal conductivity of copper-graphene composite films synthesized by electrochemical deposition with exfoliated graphene platelets. Metall Mater Trans B 2011;43:316–24.
[348] Chen L, Huang Z, Kumar S. Impact of bonding at multi-layer graphene/metal interfaces on thermal boundary conductance. RSC Adv 2014;4:35852–61.
[349] Jia FL, Wei KX, Wei W, Chu FQ, Du QB, Alexandrov IV, et al. Enhanced thermal conductivity and tensile strength of copper matrix composite with few-layer graphene nanoplates. J Mater Eng Perform 2021;30:7682–9.
[350] Malekpour H, Ramnani P, Srinivasan S, Balasubramanian G, Nika DL, Mulchandani A, et al. Thermal conductivity of graphene with defects induced by electron beam irradiation. Nanoscale 2016;8:14608–16.
[351] Ma F, Zheng HB, Sun YJ, Yang D, Xu KW, Chu PK. Strain effect on lattice vibration, heat capacity, and thermal conductivity of graphene. Appl Phys Lett 2012;101.
[352] Kuang Y, Lindsay L, Shi S, Wang X, Huang B. Thermal conductivity of graphene mediated by strain and size. Int J Heat Mass Tran 2016;101:772–8.
[353] Guo M, Qian Y, Qi H, Bi K, Chen Y. Experimental measurements on the thermal conductivity of strained monolayer graphene. Carbon 2020;157:185–90.
[354] Kuang Y, Lindsay L, Huang B. Unusual enhancement in intrinsic thermal conductivity of multilayer graphene by tensile strains. Nano Lett 2015;15:6121–7.
[355] Bae M-H, Li Z, Aksamija Z, Martin PN, Xiong F, Ong Z-Y, et al. Ballistic to diffusive crossover of heat flow in graphene ribbons. Nat Commun 2013;4:1734.
[356] Chen J, Liu B. Ballistic heat conduction characteristics of graphene nanoribbons. Phys E Low-dimens Syst Nanostruct 2022;139:115146.
[357] Zheng W, Huang B, Li H, Koh YK. Achieving huge thermal conductance of metallic nitride on graphene through enhanced elastic and inelastic phonon transmission. ACS Appl Mater Interfaces 2018;10:35487–94.
[358] Koh YK, Bae M-H, Cahill DG, Pop E. Heat conduction across monolayer and few-layer graphenes. Nano Lett 2010;10:4363–8.
[359] Hopkins PE, Baraket M, Barnat EV, Beechem TE, Kearney SP, Duda JC, et al. Manipulating thermal conductance at metal–graphene contacts via chemical functionalization. Nano Lett 2012;12:590–5.
[360] Wang J, Wang Z, Yang K, Chen N, Ni J, Song J, et al. Enhanced heat transport capability across boron nitride/copper interface through inelastic phonon scattering. Adv Funct Mater 2022;32.
[361] Wang X, Wang X, Wang Z, Guo Y, Wang Y. Enhancing mechanism of interfacial metal element on the thermal transport across Cu-graphene interfaces revealed by molecular dynamics simulations. Mater Today Commun 2020;25.
[362] Yang M, Liu Y, Fan T, Zhang D. Metal-graphene interfaces in epitaxial and bulk systems: a review. Prog Mater Sci 2020;110.
[363] Batzill M. The surface science of graphene: metal interfaces, CVD synthesis, nanoribbons, chemical modifications, and defects. Surf Sci Rep 2012;67:83–115.
[364] Khomyakov PA, Giovannetti G, Rusu PC, Brocks G, van den Brink J, Kelly PJ. First-principles study of the interaction and charge transfer between graphene and metals. Phys Rev B 2009;79:195425.
[365] Ran Q, Gao M, Guan X, Wang Y, Yu Z. First-principles investigation on bonding formation and electronic structure of metal-graphene contacts. Appl Phys Lett 2009;94.
[366] Villaroman D, Wang X, Dai W, Gan L, Wu R, Luo Z, et al. Interfacial thermal resistance across graphene/Al2O3 and graphene/metal interfaces and post-annealing effects. Carbon 2017;123:18–25.
[367] Zhou J, Yang K, Yang B, Zhong B, Yao S, Ma Y, et al. Graphene layer number-dependent heat transport across nickel/graphene/nickel interfaces. ACS Appl Mater Interfaces 2022;14:35237–45.
[368] Song M, Jin J, Wang L, Li S, Wang H, Tang S, et al. Interfacial characteristics of graphene-reinforced iron composites: a molecular dynamics study. Crystals 2022;13.
[369] Zhao W, Zhao Z, Bai P, Zhang L, Han B, Du W. The interfacial characteristics of Graphene/Al(4)C(3) in Graphene/AlSi10Mg composites prepared by selective laser melting: first principles and experimental results. Materials 2020;13.
[370] Zhang L, Zhao Z, Bai P, Du W, Liao H, Li Y, et al. The interfacial structure of α-Ti/TiC in graphene-reinforced Ti6Al4V matrix composite coating prepared by laser cladding: first-principles and experimental. Appl Phys A 2021;127.
[371] Xin H, Borduin R, Jiang W, Liechti KM, Li W. Adhesion energy of as-grown graphene on copper foil with a blister test. Carbon 2017;123:243–9.
[372] Helfrecht BA, Guzman DM, Onofrio N, Strachan AH. Interactions between copper and transition metal dichalcogenides: a density functional theory study. Phys Rev Mater 2017;1.
[373] Han Y, Lai KC, Lii-Rosales A, Tringides MC, Evans JW, Thiel PA. Surface energies, adhesion energies, and exfoliation energies relevant to copper-graphene and copper-graphite systems. Surf Sci 2019;685:48–58.
[374] Teng H, Jiang Y, Tan Z, Liu P, Fan G, Xiong D-B, et al. Towards an atomic-scale understanding of interface characteristics in graphene/Al composites. Mater Today Commun 2022;33.
[375] Hou B, Liu P, Wang A, Xie J. Interface optimization strategy for enhancing the mechanical and thermal properties of aligned graphene/Al composite. J Alloys Compd 2022:900.
[376] Dahal A, Batzill M. Graphene-nickel interfaces: a review. Nanoscale 2014;6:2548–62.
[377] Lahiri J, S Miller T, J Ross A, Adamska L, Oleynik II, Batzill M. Graphene growth and stability at nickel surfaces. New J Phys 2011;13.
[378] Fonseca AF, Liang T, Zhang D, Choudhary K, Phillpot SR, Sinnott SB. Graphene-titanium interfaces from molecular dynamics simulations. ACS Appl Mater Interfaces 2017;9:33288–97.
[379] Hsu AL, Koch RJ, Ong MT, Fang W, Hofmann M, Kim KK, et al. Surface-induced hybridization between graphene and titanium. ACS Nano 2014;8:7704–13.
[380] Gao X, Wang S, Lin S. Defective hexagonal boron nitride nanosheet on Ni(111) and Cu(111): stability, electronic structures, and potential applications. ACS Appl Mater Interfaces 2016;8:24238–47.
[381] Mattevi C, Kim H, Chhowalla M. A review of chemical vapour deposition of graphene on copper. J Mater Chem 2011;21:3324–34.
[382] López GA, Mittemeijer EJ. The solubility of C in solid Cu. Scr Mater 2004;51:1–5.
[383] Bandyopadhyay D, Sharma RC, Chakraborti N. The C-Hf-Ti system (Carbon-Hafnium-Titanium). J Phase Equil 2000;21:535–8.
[384] Dabouz R, Bendoumia M, Belaid L, Azzaz M. Dissolution of Al 6%wt c mixture using mechanical alloying. Defect Diffusion Forum 2019;391:82–7.
[385] Li H, Sun J, Zang J, Su N, Feng X, Shen Y. Thermal conductivity of graphene nanoplates reinforced Cu Cr composite coatings by mechanical alloying method. Surf Coating Technol 2021;405.
[386] Chang G, Wang L, Zhang Y, Li X, Chen K, Kan D, et al. Superior thermal conductivity of graphene Film/Cu-Zr alloy composites for thermal management applications. ACS Appl Mater Interfaces 2022;14:56156–68.
[387] Chu K, Wang F, Li Y-b, Wang X-h, Huang D-j, Geng Z-r. Interface and mechanical/thermal properties of graphene/copper composite with Mo2C nanoparticles grown on graphene. Compos Appl Sci Manuf 2018;109:267–79.
[388] Nazeer F, Ma Z, Gao L, Malik A, Khan MA, Abrar S, et al. Effect of graphene on thermal and mechanical properties of copper-titanium carbide composites. Vacuum 2020;173.
[389] Lingling Y, Yanjie Z, Haokai L, Tao G, Hui T, Shuangdong Y, et al. Co-deposition and thermal conductivity of nickel–graphene composite coatings on copper surface. Appl Phys A 2023;129.
[390] Mastrucci A, van Ruijven B, Byers E, Poblete-Cazenave M, Pachauri S. Global scenarios of residential heating and cooling energy demand and CO2 emissions. Clim Change 2021;168:14.

[391] Pradhan SK, Sahoo MR, Ratha S, Polai B, Mitra A, Sathpathy B, et al. Graphene-incorporated aluminum with enhanced thermal and mechanical properties for solar heat collectors. AIP Adv 2020;10.
[392] Sainudeen SS, Joseph A, Joseph M, Sajith V. Heat transfer phenomena of copper-graphene nanocomposite coated aluminium heat spreaders: an interferometric study. Appl Therm Eng 2022;212.
[393] Rho H, Jang YS, Bae H, Cha AN, Lee SH, Ha JS. Fanless, porous graphene-copper composite heat sink for micro devices. Sci Rep 2021;11:17607.
[394] Wang S, Wang H, Chang M, Xu J, Wang J, Yang X, et al. A novel battery thermal management system for an unmanned aerial vehicle using the graphene directional heat transfer structure. J Power Sources 2023;588:233726.
[395] Yu K, Yang X, Cheng Y, Li C. Thermal analysis and two-directional air flow thermal management for lithium-ion battery pack. J Power Sources 2014;270:193–200.
[396] Nath P, Chopra KL. Thermal conductivity of copper films. Thin Solid Films 1974;20:53–62.
[397] Fang J, Xu X, Zhang Y, Ren Q, Wei N, Zhao P. Enhanced heat dissipation for macroscopic metals achieved by a single-layer graphene. Adv Mater Interfac 2024;11:2300877.
[398] Rho H, Lee S, Bae S, Kim T-W, Su Lee D, Jung Lee H, et al. Three-dimensional porous copper-graphene heterostructures with durability and high heat dissipation performance. Sci Rep 2015;5:12710.
[399] Cho H, Rho H, Kim JH, Chae S-H, Pham TV, Seo TH, et al. Graphene–carbon–metal composite film for a flexible heat sink. ACS Appl Mater Interfaces 2017;9:40801–9.
[400] Heu CS, Kim SW, Lee K-S, Kim DR. Fabrication of three-dimensional metal-graphene network phase change composite for high thermal conductivity and suppressed subcooling phenomena. Energy Convers Manag 2017;149:608–15.
[401] Khose A, Kolhe S, Deshmukh VN. Investigations on the effect of graphene coating on thermophysical properties of aluminium and mild steel for cross flow heat exchanger. Mater Today Proc 2022;56:2858–64.
[402] Luo W, Wei B, Luo T, Li B, Zhu G. 3D network of liquid metal-embedded graphene via surface coating for flexible thermal management. Small 2024;20:2406574.
[403] Gibson I, Rosen DW, Stucker B, Khorasani M, Rosen D, Stucker B, et al. Additive manufacturing technologies. Springer; 2021.
[404] Calignano F, Manfredi D, Ambrosio EP, Biamino S, Lombardi M, Atzeni E, et al. Overview on additive manufacturing technologies. Proc IEEE 2017;105:593–612.
[405] Alinejadian N, Kazemi SH, Odnevall I. SLM-Processed MoS(2)/Mo(2)S(3) nanocomposite for energy conversion/storage applications. Sci Rep 2022;12:5030.
[406] Jiang B, Zhenglong L, Xi C, Peng L, Nannan L, Yanbin C. Microstructure and mechanical properties of TiB2-reinforced 7075 aluminum matrix composites fabricated by laser melting deposition. Ceram Int 2019;45:5680–92.
[407] Wen X, Wang Q, Mu Q, Kang N, Sui S, Yang H, et al. Laser solid forming additive manufacturing TiB2 reinforced 2024Al composite: microstructure and mechanical properties. Mater Sci Eng 2019;745:319–25.
[408] Li XP, Ji G, Chen Z, Addad A, Wu Y, Wang HW, et al. Selective laser melting of nano-TiB2 decorated AlSi10Mg alloy with high fracture strength and ductility. Acta Mater 2017;129:183–93.
[409] Zhang S, Wei P, Chen Z, Li B, Huang K, Zou Y, et al. Graphene/ZrO2/aluminum alloy composite with enhanced strength and ductility fabricated by laser powder bed fusion. J Alloys Compd 2022;910:164941.
[410] Li J, Zhang P, He H, Shi B. Enhanced the thermal conductivity of flexible copper foil by introducing graphene. Mater Des 2020;187:108373.